UNIVERSIDAD NACIONAL AUTONOMA DE MEXICO

INSTITUTO DE FISIOLOGÍA CELULAR

DOCTORADO EN CIENCIAS BIOMÉDICAS

El sistema eferente colinérgico controla la descarga aferente vía la modulación de la corriente de potasio tipo M en las neuronas aferentes vestibulares

Tesis

Que para obtener el grado de

DOCTORA EN CIENCIAS

Presenta:

LBM María Cristina Pérez Flores

Tutor

Dr. Enrique Soto Eguibar

Abril de 2010

AGRADEZCO AL CONSEJO NACIONAL DE CIENCIA Y TECNOLOGÍA (CONACyT) POR EL APOYO OTORGADO PARA REALIZAR MIS ESTUDIOS DE DOCTORADO EN CIENCIAS BIOMÉDICAS MEDIANTE LA BECA NO. 185855.

AGRADEZCO A LA DIRECCIÓN GENERAL DE ESTUDIOS DE POSGRADO DE LA UNIVERSIDAD NACIONAL AUTONOMA DE MÉXICO POR EL COMPLEMENTO DE BECA QUE ME BRINDÓ DURANTE MIS ESTUDIOS DE DOCTORADO.

Agradecimientos

A los doctores Enrique y Rosario, por permitirme trabajar con ustedes, por su apoyo profesional y personal en todo momento. Gracias por su confianza y amistad.

A mis padres Paz y Esteban por darme una vida llena de amor, cariño y confianza. Por todos sus esfuerzos para que nunca me faltara nada y tuviera las herramientas necesarias para desarrollarme académicamente. Son excelentes padres y seres humanos.

A mis hijas Cristi y Mari Jose, porque todos los días llenan de satisfacción y alegría mi vida. A José Antonio mi esposo, gracias por amarme y alentarme a seguir adelante. Gracias por estar conmigo.

A mis hermanas Blanca, Columba por su cariño y apoyo en el cuidado de mis hijas cuando yo estuve ausente. A mi hermana Pilar y a José, por su amistad, ayuda desinteresada y confianza.

A todos mis amigos, que hicieron muy grato el trabajo en el laboratorio. En especial a Agenor, por enseñarme todas las técnicas utilizadas para la realización de esta tesis.

Índice

Resumen

Diversas evidencias muestran la expresión de receptores muscarínicos y nicotínicos en las células ciliadas y en las neuronas aferentes del vestíbulo. Éstos receptores participan en la modulación eferente de la actividad eléctrica de las neuronas aferentes. Sin embargo los mecanismos celulares que subyacen a este control postsináptico en las neuronas se desconocen. El propósito de este trabajo fue demostrar que la activación de los receptores muscarínicos en las neuronas aferentes vestibulares inhibe una corriente de potasio tipo M, lo cual modifica la actividad eléctrica de las neuronas aferentes modulando así su ganancia ante la entrada sináptica proveniente de las células ciliadas y su actividad eléctrica en respuesta a estímulos mecánicos.

Realizamos registros utilizando la técnica de patch clamp en la configuración de célula completa, en neuronas aferentes vestibulares aisladas de ratas Wistar (días postparto 7-10) que se mantuvieron en cultivo primario (18-24 h). La corriente M ($I_{K,M}$) fue estudiada durante su desactivación al aplicar un pulso hiperpolarizante a -60 mV. En el 68 % (*n* = 97) de las células estudiadas, aquellas con alrededor de 42 pF de capacitancia de membrana, la aplicación de los bloqueadores selectivos de los canales KCNQ linopirdina y XE-991 disminuyeron la amplitud de la corriente $I_{K,M}$ en un 54% ± 7% y 50% ± 3% respectivamente. El agonista muscarínico oxotremorina-M también disminuyó significativamente la corriente $I_{K,M}$ en un 58% ± 12%. El efecto de oxotremorina-M fue bloqueado por atropina, corroborando su naturaleza colinérgica. El bloqueador selectivo de los canales erg E-4031 no modificó significativamente la amplitud de la corriente $I_{K,M}$. En experimentos de fijación de corriente, linopirdina, XE-991 y oxotremorina-M

modificaron la descarga de las neuronas en respuesta a pulsos de corriente, aumentando su frecuencia de descarga de potenciales de acción. Finalmente realizamos experimentos para estudiar la participación de la PLC en la inhibición de la $I_{K,M}$, nuestros resultados mostraron que en las neuronas aferentes vestibulares, la inhibición de la PLC (mediante la aplicación del inhibidor selectivo U73122 10 μM) atenúa significativamente el efecto inhibidor de oxo-M sobre la corriente $I_{K,M.}$ Observamos que el efecto de U73122 fue específico ya que al utilizar su análogo inactivo el U73343 no obtuvimos reducción significativa en el efecto inhibidor de oxo-M. También encontramos que la depleción intracelular de PIP_2 mediante el uso de poli-L-lisina reduce la amplitud de la corriente $I_{K,M.}$

Nuestros resultados indican que las neuronas aferentes vestibulares con mayor diámetro somático (muy probablemente las neuronas con terminales en cáliz) expresan la corriente $I_{K,M}$ y que la modulación de esta corriente por activación de los receptores muscarínicos constituye un mecanismo celular fundamental mediante el cual el sistema eferente controla la ganancia del sistema aferente en el vestíbulo.

1. INTRODUCCION

1.1 Generalidades

El oído interno en los mamíferos está formado por la cóclea y el aparato vestibular. Este último tiene como funciones: generar un marco de referencia egocéntrico y de la velocidad de desplazamiento del sujeto en su entorno, generar señales que contribuyen a mantener el equilibrio (ajustando la actividad muscular y la posición corporal), y contribuir a la estabilización de la posición de los ojos. En en estos procesos participan de forma conjunta la información vestibular, la información visual y la somatosensorial para generar respuestas motoras apropiadas. La integración de esta información se realiza a nivel central tanto en los núcleos vestibulares como en el cerebelo y en los núcleos oculomotores (Gacek, 1980).

En los mamiferos, el aparato vestibular está formado por dos órganos otolíticos (utrículo y sáculo), los cuales detectan aceleraciones lineales y tres canales semicirculares (lateral, posterior y anterior) que detectan aceleraciones angulares (Wersäll y Bagger-Sjöbäck, 1974) (Figura 1).

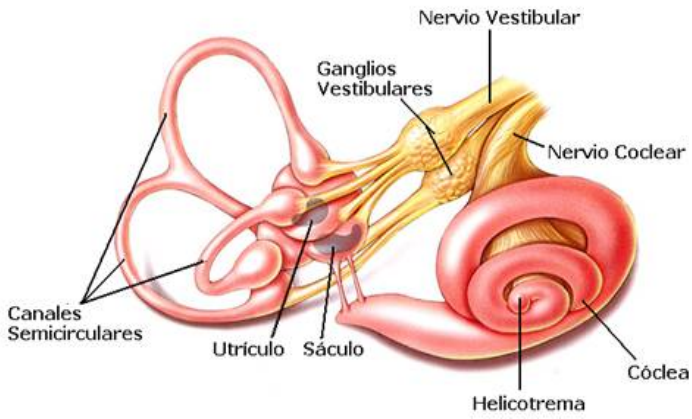

Figura 1. Esquema del sistema vestibular. El vestíbulo está formado por tres canales semicirculares: anterior, posterior y horizontal, los cuales detectan aceleraciones angulares y dos órganos otolíticos: utrículo y sáculo, que responden a las aceleraciones lineales.

El sistema vestibular difiere de otros sentidos en muchos aspectos. Notablemente, el procesamiento vestibular a nivel central es altamente convergente y polimodal. Por ejemplo, interacciones canal/otolito tienen lugar en el tallo cerebral y cerebelo inmediatamente en la primera sinapsis. Además las interacciones visuo vestibular y propioceptivo-vestibular ocurren a todos los niveles vestibulares centrales y son vitales para el control de la postura y la estabilización de la mirada. Debido a la extensa convergencia multimodal con señales motoras y sensitivas, la estimulación vestibular no produce por sí misma una sensación consciente. Sin embargo el sistema vestibular juega un papel importante en la vida diaria porque contribuye a una gran variedad de funciones, desde actividades reflejas hasta altos niveles de percepción y conciencia (Angelaki y Cullen, 2008).

1.2 Células ciliadas

El epitelio sensorial del laberinto membranoso está formado por células especializadas en la mecanorrecepción denominadas células ciliadas, las cuales se dividen en tipo I y tipo II, tomando como principal criterio la forma de la sinapsis aferente (Figura 2). En los mamíferos, las células tipo I tienen forma de ánfora y las fibras aferentes hacen sinapsis con ellas formando un cáliz que rodea la porción basolateral de la célula. Las células tipo II son cilíndricas y las fibras aferente y eferente hacen contacto directo en forma de botón sináptico con la célula ciliada (Young, 1984; Anniko, 1988).

1.3 Neuronas aferentes vestibulares

Los órganos vestibulares son inervados por neuronas aferentes y eferentes. Las neuronas aferentes son de tipo bipolar, inervan las células ciliadas en el vestíbulo y envían axones hacia los núcleos vestibulares en el mesencéfalo y al cerebelo (Bäurle y Guilding, 1998). Los cuerpos celulares de las neuronas aferentes se encuentran en el ganglio vestibular también llamado ganglio de Scarpa (Figura 3).

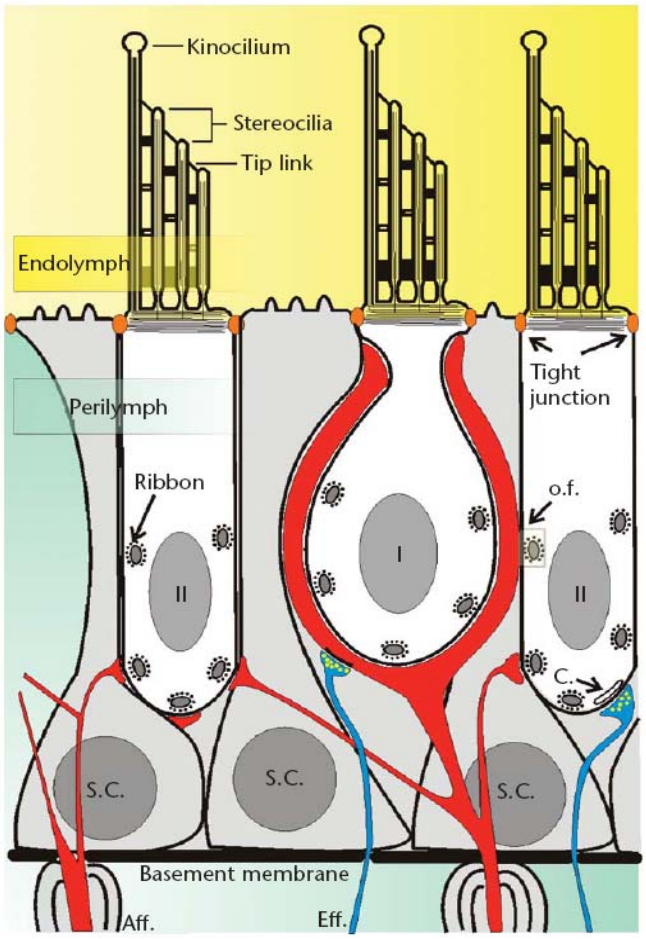

Figura 2. Esquema de las células ciliadas tipo I y II. Las células tipo I tienen la parte basolateral rodeada por un cáliz formado por la neurona aferente, sobre ésta estructura hacen contacto las terminales eferentes. Las células ciliadas tipo II tienen el cuerpo de forma cilíndrica, y hacen contacto sináptico en forma de botón con la neurona aferente. La neurona eferente hace sinapsis directamente sobre la célula ciliada. Tomado de Eatock y Hutzler, 1992.

Las neuronas aferentes vestibulares tienen diámetros somáticos variables que van desde 8 µm hasta 35 µm según la especie. El número de neuronas por ganglio también varía según la especie, en el axolotl existen 1987 ± 131 neuronas

(Limón, 1998), en el gato se han cuantificado 12376 neuronas, en la chinchilla 7772, en el conejillo de indias 8231, en la rata 8449 y en el humano 18500 (Bäurle y Guildin, 1998). Los cuerpos celulares de las neuronas aferentes vestibulares se encuentran normalmente mielinizados excepto -curiosamente- en el hombre (Ylikoski, 1983). En la rata, la mielina que rodea el cuerpo y las dendritas de la neurona, es de tipo compacta y expresa la glicoproteína (P0), indicando que la mielinización se realiza por células de Schwann. La mielina que rodea al axón mas allá de la zona de transición es exclusivamente de tipo central ya que expresa a la proteína básica de mielina (Toesca, 1996).

El diámetro de las fibras aferentes está relacionado con el tipo de contacto

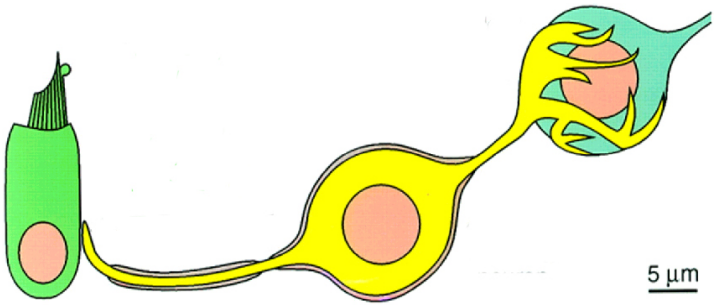

Figura 3. Esquema de una neurona aferente vestibular y sus relaciones sinápticas. A nivel periférico establece contacto sináptico con la célula ciliada. A nivel central con neuronas de segundo orden, en los núcleos vestibulares (algunas aferentes pudieran proyectar directamente a cerebelo).

sináptico entre la aferente y la célula ciliada. En los mamíferos las fibras gruesas establecen sinapsis en forma de cáliz con las células ciliadas tipo I, las fibras delgadas en forma de botón con células ciliadas tipo II y las de diámetro intermedio pueden ser dimórficas, es decir, pueden tener ambos tipos de sinapsis y contactar tanto células tipo I como tipo II (Fernández y cols., 1988). En el caso de los anfibios, existe también una distribución de diámetros de las fibras aferentes que va de gruesas a delgadas a pesar de que las terminales sinápticas

son todas en forma de botón (Honrubia y cols., 1984; Soto y cols., 1994a; Guevara, 1995).

Las neuronas aferentes vestibulares constituyen una población heterogénea, lo cual refleja la presencia de vías que posiblemente contribuyen a los procesos de segregación de la información vestibular. Éstas neuronas han sido clasificadas basándose en su patrón de descarga basal (en ausencia de un estímulo externo) en regulares e irregulares (Baird y cols., 1988; Curthoys, 1982; Estes y cols., 1975; Goldberg y cols., 1990a; Goldberg y cols., 1990b; Schneider y

Tabla I. Características de las neuronas aferentes con descarga regular e irregular registradas en el nervio vestibular de mamíferos.

Descarga Irregular	**Descarga regular**
[a]Neuronas con axones gruesos y medianos que inervan las zonas centrales y estriolares, formando sinapsis tipo cáliz y dimórficas con las células ciliadas.	Neuronas con axones medianos y delgados que inervan las zonas periféricas y forman sinapsis en forma de botón y dimórficas.
[b]Respuestas fásico-tónicas, incluyendo sensibilidad a la velocidad del desplazamiento de la cúpula o la otoconia.	Respuestas tónicas, que es lo esperado para la macromecánica de los órganos vestibulares.
[b]Alta sensibilidad a fuerzas lineales o angulares que actúan en la cabeza.	Baja sensibilidad a fuerzas lineales o angulares.
[c]Alta respuesta a la estimulación de las fibras eferentes.	Baja respuesta a la estimulación eléctrica de las fibras eferentes.
[d]Bajos umbrales a estímulos cortos y altas respuestas a corrientes galvánicas constantes (ambas en el líquido perilinfático)	Altos umbrales a pequeñas respuestas a los mismos estímulos.

[a]Goldberg y Fernández, 1977; Yagi y cols., 1977; Baird y cols., 1988; Goldberg y cols., 1990a; Lysakowski y cols., 1995. [b]Goldberg y Fernández 1971; Yagi y cols., 1977; Baird y cols., 1988; Goldberg y cols., 1990b; Lysakowski y cols., 1995. [c]Goldberg y Fernández, 1980; Mc Cue y Guinan 1994. [d]Ezure y cols., 1983; Goldberg y cols., 1984, 1987; Brontë-Stewart y Lisberg, 1994.

Anderson, 1976; Tomko y cols., 1981; Yagi y cols, 1977), sus principales características se muestran en la Tabla I.

En la rata y en el gato, la proteína fijadora de calcio calbindina, sólo se encuentra en una subpoblación de neuronas grandes (Sans y cols., 1986, Demêmes y cols., 1992 y Bäurle y cols., 1997). En la rata existe además otra subpoblación de neuronas pequeñas que es positiva a calretinina. Las dos subpoblaciones positivas para proteínas fijadoras de calcio también expresan gran cantidad de neurofilamentos en el citoplasma.

1.3.1 Corrientes iónicas dependientes de voltaje en las neuronas aferentes vestibulares

La descarga en las neuronas aferentes vestibulares está determinada por la entrada sináptica y por sus propiedades intrínsecas (Goldberg y cols., 1984). En neuronas aferentes vestibulares de ratón aisladas en forma aguda, se describieron un conjunto de corrientes de Ca^{2+} activadas por voltajes altos (HVA) que corresponden a corrientes tipo L, N, P y Q. Todas estas corrientes identificadas con base en su sensibilidad a toxinas y bloqueadores. En las neuronas de mayor diámetro, se encontró una corriente de Ca^{2+} que se activa a voltajes bajos (LVA) (Desmadryl y cols., 1997). El mismo grupo, en 1999 describió el desarrollo de las corrientes de Ca^{2+} durante la etapa embrionaria (E). Encontraron dos poblaciones neuronales de acuerdo a la amplitud de la corriente de calcio de bajo umbral durante el desarrollo embrionario. En una población, la densidad de esta corriente empieza a disminuir entre la etapa E17 y el nacimiento, tendiendo a desaparecer en etapas más adultas. En la otra población, se observa el proceso contrario, a

partir de E17 aumenta la densidad promedio de esta corriente. En relación con las corrientes tipo L sensible a dihidropiridinas encontraron que ésta permanece constante desde E15 hasta el nacimiento. Las corrientes tipo N y Q (discernidas usando ω-conotoxina GVIA e IVA) incrementaron su magnitud de forma continua. Por su parte, la corriente tipo P sensible a bajas concentraciones de ω-conotoxina IVA, se incrementa notablemente en los días E15 a E17 y luego decrece de forma significativa. El cambio que encuentran en las corrientes tipo LVA y en la corriente tipo P coincide con los máximos de crecimiento neuronal y la formación de sinapsis, lo que sugiere un papel específico para las corrientes de Ca^{2+} en la ontogenia de las neuronas aferentes (Chambard y cols., 1999).

En neuronas del ganglio vestibular de ratón y en la rata también se ha encontrado una corriente de sodio sensible a TTX (Chabbert y cols., 1997; Soto y cols., 2002). Así como tres corrientes de potasio dependientes de voltaje en neuronas aisladas del ganglio vestibular del ratón neonato. La primera corriente es sensible a TEA pero no a 4 AP (I_{TEA}), esta corriente se activa lentamente (τ_m = 38.4 ms) alrededor de -40 mV e inactiva el 84% durante pulsos de 10 segundos (Figura 4). La segunda corriente es sensible a 0.5 mM de 4 AP (Figura 4) y α-dendrotoxina (I_{DTX}), la activación de esta corriente comienza en -60 mV y su cinética es 10 veces más rápida que I_{TEA} e inactiva sólo el 19%. La tercera corriente también es sensible a 4 AP pero su sensibilidad es menor (máximo bloqueo a 2 mM, Figura 4); es sensible a la "sustancia depresora de la sangre (BDS-1)" (I_{BDS}). Esta corriente se activa alrededor de -60 mV (τ_m = 2.3 ms) e inactiva completamente en función del voltaje con una $V_{1/2}$ de -65.8 mV. I_{TEA}, I_{DTX}

e I_{BDS} se encontraron en el 100% de las neuronas estudiadas (Figura 4) (Chabbert y cols, 2001a). En nuestro laboratorio reportamos además la expresión de la corriente de potasio activada por Ca^{2+}, esta corriente está formada por una corriente de alta conductancia (BK), una de conductancia intermedia (IK), una de

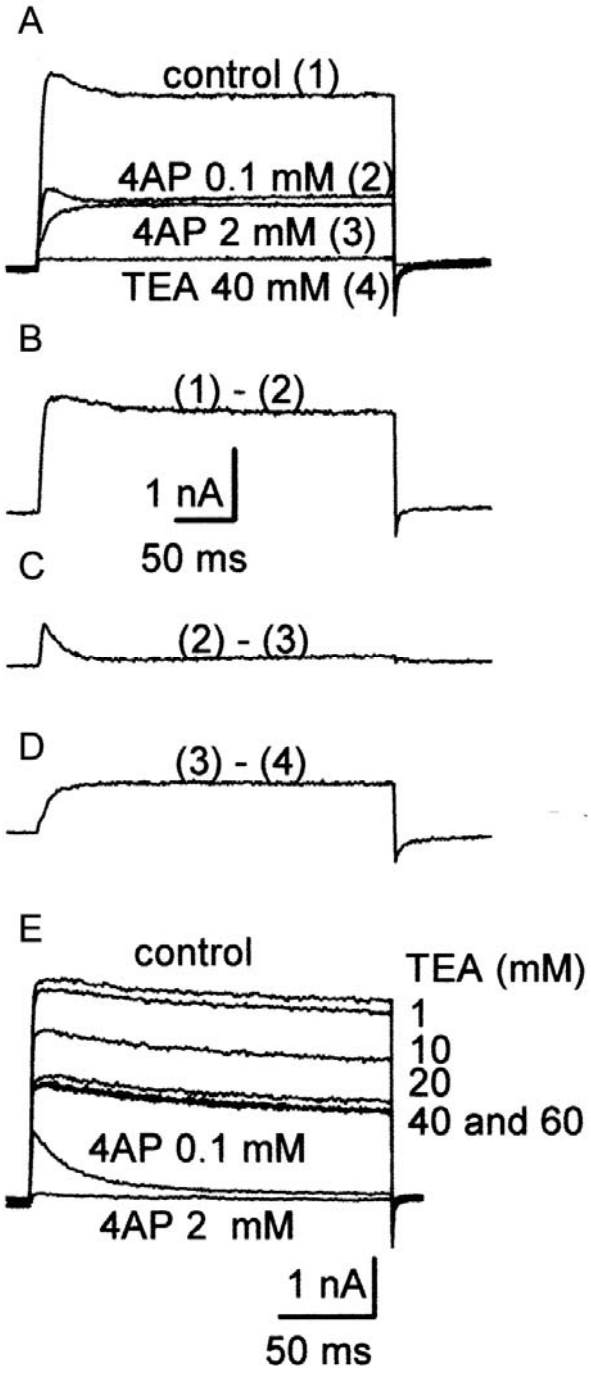

Figura 4. Separación farmacológica de los diferentes componentes de la corriente de potasio, utilizando 4-aminopiridina (4-AP) y tetraetilamonio (TEA). En A, trazos representativos provocados a -10 mV desde un potencial de sotenimiento de -100 mV, solución control (1), presencia de 0.1 mM de 4-AP (2), 2mM de 4-AP (3), y 40 mM TEA (4) en la misma célula. Las dos corrientes sensibles a 4-AP (B y C) y la corriente sensible a TEA (D). En E, la aplicación secuencial de dosis crecientes de TEA, seguidas de la perfusión de 0.1 y 2 mM de 4-AP. Tomado de Chabbert y cols., 2001a.

baja conductancia (SK) y una corriente resistente a los bloqueadores de las corrientes de K^+ activadas por Ca^{2+} que denominamos como resistente (IR) (Figura 5) (Limón y cols., 2005). La expresión de dichas corrientes está correlacionada con la capacitancia de las neuronas aferentes vestibulares, así como con la expresión de la corriente de Ca^{2+} tipo LVA. La corriente tipo BK se expresó preferencialmente en las células que también expresan la corriente de Ca^{2+} LVA. Experimentos con fijación de corriente mostraron que la corriente BK participa de forma significativa en la determinación de la descarga de las aferentes vestibulares en la rata.

Adicionalmente, resultados preliminares de nuestro grupo de investigación indican que las neuronas aferentes vestibulares expresan una corriente de K^+ activada por Na^+ (Soto y cols., 2006) y una corriente de K^+ rectificadora de entrada (I_h) cuya densidad es significativamente mayor en neuronas de ratas adultas en

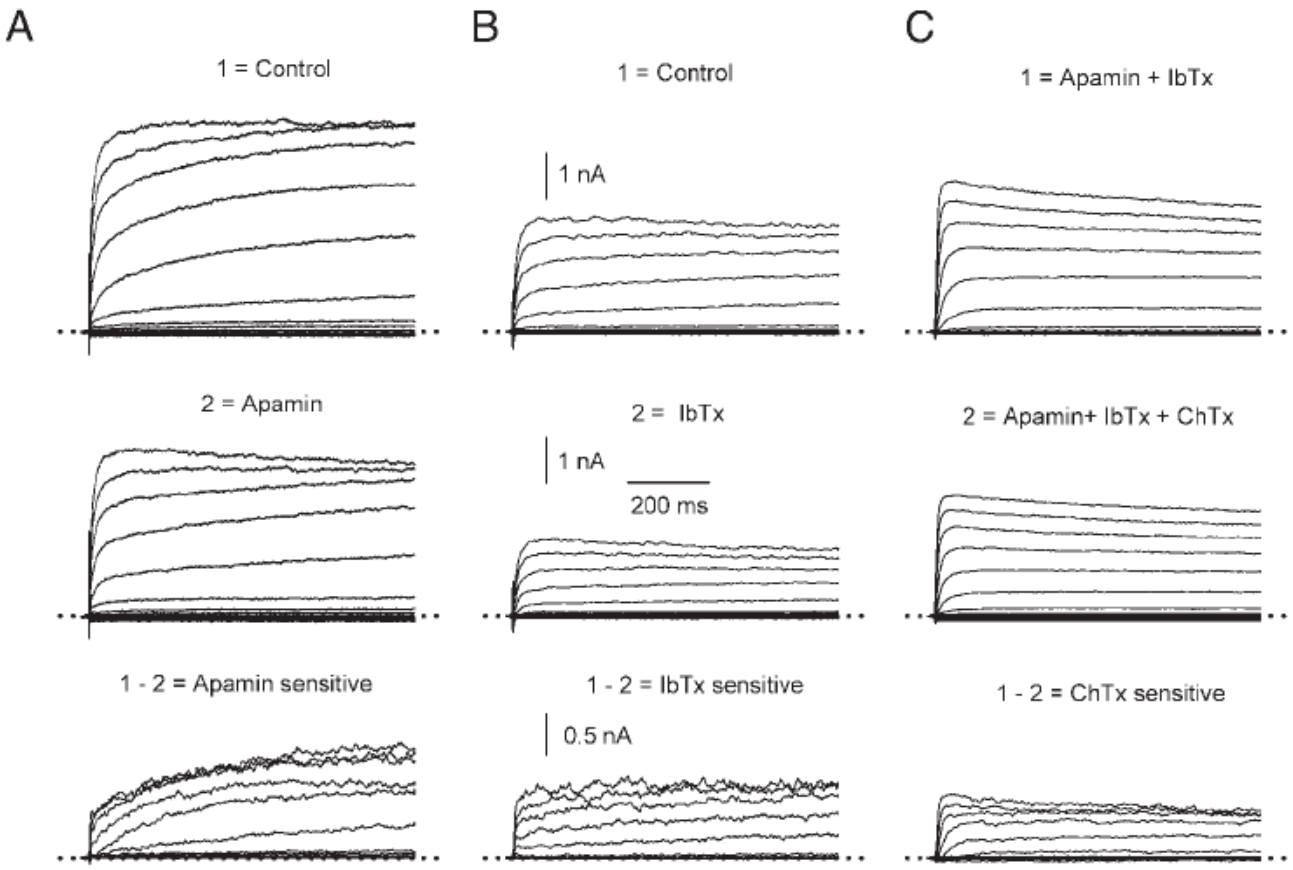

Figura 5. Subtipos de corrientes de potasio activadas por calcio en las neuronas aferentes vestibulares. En A y B se muestra el efecto de apamina e iberiotoxina (IbTx, 100 nM en ambos casos) sobre la corriente saliente provocada con un pulso a 50 mV con un potencial de sostenimiento de -60 mV. Arriba, la corriente control, en medio, durante la perfusión de la toxina y abajo la corriente sensible a la toxina obtenida por sustracción. En C, el efecto de caribdotoxina (ChTx, 100 nM) sobre la corriente resistente a apamina e IbTx. La perfusión de caribdotoxina después de bloquear la corriente de alta conductancia (BK) y de baja conductancia (SK) permitió el aislamiento de la corriente de conductancia intermedia (IK). Tomado de Limón y cols., 2005.

comparación a la I_h de neuronas de ratas neonatas (Soto y cols., 2008a).

1.4 Sinapsis célula ciliada-neurona aferente

El tipo de sinapsis entre la neurona aferente y la célula ciliada se ha usado desde 1956 para clasificar a éstas últimas en dos tipos. En las células ciliadas tipo I, la neurona aferente forma un cáliz que rodea la región basolateral de la célula ciliada; en las células ciliadas tipo II, la sinapsis es en forma de botón (Wersäll, 1956). Este arreglo estructural determina que la célula blanco de la inervación eferente sea diferente en cada caso (Figura 2). En las células ciliadas tipo I, las fibras eferentes (de control) establecen contacto presináptico sobre las neuronas aferentes, mientras que en las células ciliadas tipo II, las neuronas eferentes hacen contacto sináptico directamente sobre las células ciliadas.

La estructura sináptica formada entre las células ciliadas tipo I y las neuronas aferentes, depende de receptores en la membrana de ambas células. Se ha sugerido que tanto la formación como el mantenimiento de la sinapsis se debe al Factor Neurotrófico Derivado del Cerebro *(Brain-derived neurotrophic factor -BDNF-)* el cual serviría como puente entre el receptor a tirosina cinasa B en la neurona aferente (*Tirosine receptor kinase -TrkB-, receptor de alta afinidad para el BDNF)* y el receptor TrKB truncado presente en la célula ciliada tipo I. Por lo tanto, el 34% de las neuronas del ganglio vestibular que no expresan el receptor TrkB (Ernfors y cols., 1995; Fritzsch y cols., 1997) no podrían formar sinapsis en forma de cáliz. Lo que sugiere además, que el tipo de sinapsis que se forma estaría determinado por la célula ciliada, lo que podría explicar la existencia de las fibras dimórficas, ya que si una fibra aferente inerva a dos células ciliadas y solo una de

ellas expresa el receptor TrkB truncado, con esa célula ciliada formará una sinapsis en forma de cáliz y con la otra, simplemente en forma de botón.

1.5 Neurotransmisión aferente

Las neuronas aferentes del sistema vestibular aún en ausencia de estimulación presentan descarga eléctrica basal, la cual es provocada por la liberación de neurotransmisor de las células ciliadas. Se ha demostrado que la transmisión sináptica entre las células ciliadas y las neuronas aferentes tanto en el sistema vestibular como en la cóclea es mediada principalmente por glutamato (Annoni y cols., 1984; Soto y Vega, 1988; Prigioni y cols., 1990; Puel y cols., 1991a y 1991b y Ruel y cols., 1999). Diversos trabajos tanto electrofisiológicos, como inmunohistoquímicos y de biología molecular, sugieren que en la sinapsis aferente participan receptores a glutamato de tipo NMDA y también de tipo no-NMDA. En los roedores, durante el desarrollo se ha detectado la expresión de la subunidad NR1 y posteriormente, las terminales en forma de cáliz expresan las subunidades NR1, NR2A y NR2B. En cambio las células ciliadas tipo II así como sus terminales en forma de botón no expresan estas subunidades (Ishiyama y cols., 2002; Puyal y cols., 2002). En el ganglio vestibular de la rata se expresan las subunidades NR1, moderadamente NR2B y NR2D y en menor proporción NR2A y NR2C (Niedzielski y Wenthold, 1995). La aplicación de AMPA y glutamato en las neuronas vestibulares en cultivo aisladas del ratón, incrementa la concentración de Ca^{2+} intracelular a través de receptores AMPA formados por las subunidades GluR2/3 y GluR4 (Rabejac y cols., 1997). En el ganglio vestibular de la rata se ha encontrado la expresión de las subunidades GluR2-4, GluR5 y 6 y KA1 y 2, las

subunidades GluR1 y 7 parecen no estar presentes en el vestíbulo (Demêmes y cols., 1995; Matsubara y cols., 1999; Soto y Vega, 1988; Dechesne y cols., 1991). Sin embargo, hasta el momento se desconoce si existen subpoblaciones neuronales según el tipo de receptor presente en las neuronas aferentes, y que papel específico desempeña cada subtipo de receptor. Por ejemplo se ha sugerido que los receptores tipo NMDA están relacionados con respuestas de larga duración, en tanto los receptores AMPA determinarían la actividad basal y las respuestas de tipo fásico (Soto y Vega, 1988; Soto y cols., 1994b).

1.5.1 Modulación de la neurotransmisión aferente

Existen reportes que sugieren que la activación de ciertos receptores en la membrana postsináptica modulan la descarga aferente vestibular. Tal es el caso de los receptores a opioides μ que potencian la respuesta de las neuronas aferentes al agonista AMPA en vestíbulo de ajolote (Vega y Soto, 2003). En el vestíbulo de mamífero mediante técnicas de biología molecular se encontró que el receptor opioide μ se expresa en el soma de las neuronas aferentes, en las terminales en forma de cáliz, dimórficas y en botón. No se observó reactividad a este receptor en las fibras eferentes (Popper y cols., 2004). Sin embargo el mecanismo celular, por el cual la activación del receptor opioide μ facilita la descarga aferente aún se desconoce.

El óxido nítrico (NO) también incrementa la descarga aferente; sin embargo, no se conoce el mecanismo celular involucrado. A través de la técnica de la NADPH-diaforasa se encontró una marcada reacción a esta enzima en las células

ciliadas del sistema vestibular del ajolote, así como en algunas fibras que inervan el epitelio y en los somas de las neuronas aferentes vestibulares (Flores y cols., 1996). Mediante registros de la actividad de las fibras aferentes se ha encontrado que los inhibidores de la sintasa de NO inhiben la actividad eléctrica de las fibras aferentes, mientras que la perfusión de donadores de NO, tuvieron un efecto dual (Flores y cols., 2001). Estos resultados sugieren la participación del NO en la codificación sensorial del vestíbulo y de acuerdo a estos resultados podría tener un papel facilitador sobre la descarga basal y la respuesta a estímulos mecánicos. En el sistema vestibular del cobayo mediante el uso del indicador fluorescente diacetato 4,5-diaminofluoresceina, se demostró la producción de NO en las células ciliadas del utrículo (Takumida y Anniko, 2001). Posteriormente se estudió la expresión de la sintasa de NO neuronal (nNOS) e inducible (iNOS) así como de nitrotirosina. La nNOS y la iNOS son sobreexpresadas en el epitelio vestibular cuando los cobayos son tratados con gentamicina después de 7 días. La nitrotirosina incrementa sus niveles en las terminales aferentes en forma de cáliz (Hong y cols., 2006). En células ciliadas aisladas de la cresta de los canales semicirculares de la rata, se demostró que el NO inhibe la corriente de calcio de manera independiente de voltaje, mediante la activación de la vía de señalización del GMPc y por acción directa sobre el canal a través de un reacción de nitrosilación. Esto refleja una importante regulación del calcio intracelular en la célula ciliada así como en la transmisión sináptica (Almanza y cols., 2007).

Otras substancias como la histamina, el ATP y los canabinoides también se ha reportado tienen un papel modulador sobre la descarga aferente. En el caso de la histamina su acción parece estar mediada por receptores tipo H_3, ya que la

aplicación de antagonistas (betahistina, clobenpropit y tioperamida) de este receptor disminuyen la descarga de las neuronas aferentes vestibulares del ajolote (Chávez y cols, 2005), y la betahistina produce una modulación bifásica, excitadora-inhibitoria, en la actividad aferente vestibular en el oído aislado de roedores (Soto y cols., 2008b).

Por otro lado, el ATP extracelular a través de la activación de receptores P_{2X} en las células ciliadas aisladas de la cresta del cobayo, controla directamente la entrada de Ca^{2+} en la célula ciliada, (Rennie y Ashmore, 1993; Nagata y cols., 2000; Kreindler y cols., 2001). La aplicación de agonistas de canabinoides tienen un efecto bifásico, tanto excitador como inhibidor en la descarga de las neuronas aferentes (el efecto depende de la concentración utilizada), el efecto parece ser mediado por receptores CB1 (Carrillo, 2005).

1.6 Neurotransmisión eferente

El epitelio vestibular está inervado por fibras eferentes, cuyos cuerpos celulares se encuentran ubicados bilateralmente en el tallo cerebral, en la región dorsolateral a la eminencia del nervio facial, en la cercanía del núcleo abducens y ventral al núcleo vestibular medial en la formación reticular del tallo cerebral (Perachio y Kevetter, 1989; Bridgeman y cols., 1996). Las fibras eferentes hacen sinapsis con las células ciliadas tipo II y en el caso de las células ciliadas tipo I la terminal eferente hace sinapsis con la fibra aferente en forma de cáliz. El principal neurotransmisor liberado por estas fibras es la acetilcolina. Se ha encontrado que la estimulación de las fibras eferentes produce efectos variables e incluso contrarios sobre la actividad de las fibras aferentes vestibulares, aumentando

(Goldberg y Fernández, 1980; Highstein y Baker, 1985) o inhibiendo la descarga eléctrica de estas neuronas (Valli y cols., 1984). En algunos casos se han observado efectos mixtos (Bernard y cols., 1985). La acetilcolina actuaría sobre receptores nicotínicos y muscarínicos. En las células ciliadas se han identificado receptores de tipo nicotínico α9 y α10 y en las neuronas aferentes receptores nicotínicos α4-7, β2 y β3 (Eróstegui y cols., 1994; Elgoyhen y cols., 1994; Elgoyhen, 2001; Wackym y cols., 1995; Hiel y cols., 1996). Mediante estudios de hibridación in situ en roedores, se ha demostrado que existen subpoblaciones de neuronas que expresan diferentes subunidades del receptor a ACh (mAChR) (Wackym y cols., 1995; Hiel y cols., 1996).

Con respecto a los receptores muscarínicos, estudios mediante reacción en cadena de la polimerasa con transcriptasa inversa (RT-PCR) muestran que tanto en el vestíbulo como en las neuronas aferentes se expresan los cinco subtipos de receptores muscarínicos (m1 - m5) en la rata, en el humano sólo los receptores tipo m1, m2 y m5 fueron amplificados tanto del ganglio vestibular como del epitelio sensorial (Wackym y cols. 1996). En las células ciliadas tipo II se ha descrito también la presencia de receptores muscarínicos en la rana (Guth y cols., 1994; Derbenev y cols., 2005). En el sistema vestibular de la paloma, utilizando inmunohistoquímica se localizaron los cinco subtipos de mAChR que además modulan una corriente rectificante de entrada (Li y cols., 2007).

En las células ciliadas de la cóclea aisladas del pollo, la activación de receptores muscarínicos hiperpolarizó el potencial de membrana mediante la activación de una corriente de K^+ dependiente de Ca^{2+} (Shigemoto y Ohmori,

1991). Mientras que en las neuronas del ganglio espiral la aplicación de carbamilcolina inhibe una corriente lenta de K^+ posiblemente a través de la activación del receptor M1 (Yamaguchi y Ohmori, 1993). La aplicación de acetilcolina en neuronas del ganglio espiral aisladas de la rata, induce la activación de receptores muscarínicos que promueven la movilización del calcio intracelular (Rome y cols., 1999). Los datos obtenidos en el sistema vestibular sugieren que la sinapsis eferente posee un componente muscarínico el cual puede representar un importante blanco terapéutico en pacientes con alteraciones vestibulares. Entre las drogas que modulan la actividad colinérgica y que son utilizadas en clínica para el tratamiento de trastornos vestibulares, se encuentra la escopolamina, fisostigmina y neostigmina.

1.7 Características y papel funcional de la corriente M.

La corriente M ($I_{K,M}$) es una corriente de potasio dependiente de voltaje, no inactivante, la cual está activa alrededor del potencial de membrana en reposo y que modula de manera importante la excitabilidad neuronal (Brown y Adams, 1980; Constanti y Brown, 1981; Aiken y cols., 1995; Marrion, 1997). La corriente $I_{K,M}$ es generada por las subunidades de los canales KCNQ, particularmente por los heterómeros KCNQ2-KCNQ3 y KCNQ3-KCNQ5 (Schroeder y cols., 2000; Lerche y cols., 2000) y homómeros de la subunidad KCNQ4 (Søgaard y cols., 2001). Las subunidades de los canales de la familia erg (ether-a-go-go-related gene) particularmente, los heterómeros erg1-erg2 (Meves y cols., 1999; Selyanko y cols., 2002) también producen corrientes tipo M. Esta corriente es modulada por la activación de receptores acoplados a proteínas G, incluyendo los receptores

muscarínicos, por esta razón se le denomina corriente M (Brown y Adams, 1980; Robbins, 2001).

La corriente M fue originalmente descrita en neuronas simpáticas de la rana toro como una corriente de K^+ que es modulada por el agonista colinérgico muscarina a través de los receptores M1 y M3 (Brown y Adams, 1980). Ha sido ampliamente caracterizada en neuronas parasimpáticas de la rana y rata (Constanti y Brown, 1981), en neuronas de hipocampo de la región CA1 (Yue y Yaari, 2004, 2006; Shah y cols., 2008), neuronas de la corteza olfatoria (Constanti y Sim, 1987), en células NG108-15 (mouse neuroblastoma x rat glioma hybrid cells) (Meves y cols., 1999; Selyanko y cols., 1999), células de músculo liso gástrico (Clapp y cols., 1992), lactotropos (Sankaranarayanan y Simasko, 1996) y en los bastones de la retina (Kurenny y Barnes, 1994, 1997).

En neuronas simpáticas de la rata, la corriente M puede distinguirse de otras corrientes de potasio por, (1) su rango de activación a potenciales más negativos que otras corrientes de potasio ($V_{1/2}$ = -45 mV) (Constanti y Brown, 1981) comparado con el rectificador retardado ($V_{1/2}$ = -6 mV) (Belluzzi y cols., 1985a) y el de la corriente inactivante I_A ($V_{1/2}$= -30 mV) (Belluzzi y cols., 1985b), (2) su cinética de activación y desactivación es sustancialmente lenta con respecto a la de otras corrientes de potasio (aproximadamente 10 veces más lenta) (Owen y cols, 1990).

La corriente M tiene como correlato molecular subunidades de las familias de canales KCNQ y erg, los cuales forman heterómeros que originan dicha corriente.

1.7.1 Canales de potasio de la familia KCNQ

Los miembros de la familia KCNQ, ahora denominados Kv7 desempeñan papeles importantes en la función del corazón, cerebro, oído, vestíbulo y en diversos tejidos epiteliales (Jentsch, 2000; Jespersen y cols., 2005). Los miembros de esta familia de canales han sido ampliamente caracterizados funcionalmente, sin embargo se conoce muy poco acerca de sus características estructurales y de ensamble. Esto es de particular importancia debido a que diversas enfermedades (como la Epilepsia Benigna Neonatal, el Sindrome de QT largo, o el de Jervell-Lange Nielsen, entre otros) son debidas a mutaciones, producidas por la sustitución de ciertos aminoácidos en las regiones citoplasmáticas de la proteína (Jentsch, 2000).

En los mamíferos se han descrito 5 subtipos de canales KCNQ (KCNQ1-5) (Gutman y cols., 2003). Estudios funcionales indican que cada subunidad tiene diferente preferencia para ensamblarse. La subunidad KCNQ1 responsable de generar la corriente I_{Ks}, presente en miocitos cardiacos, no se ensambla con ninguna otra subunidad. La subunidad KCNQ3 puede formar heterotetrameros con todas las demás, excepto con KCNQ1, y es escasamente expresada como homotetramero (Schwake y cols., 2000). Los otros miembros de la familia, KCNQ2, KCNQ4 y KCNQ5 pueden formar homotetrámeros funcionales y heterotetrámeros funcionales con KCNQ3. Todas estas combinaciones confieren diferentes propiedades biofísicas, lo que produce la diversidad funcional de la corriente (Hadley y cols., 2000; Kubisch y cols., 1999; Schwake y cols., 2000; Selyanko y cols., 2002; Wang y cols., 1998).

1.7.2 Canales erg

Los canales EAG (ether-à-go-go gene) forman una familia de canales de K^+ activados por voltaje con tres subfamilias: canales eag, elk (eag-like) y erg (eag-related gene), los cuales han sido descritos en *Drosophila* y en mamíferos (Warmke y cols., 1991; Ludwig y cols., 1994; Warmke y Ganetzky, 1994; Titus y cols., 1997; Wang y cols., 1997). De los canales erg en la rata se han descrito las subunidades: erg1 (Bauer y cols., 1998), erg2 y erg3 (Shi y cols., 1997), sus homologos en los seres humanos son los canales HERG. Estos canales son tetrámeros formados por cuatro subunidades, cada una con seis segmentos transmenbrana al igual que los canales Kv (*Shaker*-related) (Marais-Cabral y cols., 1998). La corriente erg presenta rectificación entrante, ésta se debe a dos propiedades biofísicas atípicas: una cinética de activación lenta e inactivación rápida (Shibasaki, 1987). Como resultado observamos una corriente saliente de lenta activación a potenciales positivos. La combinación del proceso de desactivación lenta y la recuperación rápida de la inactivación, producen una cola de corriente transitoria de gran amplitud, la cual fluye durante la hiperpolarización, tal y como se ha observado en la fase de repolarización del potencial de acción cardiaco (Tristani-Firouzi y Sanguinetti (2003).

1.7.3 Canales KCNQ y erg en el oído interno

Estudios de inmunohistoquímica han permitido demostrar que en roedores la subunidad KCNQ1 se expresa en la superficie apical de las células oscuras del sistema vestibular (Shen y Marcus, 1998). Las subunidades KCNQ3 y KCNQ5 están presentes en las células ciliadas y la subunidad KCNQ5 se expresa en las

células de soporte y en las neuronas aferentes vestibulares que inervan en forma de cáliz (Hurley y cols., 2006). La subunidad KCNQ4 se expresa abundantemente en las estructuras del oído interno, están presentes en las terminales en forma de cáliz y en células ciliadas tipo I y II. (Kharkovets y cols., 2000; Hurley y cols., 2006; Rocha-Sanchez y cols., 2007; Holt y cols., 2007). Se encontró también inmunoreactividad a la subunidad Herg en las células ciliadas y en las terminales en cáliz (después del día 4 posnatal). La subunidad erg1 parece concentrarse más en las terminales aferentes que en las células ciliadas (Hurley y cols., 2006). Debido a que la subunidad KCNQ4 está altamente expresada en los cálices (Kharkovets y cols., 2000, Hurley y cols., 2006) y en el ganglio vestibular (Rocha-Sanchez y cols., 2007), existe la posibilidad de que los canales con subunidades KCNQ4 estén participando en la generación de la una corriente de potasio tipo M (Kubisch y cols., 1999; Søgaard y cols., 2001; Holt y cols., 2007). Apoyando este resultado, la deleción de la subunidad KCNQ4 provoca la pérdida de una conductancia de potasio activada a bajo umbral ($G_{K,n}$) en las células ciliadas externas de la cóclea (Kharkovets y cols., 2006).

Se ha reportado también la presencia del RNAm para las subunidades de los canales tipo erg (erg1, erg2 y erg3) y para las subunidades KCNQ3, KCNQ4 y KCNQ5 tanto en epitelio utricular como en el ganglio vestibular (Hurley y cols., 2006). Estos autores no detectan la expresión de la subunidad KCNQ2. Considerando la presencia de subunidades KCNQ y erg (las cuales en otros sistemas subyacen la corriente $I_{K,M}$) en el epitelio vestibular y en las neuronas aferentes, en este trabajo nos propusimos estudiar las características de la corriente M en las NAV, su modulación por la activación de receptores

muscarínicos, la vía de segundos mensajeros que participa en la modulación de la corriente luego de la activiación de los receptores mACh, y el efecto de la modulación de la corriente sobre la descarga de las neuronas aferentes.

1.7.4 Modulación de la corriente $I_{K,M}$ por activación de receptores muscarínicos.

Los canales de potasio KCNQ son modulados por diferentes neurotransmisores que actúan a través de proteínas Gαq/11 en varios tipos neuronales, entre los receptores que modulan dicha corriente destacan los mAChR (Caulfield y cols., 1994; Marrion, 1997; Cruzblanca y cols., 1998; Haley y cols., 1998). Existen cinco subtipos de mAChR clasificados con base a su farmacología y a la vía de segundos mensajeros que activan, se les denomina M1-M5. Los receptores impares (M1, M3 y M5) están acoplados a la subunidad Gαq/11 de la proteína G y activan a la Fosfolipasa C (PLC -*Phospholipase C*-), mientras que los receptores M2 y M4 están acoplados a las subunidades α Gi y Go e inhiben a la adenilato ciclasa (Caulfield y cols., 1998). Diversos estudios han abordado el estudio del mecanismo mediante el cuál la activación del receptor M1 inhibe la corriente $I_{K,M}$ (Suh y cols., 2004; Jensen y cols., 2009). Se ha propuesto, que la inhibición de la corriente es el resultado de la activación de la proteína Gq/11, su subunidad α es la fracción que activa a la PLC y ésta a su vez hidroliza el fosfatidilinositol-bi-fosfato (PIP_2 -*phosphatidylinositol-bis-phosphate*-) provocando su depleción y una disminución subsecuente de la probabilidad de apertura de los canales KCNQ (Brown y Yu, 2000). Por su parte, la fracción Gβγ

puede difundir y activar también a la PLC, según estudios en que determinaron los niveles de PIP_2 en células en cultivo (Liu y Wu, 2004), además incrementa la fuerza de interacción entre PIP_2 y el canal de potasio activado por receptores muscarínicos (KACh) en células atriales de embrión de pollo (Mirshahi y cols., 2003). Los incrementos de la concentración de calcio intracelular también parecen modificar significativamente la probabilidad de apertura de los canales tipo M, de

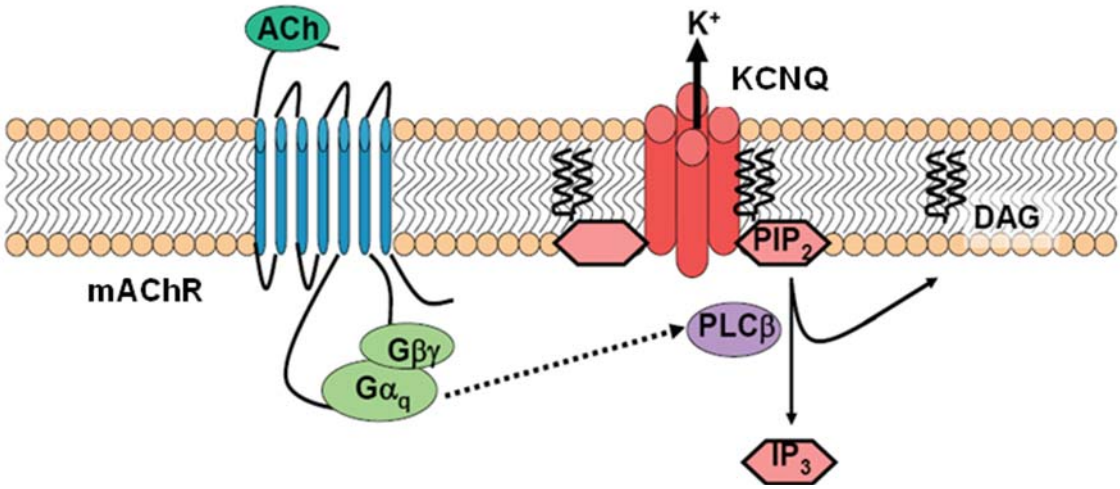

Figura 6. Modulación muscarínica de la corriente $I_{K,M}$. En el esquema se muestra de izquierda a derecha, la activación del receptor muscarínico estimula a la PLC a través de la proteína Gαq. La PLC hidroliza el PIP_2 que está unido al extremo carboxilo del canal KCNQ y sintetiza IP_3 y DAG. De esta manera la depleción de PIP_2 provoca el cierre del canal de potasio.

hecho, existe evidencia de que ésta es la vía mediante la cual la bradicinina (Cruzblanca y cols., 1998) y algunos nucleótidos (Bofill-Cardona y cols., 2000), pero no la acetilcolina (Del Río y cols., 1999), modulan la corriente M.

El PIP_2 es un fosfolípido de la membrana celular que se encuentra en poca abundancia, se le han atribuido importantes funciones en los procesos celulares, tales como la generación de segundos mensajeros (diacilglicerol –DAG- e inositol

1,4,5-trifosfato –IP_3-), control de la actividad de transportadores y en las propiedades de apertura de algunos canales iónicos, por ejemplo: los canales KCNQ (Suh y cols., 2006) (Figura 6). El PIP_2 activa directamente a todos los miembros de la familia KCNQ probablemente debido a una interacción electrostática con una región muy conservada de aminoácidos básicos localizados en la porción carboxilo terminal en el dominio transmembrana S6 (Lopes y cols., 2002; Zhang y cols., 2003). Recientemente se encontró que el proceso de fosforilación está relacionado con la regulación tónica de la corriente M en las neuronas del ganglio cervical superior, en particular una proteína de unión a cinasa A (AKAP150) la cual se une a la proteína cinasa C y esta a su vez fosforila las subunidades KCNQ incrementando su sensibilidad a la estimulación muscarínica (Hoshi y cols., 2003).

Un paso importante en el estudio de la función de los canales de K^+ en la descarga de las neuronas aferentes es determinar la presencia y el papel funcional de la corriente $I_{K,M}$ en el patrón de descarga, la cual posiblemente sea el blanco principal de la entrada eferente colinérgica a las neuronas aferentes vestibulares. Con este propósito, utilizamos neuronas aferentes vestibulares en cultivo primario de rata y estudiamos las propiedades farmacológicas y electrofisiológicas de la corriente $I_{K,M}$.

2. PLANTEAMIENTO DEL PROBLEMA

No se conoce el mecanismo celular por el cual el sistema eferente (cuyo principal neurotransmisor es la acetilcolina) ejerce su influencia sobre la descarga de las neuronas aferentes vestibulares (NAV). Debido a que los mecanismos de control central de la entrada aferente parecen jugar un papel fundamental en la percepción de los movimientos del organismo y particularmente en la capacidad de los sujetos para discernir entre movimientos propios de aquellos que son generados por el entorno, es que decidimos estudiar a nivel celular uno de los procesos que median la respuesta de las neuronas aferentes a la entrada eferente colinérgica. Considerando que las NAV expresan subunidades KCNQ, las cuales en otros sistemas generan una corriente tipo M, aunado con el hecho de que las vías eferentes liberan ACh como neurotransmisores, y que se ha determinado que las NAV expresan receptores muscarínicos, decidimos estudiar si las NAV expresan una corriente de potasio tipo M, y si la inhibición de esta corriente por activación de receptores muscarínicos, media la entrada excitadora a través de la cual el sistema eferente colinérgico modula la actividad eléctrica de las neuronas aferentes vestibulares.

3. HIPÓTESIS

La activación de los receptores muscarínicos en las neuronas aferentes vestibulares inhibe la corriente M, modificando su patrón de descarga. A nivel intracelular la activación de receptores muscarínicos produce su efecto sobre la corriente $I_{K,M}$ a través de la activación de la PLC y una depleción subsecuente de los niveles de PIP_2.

4. OBJETIVO GENERAL

Caracterizar la sensibilidad al voltaje y sensibilidad farmacológica de la corriente $I_{K,M}$ en las NAV, así como evaluar su papel funcional en el patrón de disparo de estas neuronas, además de mostrar la participación de la PLC y el PIP_2 en la inhibición de la corriente $I_{K,M}$.

4.1 Objetivos particulares

1. Analizar las características electrofisiológicas de I_{KM} en las NAV y compararlas con la corriente nativa reportada en neuronas de los ganglios simpáticos.
2. Estudiar el efecto de linopirdina y XE-991 (bloqueadores selectivos de canales KCNQ) sobre la amplitud de la corriente $I_{K,M}$ medida durante su desactivación.
3. Evaluar el efecto de linopirdina y XE-991 en el patrón de descarga de las NAV.
4. Analizar el efecto de Oxotremorina-M (agonista muscarínico) sobre la amplitud de la corriente M, así como en la frecuencia de disparo de las NAV.
5. Evaluar la presencia de la corriente $I_{K,M}$ en NAV de ratas P25-P30. Debido a que el sistema eferente madura por completo durante la 3ª semana posnatal.

6. Determinar si las subunidades de los canales de potasio tipo erg participan en la generación de la corriente $I_{K,M}$ en las NAV, mediante la aplicación del antagonista E-4031.

7. Evaluar la participación de la PLC en la inhibición de la corriente $I_{K,M}$, utilizando el inhibidor U73122 y su análogo inactivo U73343.

8. Estudiar el efecto de la depleción intracelular de PIP_2 sobre la amplitud de la corriente $I_{K,M}$.

5. MATERIAL Y METODOS

En los experimentos se usaron ratas neonatas Wistar de 7 a 10 días postparto (P7-P10), antes de que los cuerpos celulares estén mielinizados (Dechesne y cols., 1987; Toesca, 1996), y un grupo de ratas adultas (P25–P30). Todos los animales fueron proporcionados por el bioterio "Claude Bernard" de la Universidad Autónoma de Puebla.

5.1 Cultivo de neuronas aferentes

Para el cultivo de las neuronas aferentes, las ratas se sacrificaron por decapitación y las cabezas se rociaron con etanol al 70 %. Se retiró el maxilar inferior y el cráneo se introdujo en medio de cultivo L-15 (Gibco, Grand Island, NY). Los ganglios vestibulares se identificaron a través de un microscopio estereoscópico (Nikon, Japan). Se disecaron los ganglios vestibulares y se colocaron en medio de cultivo L-15, adicionado con colagenasa IA 1.25 mg/mL (Sigma Chemicals, St. Louis, MO, USA) y tripsina 1.25 mg/mL (USB, Cleveland, OH, USA) por 30 minutos a 37ºC. Después, los ganglios se centrifugaron en medio de cultivo tres veces por 5 minutos a 4000 rpm. Posteriormente las células se suspendieron en medio de cultivo L-15 suplementado con suero bovino fetal 10% (Gibco), penicilina 100 UI/ml (Lakeside, Toluca, México), fungizone® 2.5 µg/ml (Gibco), $NaHCO_3$ 15.7 mM (Merck KGaA, Darmstadt, Germany), HEPES (4-(2-hydroxyethyl)-1-piperazineethanesulfonic acid) 15.8 mM (Sigma Chemicals), pH 7.7 con NaOH. Previamente el medio de cultivo se incubó durante 30 minutos en CO_2 al 5%. La suspensión celular se colocó en cajas de petri de 35 mm para cultivo (Nunc, Roskilde, Denmark), pre-tratadas con poli-D-lisina, (100 µg/mL) (Sigma Chemicals,

St. Louis, MO, USA) durante 15 minutos. Finalmente las células se incubaron a 37ºC en una atmósfera de CO_2 al 5% durante 18 a 24 horas. Tanto el proceso de disección como el de disociación se realizaron en un cuarto de cultivo bajo una campana de flujo laminar (Nuaire, Plymouth, MN, USA) en condiciones estrictamente asépticas (Soto y cols., 2002).

5.2 Registro electrofisiológico y análisis de datos

Los experimentos se realizaron a temperatura ambiente (23 a 25 ºC) y las células fueron perfundidas con la solución extracelular correspondiente, según se indica en cada caso (Tabla II). El registro de las corrientes iónicas se llevo a cabo mediante la técnica de fijación de voltaje en su configuración de célula completa. Las pipetas de registro se fabricaron a partir de capilares de borosilicato, de 1.2mm de diámetro (WPI, Sarasota, FL, USA) con un estirador horizontal (P80/PC

Tabla II. Soluciones de registro (mM).

	KCl	KF	Colina	NaCl	$CdCl_2$	$MgCl_2$	$CaCl_2$	4-AP	HEPES	Glucosa	EGTA	Mg-ATP	Na-GTP
Extracelular	5.4			140	-	1.2	3.6	-	10	10	-	-	-
Intracelular	140			10	-	-	0.134	-	5	-	10	2	1
Extracelular Modificada		5.4	130	-	0.3	1.2	1.8	10	10	30	-	-	-
Intracelular Modificada		140	10	-	-	-	0.134	-	5	-	10	2	1

El pH de las soluciones intracelular y extracelular se ajustó a 7.2 y 7.4 y a una osmolaridad de 300 y 310 mOsm, respectivamente. EGTA (ethylene glycol bis(2-aminoethyl ether)-N,N,N'N'-tetraacetic acid), 4-AP (4-aminopyridine), HEPES (4-(2-hydroxyethyl)-1-piperazineethanesulfonic acid)

Sutter Instruments, San Rafael, CA, USA) y se utilizaron aquellos con resistencias entre 1 a 3 MΩ una vez llenos con la solución intracelular correspondiente (Tabla

II). En algunos experimentos (según se indica) se usó la técnica de fijación de voltaje con parche perforado. Para este procedimiento, inmediatamente antes de iniciar el registro se agregó anfotericina-B 260 µM (Sigma Chemicals, St. Louis, MO, USA) a la solución intracelular (Rae y cols., 1991).

Para el registro se utilizó un amplificador Axopatch 200B (Molecular Devices, Union City, CA, USA), los registros se digitalizaron con un convertidor analógico digital de 12 bits (Digidata 1200, Molecular Devices) controlado por el programa pClamp 9.0 (Molecular Devices). La condición de registro de célula completa de la técnica de fijación de voltaje se obtuvo después de cancelar la capacitancia de la pipeta y de formar un sello >1 GΩ. En estas condiciones la resistencia de acceso (R_a), resistencia de membrana (R_m), constante de tiempo (τ_m) y capacitancia de membrana (C_m), se calcularon en línea con el programa pClamp 9. Una vez que se registraron las propiedades pasivas, se cancelaron los transientes capacitivos y se compensó la resistencia en serie en todos los registros (≈80%). El potencial de unión líquida para las soluciones de registro fue menor a 5 mV por lo que no fue corregido.

Inicialmente estudiamos la relación dosis-efecto para los bloqueadores de la $I_{K,M}$, linopirdina y XE-991. Para estos experimentos utilizamos soluciones intracelular y extracelular modificadas (Tabla II) y las corrientes fueron provocadas con un pulso de voltaje a 30 mV con duración de 400 ms partiendo de un potencial de sostenimiento de (V_H) -60 mV. Para las relaciones dosis-efecto, la amplitud de la corriente iónica fue normalizada como el porcentaje de cambio comparada con la condición control, con el promedio y el error estándar calculado de estos

valores. Se reunieron los resultados obtenidos de varias células porque no fue posible estudiar en una sola célula todas las concentraciones.

Las curvas dosis-respuesta fueron ajustadas con la ecuación:

$$f(x) = R_{\min} \frac{R_{\max} - R_{\min}}{1+10^{(\log CI_{50} - C)H}}$$

donde R_{max} y R_{min} son el máximo y mínimo efecto, C es la concentración de la droga, CI_{50} es la concentración de la droga con la cual se obtiene la mitad del efecto inhibitorio máximo, y H es el coeficiente de Hill.

Para estudiar el efecto de varias drogas sobre la corriente $I_{K,M}$, su amplitud fue medida durante su desactivación producida por un pulso hiperpolarizante a -60 mV y duración de 1 s, desde un potencial de sostenimiento de -20 mV. Este protocolo fue utilizado tomando ventaja del lento curso temporal de la desactivación de la $I_{K,M}$. La amplitud de la corriente fue medida a -60 mV como la diferencia entre el promedio de un segmento de 10 ms, tomado en los primeros 10-20 ms del pulso hiperpolarizante, y el promedio de los últimos 20 ms del pulso (Brown y Adams, 1980; Shapiro y cols. 2000).

La conductancia de la corriente $I_{K,M}$ fue calculado midiendo la amplitud de la corriente de cola a -60 mV generada por pulsos de voltaje que parten de -80 mV a -10 mV con una duración de 1.6 s y un potencial de sostenimiento de -70 mV.

La corriente de potasio tipo erg ($I_{K(erg)}$) se estudió mediante colas de corriente a -120 mV producidas por pulsos de voltaje desde -80mV a 0 mV y duración de 4 s. La curva de activación de la $I_{K(erg)}$ se obtuvo graficando la corriente normalizada contra el pulso de voltaje.

Las curvas de conductancia fueron normalizadas y aproximadas a una función de Boltzmann:

$$g_{ion} / g_{\max} = 1 / \left\{ 1 + e^{[(Vm - V1/2)/S]} \right\}$$

donde g_{ion} es la conductancia, g_{max} es la conductancia máxima, V_m es el potencial de membrana, $V_{1/2}$ es el potencial al cual se alcanza la mitad de la corriente máxima y S es la pendiente.

En algunos experimentos, las células fueron registradas utilizando la técnica de fijación de corriente, para estudiar su potencial de membrana y su respuesta ante pulsos de corriente, así como su respuesta a la aplicación de las drogas. En estos experimentos los filtros del amplificador fueron abiertos a 10 KHz, se aplicaron pulsos de corriente desde -0.5 a 0.5 nA en pasos de 0.1 nA generados por el programa pClamp. La resistencia de membrana (R_m) se midió utilizando pulsos hiperpolarizantes. Las características del potencial de acción fueron medidas usando el programa Clampfit 9.0 y un software desarrollado en nuestro laboratorio (Soto y cols., 2000). Para esto el valor de voltaje umbral fue usado como punto de referencia. El umbral fue definido como el punto donde la segunda derivada del registro es mayor que la media más dos veces la desviación estándar de los 30 ms previos del registro (Soto y cols., 2000). La amplitud del potencial de acción se calculó como el valor al pico del potencial de acción menos el voltaje umbral. La duración del potencial de acción fue medida al 75% de la amplitud de la espiga. La posthiperpolarización *(*AHP *-after-hiperpolarization-)* fue calculada como la diferencia entre el voltaje mínimo después del potencial de acción y el

potencial de membrana, y la pendiente de la AHP se obtuvo mediante un ajuste lineal a la trayectoria de voltaje después del voltaje mínimo (Soto y cols., 2000).

Para evaluar la significancia estadística utilizamos una prueba *t de Student*, con una $P<0.05$ indicando diferencia significativa. Los resultados numéricos se muestran como la media ± el error estándar de la media, excepto donde la desviación estándar (DS) este indicada.

5.3 Soluciones de registro

La cámara de registro fue continuamente perfundida por gravedad con solución extracelular normal o solución extracelular modificada tal como se indica (Tabla II). Para obtener la curva dosis-efecto de linopirdina y XE-991, el KCl fue reemplazado con KF para bloquear la corriente de Ca^{+2} y la corriente de K^{+} activada por Ca^{+2} (Bertollini y cols., 1994).

5.4 Drogas

En la cámara de registro, las células fueron perfundidas de manera local con la solución extracelular correspondiente mediante un sistema de tubos cuadrados acoplado a un motor de pasos (Warner SF-77B, Hamden, CT, USA) y conectado a una serie de microjeringas mecánicas (Baby Bee, BAS, West Lafayette, IN, USA). La velocidad del flujo fue ajustado a 20 µL/min. Linopirdina, 4-amino-piridina, atropina, oxotremorina-M (oxo-M), anfotericina-B, U-73122, U-73343 y la poli-L-lisina (30,000-70,000 Da) fueron adquiridos en Sigma Chemicals Co. (St. Louis, MO, USA) y el XE-991 de Tocris-Cookson, Inc. (Ellisville, MO, USA). Se prepararon alícuotas de la solución stock en agua desionizada y fueron

almacenadas en refrigeración. La linopirdina, el U-73122 y el U-73343 fueron disueltos en DMSO (concentración final de DMSO 0.01%). Las alícuotas fueron disueltas finalmente en la solución extracelular correspondiente antes de iniciar el experimento.

6. RESULTADOS

Las neuronas aferentes vestibulares fueron identificadas por su birrefringencia y su forma ovoide mediante microscopía de contraste de fases (Figura 7A). Debido a que existe una correlación lineal entre el diámetro somático y la capacitancia de membrana de las neuronas mantenidas en cultivo primario (*r* = 0.92; Limón y cols., 2005) utilizamos la capacitancia como una medida indirecta del diámetro somático (Figura 7B). En solución intracelular y extracelular normal (Tabla II), las neuronas aferentes en cultivo (*n* = 101) tuvieron una C_m = 37 pF (DS = 13 pF; rango = 12 - 72 pF), R_m de 285 MΩ (DS = 153 MΩ; rango = 36 - 980 MΩ), y un potencial de membrana de -59 mV (DS= 6 mV; rango = -45 a -76 mV).

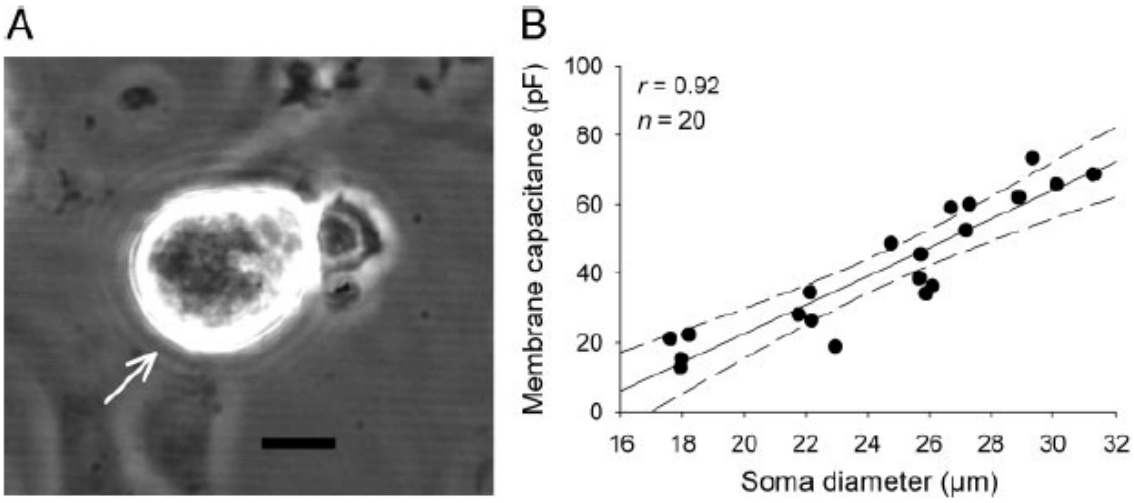

Figura 7. Correlación lineal de la capacitancia de membrana y el diámetro somático. En A, se observa una neurona aferente vestibular aislada después de permanecer 19 horas en cultivo (flecha blanca). La barra de calibración representa 10 μm. En B, se muestra la correlación entre la capacitancia de membrana y el diámetro somático. El diámetro se calculó como el promedio del eje longitudinal mayor y menor. Las líneas punteadas representan el 95 % del intervalo de confianza. Tomado de Limón y cols., 2005.

6.1 Efecto de Linopirdina y XE-991 sobre la corriente M

Para determinar si una conductancia de tipo M formaba parte de la corriente saliente de las neuronas aferentes vestibulares, aplicamos un pulso de voltaje despolarizante desde -60 mV a 30 mV, utilizamos soluciones intracelular y extracelular modificadas (Tabla II) para aislar la corriente $I_{K,M}$ de otras conductancias de potasio. Linopirdina y XE-991 fueron usados como antagonistas de la corriente $I_{K,M}$ (Lamas y cols., 1997; Wang y cols., 1998).

La linopirdina (0.1 μM a 100 μM) y el XE-991 (1 nM a 1 μM) inhibieron la corriente saliente de manera dependiente de la concentración en 78% (*n* =18, Figura 8A, B) y en 82% (*n* = 17, Figura 8C, D) de las células. En el resto de las

células, la linopirdina (*n* = 4) y el XE-991 (*n* = 3) no tuvieron efecto significativo.

La corriente sensible a linopirdina o XE-991 no mostró inactivación significativa (Figura 8B, D). La capacitancia de las neuronas que fueron sensibles a linopirdina y XE-991 fue significativamente mayor que la capacitancia de las células no sensibles (C_m = 38 ± 2 pF, *n* = 28 comparado con C_m = 26 ± 3 pF, *n* = 7; *P* = 0.005). La acción inhibidora de la linopirdina y el XE-991 sobre la corriente saliente se ajustó con una curva dosis respuesta, con una CI_{50} = 7 µM y H = 1 y con una CI_{50} = 30 nM y H = 1, respectivamente (Figura 8E). Como experimento

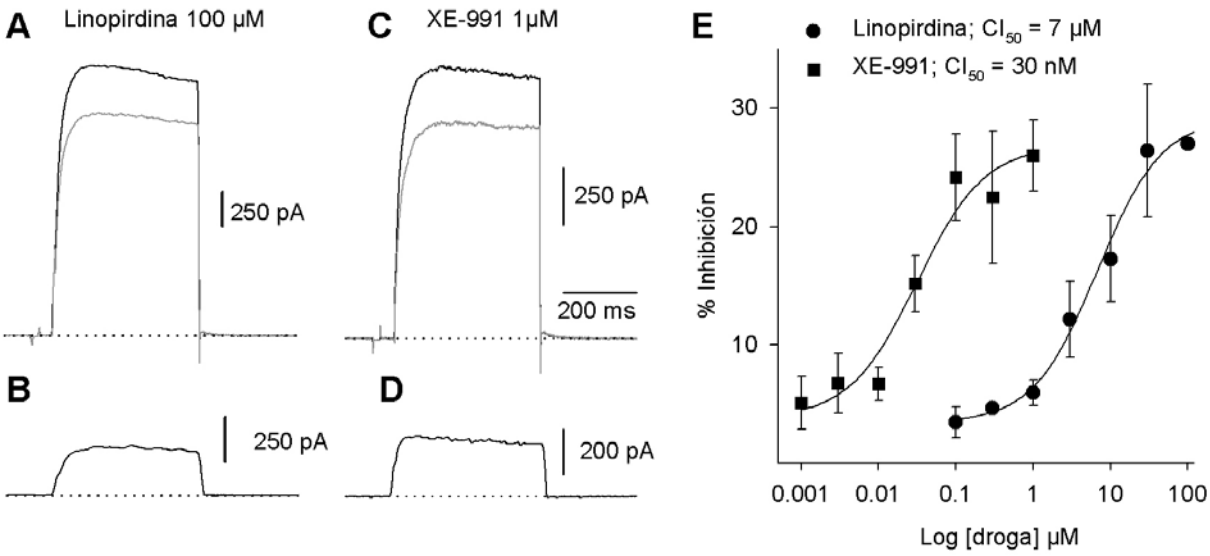

Figura 8. Corriente sensible a linopirdina y XE-991. En A y C, la aplicación de linopirdina 100 µM y XE-991 1 µM inhibieron la corriente saliente cerca del 20 %. En B y D, se muestran las corrientes sensibles a linopirdina y XE-991, fueron obtenidas por la sustracción de la corriente control menos la obtenida después de perfundir la droga. En E, la curva dosis-efecto para linopirdina y XE-991 (linopirdina, *n* = 4-6; XE-991, *n* = 3-8). Las corrientes fueron obtenidas utilizando soluciones modificadas (Tabla II) y fueron producidas por un pulso a 30 mV desde un potencial de sostenimiento de -60 mV. En ésta y las siguientes gráficas los puntos representan la media ± SE (error estándar de la media) y las líneas punteadas representan el cero de corriente o de voltaje.

control, perfundimos solución extracelular normal con DMSO 0.01% (utilizado para disolver linopirdina) y observamos que no tuvo efecto en ninguno de los casos estudiados (n = 5, datos no mostrados).

Con base en el efecto inhibitorio obtenido con linopirdina y XE-991, decidimos estudiar la acción de linopirdina 10 μM y XE-991 1 μM sobre la amplitud de la $I_{K,M}$ medida durante su desactivación (véase material y métodos). Utilizamos soluciones intracelular y extracelular normales debido a que no se contempla la participación de otras corrientes durante la desactivación (Brown y Adams, 1980; Adams y cols., 1982; Shapiro y cols., 2000). La concentración de XE-991 fue saturante (1 μM), mientras que para linopirdina no lo fue, con el propósito de evitar efectos no específicos sobre otras corrientes de K^+ (Schnee y Brown, 1998). La densidad de la corriente $I_{K,M}$ fue de 4 ± 0.4 pA/pF (*n* = 20). Típicamente los trazos de corriente replicaron las propiedades descritas para $I_{K,M}$ (Wang y cols., 1998), por ejemplo: la activación de la corriente estuvo cerca de -60 mV y la cinética de desactivación se ajustó con una función exponencial doble, las constantes de tiempo a -60 mV fueron $\iota_{rápida}$ = 76 $\pm$ 4 ms y ι_{lenta} = 789 $\pm$ 70 ms (*n* = 20, datos no mostrados). El ajuste de la desactivación con una doble exponencial, puede reflejar diferencias en el tipo de subunidades KCNQ que forman la $I_{K,M}$ o que posiblemente está formada por canales KCNQ y canales erg (Meves y cols., 1999; Selyanko y cols., 1999, 2002; Wang y cols., 1998).

La perfusión de linopirdina 10 μM disminuyó la amplitud de la $I_{K,M}$ medida durante su desactivación un 54 ± 7% en 6 células (*n* = 10) con una capacitancia de 44 ± 4 pF (Figura 9A, Tabla III). En el resto de las células, con una capacitancia

promedio de 24 ± 4 pF la inhibición fue de 19 ± 2%. La diferencia en sensibilidad a la droga y en capacitancia entre los dos grupos de células fue significativa (*P* = 0.04 y *P* = 0.02).

La curva de conductancia fue calculada de la corriente de cola a -60 mV después de pulsos de voltaje despolarizantes desde un potencial de sostenimiento de -70 mV antes y después de usar linopirdina 10 μM. La curva de la corriente sensible se ajustó con una función de Boltzmann y obtuvimos una $V_{1/2}$ = -47 ± 2 mV y un *S* = 7 ± 1 mV (*n* = 5) (Figura 9B).

De manera similar estudiamos el efecto de XE-991 durante la desactivación de la $I_{K,M}$. La perfusión de XE-991 1 μM inhibió su amplitud un 50 ± 3% en 12 células (*n* = 14) las cuales tuvieron una capacitancia de 45 ± 3 pF (Figura 10A, Tabla III). Las dos células restantes tuvieron menor capacitancia (C_m = 24 ± 8 pF) y la corriente medida en la desactivación se redujo un 10 ± 3% después de la aplicación de XE-991. La curva de conductancia para XE-991 se ajustó con una función de Boltzmann con una $V_{1/2}$ = -47 ± 2 mV y *S* = 8 ± 2 mV (*n* = 5) (Figura 10B).

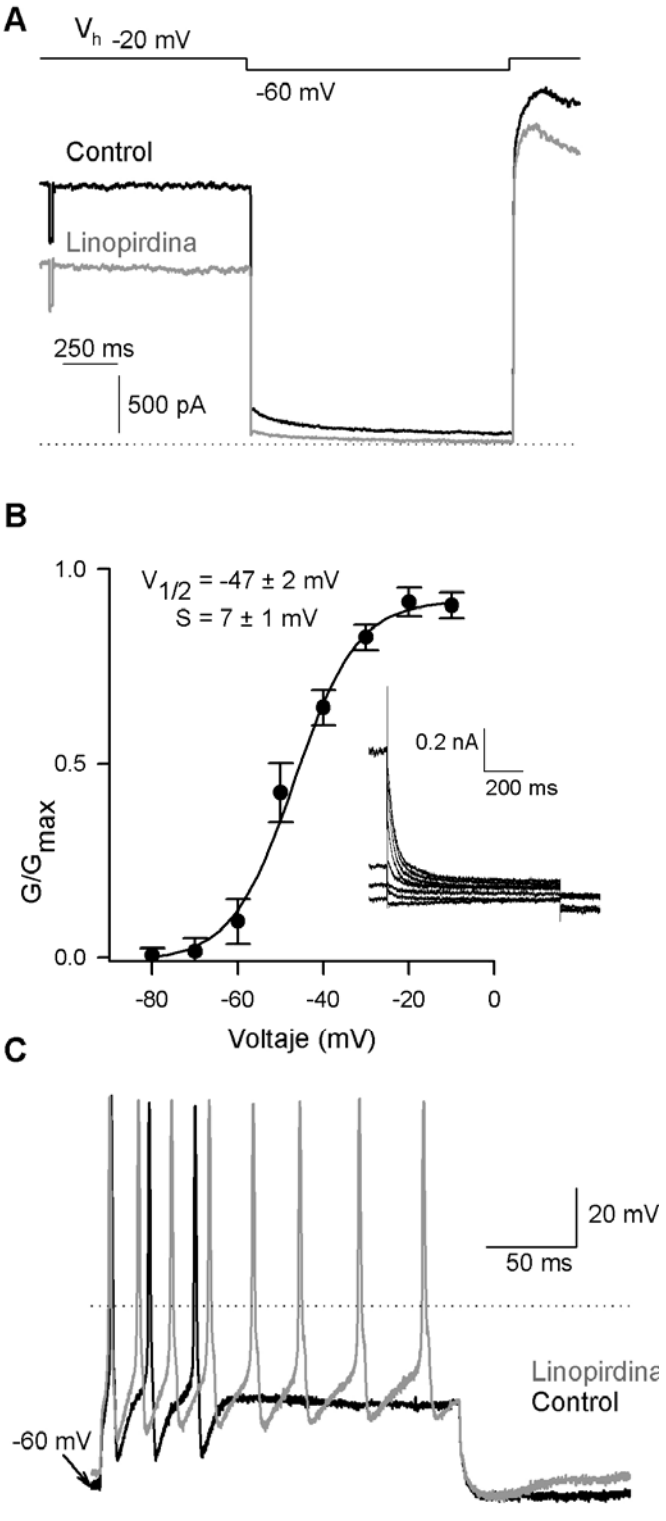

Figura 9. Efecto de linopirdina durante la desactivación de la corriente, conductancia y frecuencia de disparo de las neuronas aferentes vestibulares. En A, inhibición de la corriente con linopirdina 10 μM de alrededor de 55% (línea gris) comparada con el trazo control (línea negra). El pulso que se observa al inicio del trazo se utilizó como indicador de la estabilidad del valor de resistencia de acceso. En B, la conductancia normalizada de la corriente sensible a linopirdina 10 μM. El inserto muestra los trazos típicos de las colas de corriente de la $I_{K,M}$. En C, la respuesta de una neurona aferente a un pulso de corriente de 0.3 nA y 200 ms de duración, en condiciones control (línea negra) y después del uso de linopirdina 10 μM (línea gris). La perfusión con linopirdina incrementó el número de potenciales de acción disparados por las neuronas aferentes vestibulares y también disminuyó la amplitud de la posthiperpolarización.

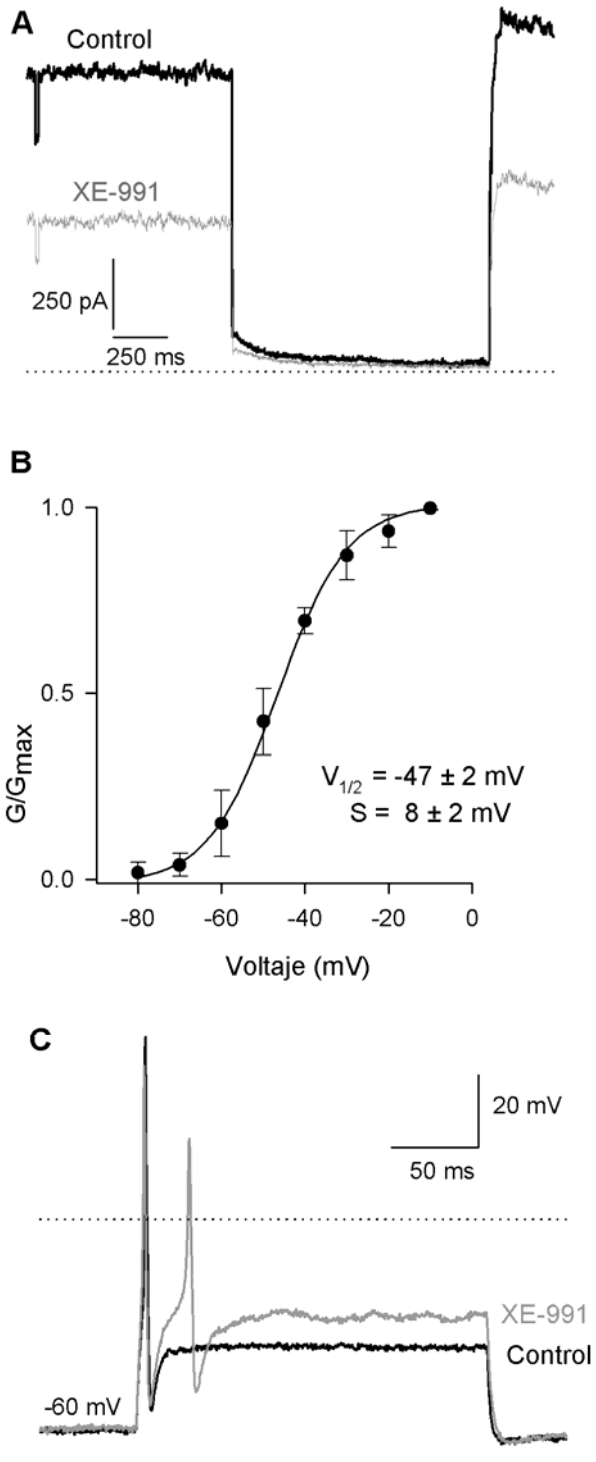

Figura 10. Efecto de XE-991 durante la desactivación de la corriente, conductancia, y frecuencia de disparo de las neuronas aferentes vestibulares. En A, se muestra la desactivación de la corriente obtenida en condiciones control (trazo negro) y después de la aplicación de XE-991 1 μM (trazo gris). XE-991 provocó la disminución de la amplitud de corriente un 47%. En B, la curva conductancia-voltaje de la corriente sensible a XE-991 1 μM. En C, la respuesta de un neurona aferente (Vm = -60 mV) a un pulso de corriente de 0.3 nA y 200 ms de duración en condiciones control (trazo negro) y durante la perfusión de XE-991 1 μM (trazo gris).

6.2 Efecto de E-4031 sobre la corriente $I_{K,M}$

Para determinar si las subunidades de los canales erg están presentes en las NAV, usamos un bloqueador selectivo de los canales erg el E-4031, en concentracion submicromolar de 100 nM (Sanguinetti y Jurkiewicz, 1990; Shi y cols., 1997; Meves y cols., 1999).

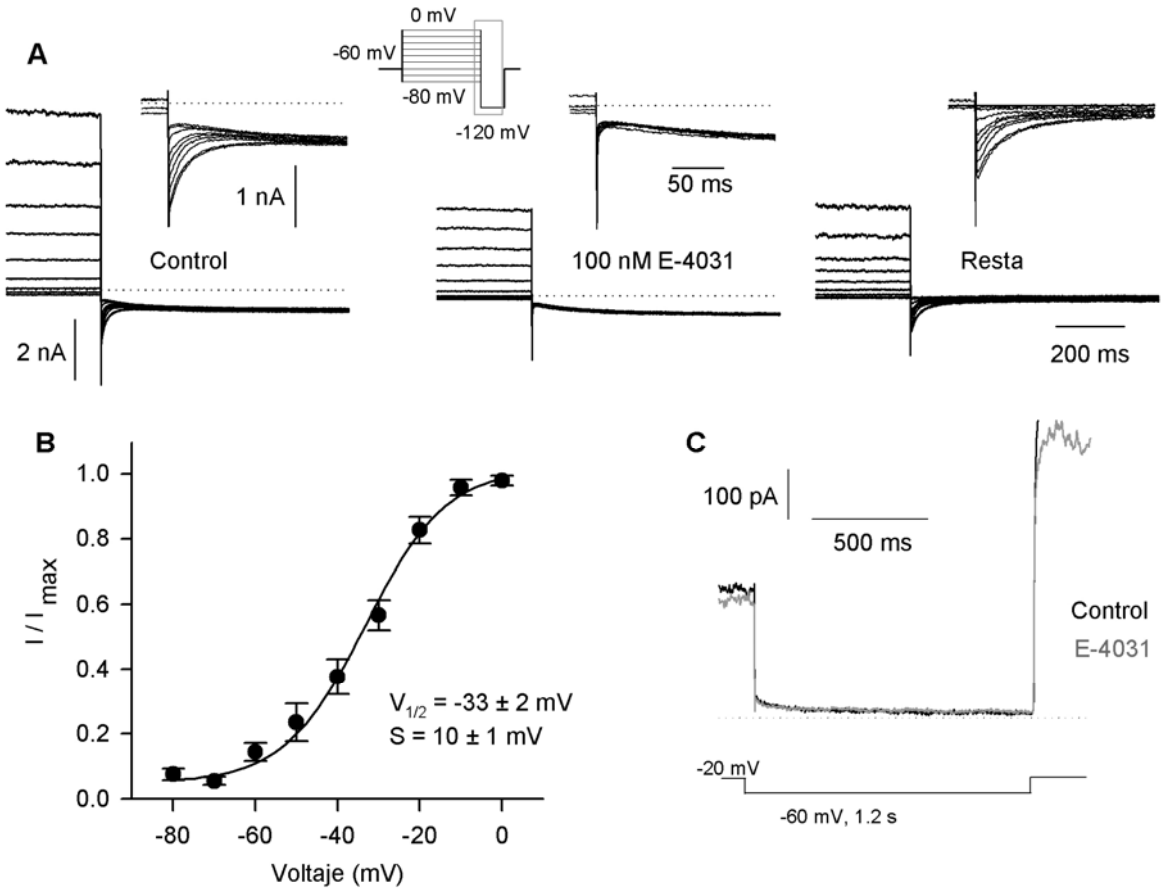

Figura 11. Efecto del bloqueador de los canales erg, E-4031. En A, la corriente de cola obtenida en condiciones control (izquierda), y después de E-4031 100 nM (centro), y la corriente sensible a E-4031 obtenida por sustracción (derecha). En el inserto se muestra el protocolo de estimulación utilizado para obtener la corriente de cola. En B, la curva de activación de la corriente sensible a E-4031. La corriente fue medida en la corriente de cola. La línea continua representa el ajuste de Bolztmann aplicado a los datos, se obtuvo una $V_{1/2}$ = -33 ± 2 mV y S = 10 ± 1 mV. En C, el E-4031 no modificó significativamente la amplitud de la corriente durante la desactivación.

La corriente $I_{K(erg)}$ en las NAV se estudió en soluciones normales. Debido a su rápida inactivación, la corriente $I_{K(erg)}$ se estudió mediante colas de corriente a -120 mV (duración 1s), generadas por pasos de voltaje despolarizantes desde -80 hasta 0 mV (duración 4s). Observamos un componente transitorio entrante mediado por canales erg y un componente lento mediado probablemente por la corriente I_h o I_{K1} (Chabbert y cols., 2001b; Soto y cols., 2008a). Cuando aplicamos el bloqueador E-4031 (100 nM) se redujo significativamente el componente transitorio sin afectar el sostenido. La corriente sensible a E-4031 se obtuvo por sustracción (Figura 11A). También observamos una disminución de la corriente saliente después de perfundir el E-4031, la cual puede ser generada por las subunidades erg1 y erg2 las cuales forman una corriente de lenta activación y que rectifica en ovocitos de *Xenopus* (Shi y cols., 1997). La curva de activación de la corriente $I_{K(erg)}$, se obtuvo graficando la amplitud al pico de la cola de corriente contra el potencial. La curva de activación se ajustó con una función de Boltzmann y se obtuvo una $V_{1/2}$ = -33 ± 2 mV y S = 10 ± 1 mV (n = 9) (Figura 11B). La corriente $I_{K(erg)}$ se expresó en todas las células registradas. La densidad de corriente no fue significativamente diferente entre las células con $I_{K,M}$ (densidad de $I_{K(erg)}$ = 24 ± 2 pA/pF; C_m = 46 ± 5 pF; n = 6) y aquellas en las que no se expresó de manera significativa la $I_{K,M}$ (densidad de $I_{(Kerg)}$ = 32 ± 12 pA/pF; C_m = 28 ± 1 pF; n = 3; P = 0.39). A pesar de que la aplicación de E-4031 bloqueó parte de la corriente saliente, no observamos cambio significativo en la amplitud de la corriente $I_{K,M}$ durante su desactivación (n = 4) (Figura 11C, Tabla III).

Tabla III. Efecto de linopirdina, XE-991, oxo-M y E-4031 durante la desactivación de la corriente $I_{K,M}$.

Bloqueador		*% disminución*	*Cm (pF)*	*n*	*P (efecto)*	*P (Cm)*
Linopirdina 10 μM	Células sensibles	54 ± 7	44 ± 4	6	0.04	
	Células no sensibles	19 ± 2	24 ± 4	4		0.02
XE-991 1 μM	Células sensibles	50 ± 3	45 ± 3	12	0.03	
	Células no sensibles	10 ± 3	24 ± 8	2		0.02
Oxo-M 10 μM	Células sensibles	58 ± 12	39 ± 3	4	0.03	
	Células no sensibles	5 ± 3	26 ± 3	3		0.03
E-4031 100 nM		-	41 ± 1	4		

6.3 Efecto de linopirdina, XE-991 y E-4031 sobre la respuesta de las neuronas aferentes vestibulares ante pulsos de corriente.

La mayoría de las NAV presentan un patrón de descarga fásico, es decir disparan uno o dos potenciales de acción en respuesta a la inyección de corriente (Limón y cols., 2005; Mercado y cols., 2006). Por el contrario en neuronas del ganglio vestibular de ratón se ha mostrado que disparan más de 2 potenciales de acción en repuesta a la inyección de corriente (Risner y Holt, 2006). En 5 células (*n* =14) con C_m = 49 ± 4 pF, la aplicación de linopirdina 10 μM convirtió la descarga de las células de un solo potencial a la descarga de 3 ± 1 potenciales de acción (rango 2-7) durante un pulso de 200 ms de duración. La perfusión de linopirdina despolarizó el potencial de membrana 2 mV sin afectar significativamente otras variables como el umbral, la posthiperpolarización o la

duración (Figura 9C). En otras 4 células, de esta serie experimental, con C_m = 34 ± 4 pF, linopirdina no provocó descarga repetitiva pero sí despolarizó el potencial de membrana de -60 ± 0.03 mV a -55 ± 2 mV (*P* = 0.042) y redujo la amplitud de la posthiperpolarización 7 ± 2 mV. Además hizo evidente una postdespolarización después del primer potencial de membrana (no mostrado), pero no fue suficiente para generar descarga repetitiva. En las 5 células restantes con C_m = 28 ± 2 pF no observamos efecto significativo de la linopirdina. La diferencia en capacitancia entre las células sensibles y no sensibles a linopirdina fue significativa con *P* = 0.02.

En 9 de 23 neuronas (C_m = 44 ± 4 pF), la perfusión de XE-991 1 μM convirtió la descarga de las células de un solo potencial a la descarga de 5 ± 1 potenciales de acción (rango 2-13) durante un pulso de corriente de 200 ms. El XE-991 redujo el potencial de membrana de -59 ± 0.4 mV a -52 ± 2 mV, la amplitud de la AHP 5 ± 1 mV, la amplitud del potencial de acción 10 ± 3 mV, y modificó el umbral de -28 ± 1 mV a -24 ± 1 mV sin afectar significativamente otros parámetros del potencial de acción tales como la pendiente de la AHP y la duración del potencial de acción. El efecto de XE-991 sobre la descarga de las neuronas aferentes fue reversible después del lavado. En otras 6 células (C_m = 41 ± 2 pF), aunque el XE-991 no modificó la descarga de la neurona, despolarizó la célula de -60 ± 1 mV a -57 ± 2 mV y disminuyó la amplitud del potencial de acción 7 ± 3 mV. En las 8 células restantes (C_m = 28±4 pF) no observamos efecto significativo (Figura 10C). La diferencia en la capacitancia entre las células sensible y no sensibles a XE-991 fue significativa con *P* = 0.006. Agrupando todos los experimentos de fijación de corriente encontramos

Tabla IV. Efecto de los bloqueadores linopirdina y XE-991, oxo-M y E-4031, en la respuesta de las neuronas aferentes vestibulares ante un pulso de corriente, las células fueron obtenidas de ratas P7-P10.

Bloqueador		Aumento número de PA	Cambio del PM (mV)	Disminución AHP (mV)	Disminución Amplitud del PA (mV)	Umbral (mV)	Cm (pF)
Linopirdina 10 μM	Células sensibles (n = 5)	3 ± 1	-60 ± 0.03 -55 ± 2	7 ± 2	-	-	49 ± 2
	Células no sensibles (n = 4)	-	-	-	-	-	28 ± 2
XE-991 1 μM	Células sensibles (n = 9)	5 ± 1	-59 ± 0.4 -52 ± 2	5 ± 1	10 ± 3	-28 ± 1 -24 ± 1	44 ± 4
		-	-60 ± 1 -57 ± 2	-	7 ± 3	-	41 ± 2
	Células no sensibles (n = 8)	-	-	-	-	-	28 ± 4
Oxo-M 10 μM	Células sensibles (n = 13)	5 ± 2	-	-	-	-34 ± 3 -28 ± 4	36 ± 4
		-	-60 ± 1 -57 ± 3	-57 ± 4 -53 ± 4	-	-	
		-	-60 ± 1 -61 ± 1	-58 ± 4 -56 ± 4	-	-	
	Células no sensibles (n = 3)	-	-	-	-	-	28 ± 5
E-4031 100 nM	Células sensibles (n= 7)	-	-	2 ± 1	8 ± 2	-	-

que las células que responden a linopirdina y XE-991 tienen una C_m = 43 ± 2 pF (*n* = 21), y las células no sensibles a estas drogas tuvieron una C_m = 27 ± 2 pF (*n* = 12; *P* < 0.001).

En condiciones de fijación de corriente la perfusión de E-4031 100 nM (*n* = 7) no modificó el patrón de descarga, el potencial de membrana, el umbral o la duración, aunque el E-4031 disminuyó la AHP 2 ± 1 mV y la pendiente de la AHP

0.4 ± 0.1 ms. Observamos de manera muy consistente que el E-4031 100 nM disminuye significativamente la amplitud de el potencial de acción de 50 ± 4 mV a 42 ± 5 mV (*n* = 7; *P* = 0.002; datos no mostrados). Este último efecto puede no estar relacionado con el bloqueo de los canales erg y puede ser provocado por una acción inespecífica del E-4031, la cual no abordamos en este trabajo. El efecto de los distintos fármacos utilizados se resume en la Tabla IV.

6.4 Estudio de la corriente $I_{K,M}$ en neuronas aferentes de rata P25-P30.

La inervación eferente en el vestíbulo de la rata se desarrolla durante las primeras 2 semanas después del nacimiento (Demêmes y cols., 2001). Por esta razón realizamos una serie experimental en ratas P25-P30, para corroborar que la $I_{K,M}$ se expresa también en neuronas de rata cuyo sistema vestibular es funcionalmente maduro. Estos experimentos fueron limitados debido a que la mayoría de las neuronas están cubiertas con una capa de mielina. Sin embargo, en cultivo algunas neuronas perdieron la capa de mielina y fueron registradas. Estas neuronas tuvieron una C_m = 30 ± 2 pF, una R_m = 276 ± 27 MΩ, y un potencial de membrana de -59 ± 2 mV (*n* = 24).

La perfusión de XE-991 1 μM (*n* = 9) disminuyó la amplitud de la corriente $I_{K,M}$ 36 ± 9 % en 8 de las células registradas (con C_m = 34 ± 4 pF, comparada con C_m =15 pF de la célula que no tuvo efecto) (Figura 12A). Paralelamente, encontramos que las neuronas maduras mostraron una corriente entrante activada por hiperpolarización de mayor densidad que la observada en neuronas de ratas neonatas (datos no mostrados). La densidad promedio de corriente entrante en

neuronas de rata P7 a P10 fue de 7 ± 1 pA/pF (*n* = 24) mientras que en ratas adultas P25 a P30 fue de 19 ± 2 pA/pF (*n* = 24) (Figura 12C y D). La diferencia en la densidad de la corriente entrante fue significativa con una *P* = 0.0007. Para el propósito de este trabajo no estudiamos con mayor detalle esta corriente.

En experimentos de fijación de corriente, el uso de XE-991 1 µM disminuyó el potencial de membrana desde -57 ± 0.2 a -54 ± 1 mV, el umbral desde -26 ± 2 a -22 ± 2 mV, la amplitud del potencial de acción desde 47 ± 6 a 29 ± 6 mV, y la AHP 3 ± 1 mV (*n* = 6; *P* < 0.05) (Figura 12B, Tabla V).

Tabla V. Efecto del bloqueador XE-991 y del agonista muscarínico oxo-M en la actividad eléctrica de las neuronas aferentes vestibulares, aisladas de ratas P25-P30.

Bloqueador	***Aumento número de PA***	***Cambio PMR***	***Umbral***	***Disminución AHP***	***Disminución amplitud PA***	***Cm (pF)***
XE-991 1 µM	-	-57 ± 0.2 -54 ± 1	-26 ± 2 -22 ± 2	3 ± 1	18	33 ± 4 (n = 6)
Oxo-M 10 µM	-	-60 ± 1 -63 ± 1	-	2 ± 2	7	30 ±3 (n = 9)

La aplicación de oxo-M 10 µM hiperpolarizó el potencial de membrana desde -60 ± 1 a -63 ± 1 mV, disminuyó la amplitud del potencial de acción desde 57 ± 3 a 50 ± 3 mV, la duración del potencial de acción se mantuvo estable (1 ± 0.1 ms) y la AHP 2 ± 2 mV (Tabla V). Además encontramos que la oxo-M disminuyó significativamente la resistencia de membrana desde 145 ± 22 a 80 ± 17 MΩ (*n* = 9; *P* = 0.001), incrementó la corriente entrante instantánea desde -0.69 ± 0.2 hasta -1.6 ± 0.3 nA, y disminuyó el componente entrante que activa

lentamente desde -0.43 ± 0.1 hasta -0.26 ± 0.05 nA (*n* = 8; *P* = 0.001, datos no mostrados).

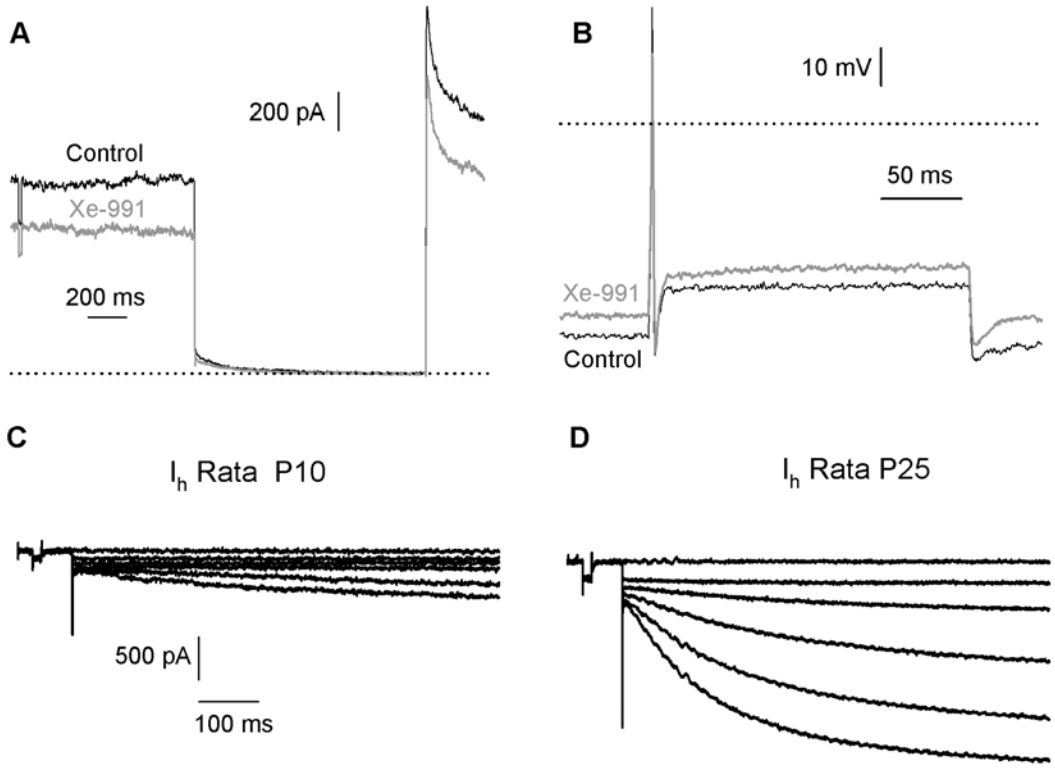

Figura 12. Efecto de XE-991 sobre la corriente $I_{K,M}$ y frecuencia de descarga en neuronas de rata P25. En A, se muestra la disminución de la corriente $I_{K,M}$,durante la aplicación de XE-991 1μM. En B, se observa el efecto de XE-991 en la frecuencia de disparo de una célula. C y D muestran la corriente rectificante de entrada regitrada en ratas de dos edades distintas.

6.5 Inhibición muscarínica de la corriente M

Evaluamos la sensibilidad de la $I_{K,M}$ a oxo-M, un agonista muscarínico de amplio espectro (Shapiro y cols., 2000; Gamper y cols., 2003). La aplicación de oxo-M (10

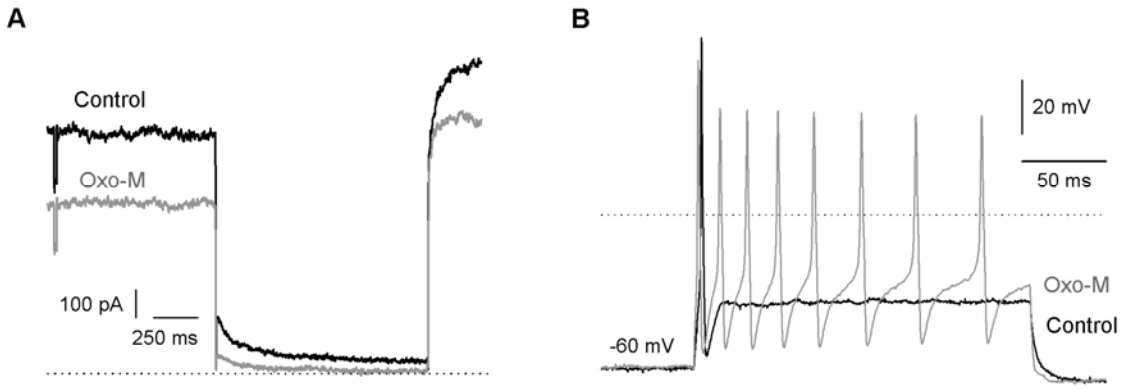

Figura 13. Efecto de Oxotremorina-M (oxo-M). En A, la desactivación de la corriente en condiciones control (trazo negro) y después de la aplicación de oxo-M 10 µM (trazo gris). Oxo-M disminuyó la amplitud de la corriente un 57%. En B, la respuesta de una neurona aferente (V_m = -60 mV) ante un pulso de corrinte de 0.6 nA y 200-ms de duración, en condiciones control (trazo negro) y después de la perfusión de oxo-M 10 µM (trazo gris).

µM) inhibió de manera parcialmente reversible la corriente saliente en un 15 ± 2% en 7 de 10 células (*n* = 7; C_m = 42 ± 3 pF), no se observó efecto significativo en las 3 células restantes (C_m = 22 ± 2 pF; *P* = 0.001). La corriente sensible a oxo-M se obtuvo sustrayendo la corriente después de aplicar oxo-M de la corriente control (datos no mostrados). El efecto de oxo-M fue bloqueado por la aplicación previa de atropina 1 µM (*n* = 5). La aplicación de atropina por sí misma no modificó la amplitud de la corriente saliente (datos no mostrados). La acción de oxo-M también se estudió durante la desactivación de la $I_{K,M}$. En 4 de 5 células (C_m = 39 ± 3 pF), oxo-M 10 µM redujo la amplitud de la corriente un 58 ± 12 %, el efecto fue parcialmente reversible (Figura 13A, Tabla III). La curva conductancia-voltaje de la corriente sensible a oxo-M se ajustó con una función de Boltzmann, se obtuvo una $V_{1/2}$ = -45 ± 3 mV y *S* = 7 ± 2 mV. La acción de oxo-M sobre la deactivación fue completamente bloqueada con la aplicación previa de atropina 1 µM (*n* = 4, no se

muestran los datos). Adicionalmente estudiamos el efecto de oxo-M utilizando la

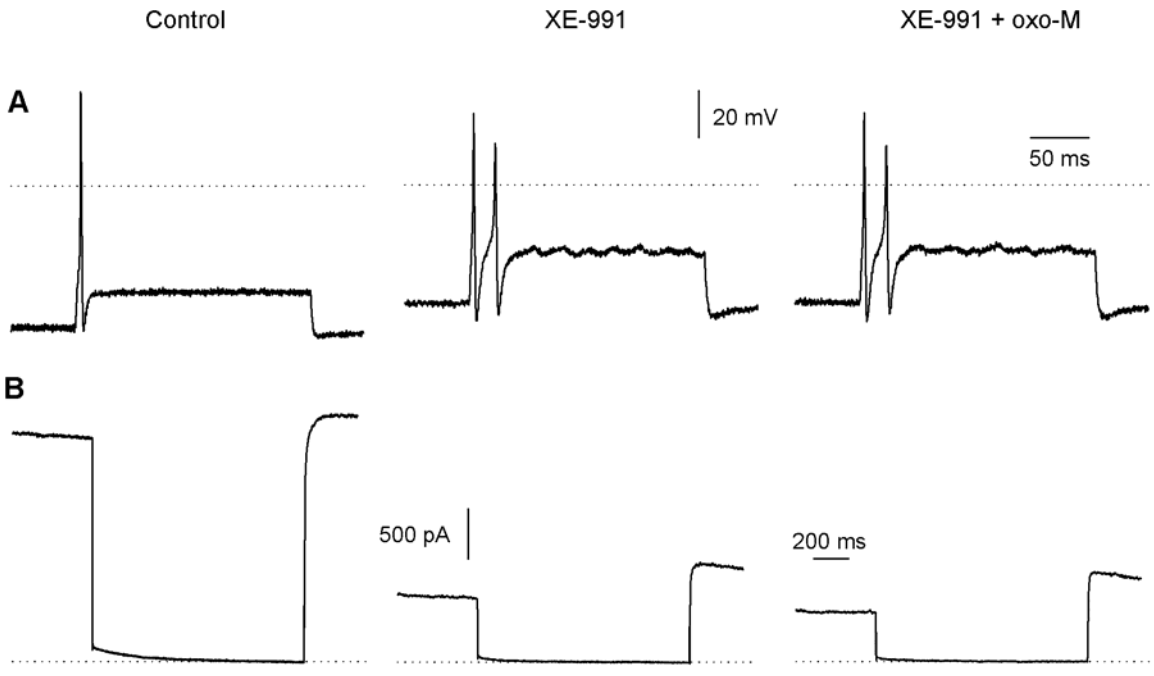

Figura 14. El XE-991 previene el efecto de oxo-M. En A, la respuesta de una neurona aferente a un pulso de corriente de 0.9 nA y 200 ms de duración, a la izquierda se muestra el trazo control, en el centro, la aplicación de XE-991 1 μM provocó el disparo de un potencial de acción y finalmente luego de la coaplicación de oxo-M 10 μM y XE-991 1μM (trazo a la derecha). En B, la desactivación de la corriente en condiciones control (izquierda), después la perfusión de XE-991 1 μM (centro), y después de la coaplicaión de oxo-M y XE-991 (derecha).

técnica de parche perforado (*n* = 3). El curso temporal, el porcentaje de inhibición y la recuperación de la corriente no fueron significativamente diferentes de los valores obtenidos en configuración de célula completa. En condiciones de fijación de corriente, la aplicación de oxo-M 10 μM incrementó la excitabilidad en 3 de 16 neuronas (C_m = 52 ± 6 pF), provocó la descarga de un solo potencial a la descarga de 5 ± 2 potenciales de acción (rango 2-8) durante un pulso de corriente de 200

ms de duración (Figura 13B) y modificó el umbral 6 mV (desde -34 a -28 mV). En otras 4 células, oxo-M despolarizó el potencial de membrana desde -60 ± 1 hasta -57 ± 3 mV y disminuyó la AHP medida al pico de -57 ± 4 a -53 ± 4 mV (*P* = 0.04). En 6 células la aplicación de oxo-M hiperpolarizó el potencial de membrana de -60 ± 1 a -61 ± 1 mV, disminuyó la amplitud de la AHP de -58 ± 4 a -56 ± 4 mV y la pendiente de la AHP desde 9 ± 2 hasta 8 ± 2 ms (*P* = 0.048). Las células sensibles a oxo-M tuvieron una C_m = 36 ± 4 pF (*n* =13). Oxo-M no provocó efecto significativo en 3 de 16 células (C_m = 28 ± 5 pF; *P* = 0.41 para la diferencia de capacitancia). La sola aplicación de oxo-M 10 µM provocó la descarga de un

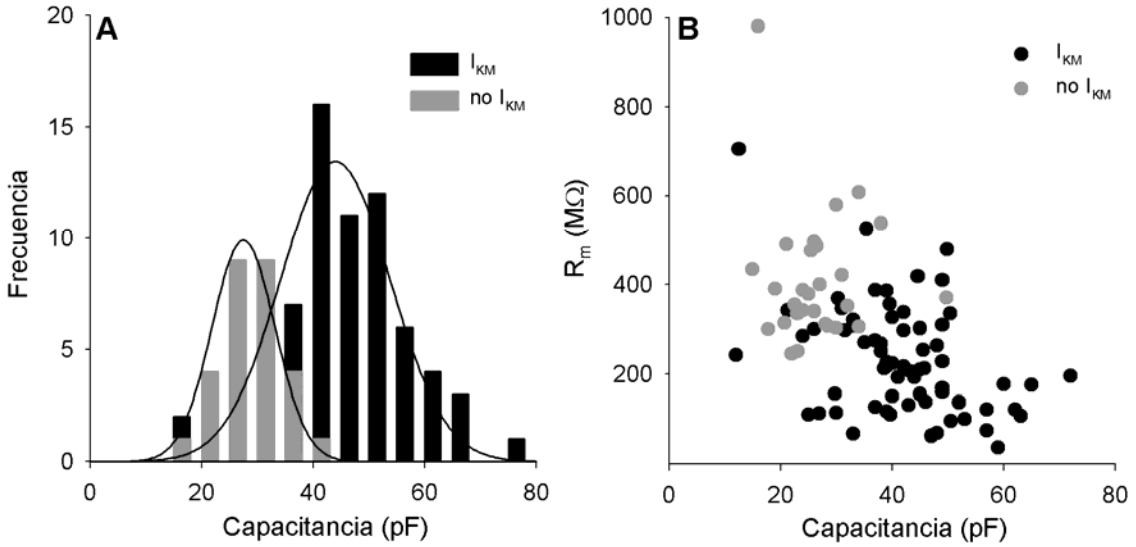

Figura 15. La expresión de $I_{K,M}$ en las neuronas aferentes vestibulares. En A, se muestra el histograma de la capacitancia de membrana de las células de acuerdo a la expresión de $I_{K,M}$. El promedio de capacitancia de las células que no tuvieron $I_{K,M}$ fue menor (26 ± 1 pF) que el de las células con $I_{K,M}$ (42 ± 1 pF; *P* < 0.001). La línea continua representa el ajuste a una función de Gauss; *r* = 0.9 y *r* = 0.99. En B, las células que expresaron $I_{K,M}$ tuvieron una menor resistencia de membrana, comparado con las células que no tuvieron $I_{K,M}$ (*P* = 0.0001, *r* = 0.13).

potencial de acción en 2 de 9 células. En 5 células despolarizó el potencial de membrana 5 ± 2 mV y no observamos efecto significativo en 2 células. La coaplicación de atropina 1 µM (*n* = 7) bloqueo de manera reversible el efecto de oxo-M (datos no mostrados). Para definir si el XE-991 y oxo-M actúan sobre los mismos canales, medimos la amplitud de la corriente $I_{K,M}$ durante la aplicación secuencial de XE-991 y oxo-M. La perfusión inicial de XE-991 1 µM disminuyó la amplitud de la corriente un 51 ± 4% (*n* = 5; *P* = 0.03). La coaplicación de oxo-M 10 µM y XE-991 1 µM produjo una disminución adicional no significativa (*n* = 5; *P* = 0.1) (Figura 14B). La aplicación de XE-991 1 µM también disminuyó la corriente sostenida (a -20 mV) un 47 ± 9% (*n* = 5; *P* = 0.04). La co-perfusión de oxo-M y XE-991 disminuyó la corriente sostenida un 7 ± 2% de manera adicional, sin embargo este efecto aditivo no fue significativo (*n* = 5; *P* = 0.08, comparado con el efecto de XE-991).En experimentos de fijación de corriente, el XE-991 1 µM incrementó la excitabilidad en 3 de 4 células convirtiendo el disparo de un solo potencial en descarga repetitiva con un promedio de 6 ± 4 potenciales de acción (rango 2-13) durante un pulso de corriente de 200 ms, además el potencial de membrana se despolarizó de -60 ± 0.5 a -52 ± 2 mV. La coaplicación de oxo-M y XE-991 después de 2 minutos de XE-991, no observamos cambios significativos en el potencial de membrana o el patrón de descarga (*n* = 4; *P* = 0.3) (Figura 14A).

6.6 Umbral, capacitancia de membrana y expresión de $I_{K,M}$

El análisis de la relación entre la C_m y la sensibilidad a linopirdina, XE-991 u oxo-M mostró que las células que expresaron la $I_{K,M}$ tuvieron una C_m de 42 ± 1 pF (*n* = 69), este valor es significativamente diferente al de las células que no expresaron

corriente $I_{K,M}$ cuya capacitancia fue de 26 ± 1 pF (*n* = 28; *P* < 0.001; Figura 15A).

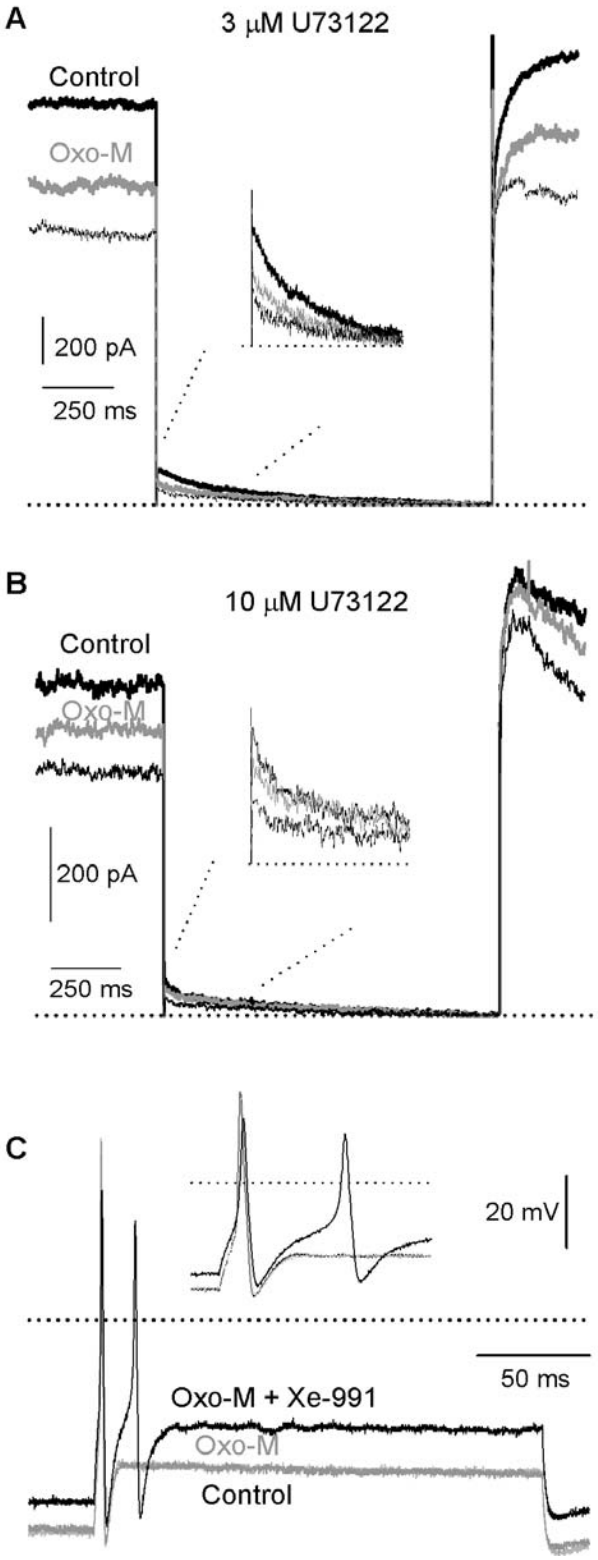

Figura 16. Efecto de los inhibidores de la PLC sobre la corriente $I_{K,M}$. En A y B, observamos la disminución de la corriente $I_{K,M}$ durante su desactivación, con 3 μM y 10 μM de U-73122 respectivamente, con 10 μM el efecto inhibidor de oxo-M es significativamente atenuado (*P* = 0.006). En C, la respuesta de una neurona aferente a un pulso de corriente de 0.6 nA y 200 ms de duración, se muestra el trazo control y el efecto de oxo-M en color gris, y luego de la coaplicación de oxo-M 10 μM y XE-991 1μM aumentó la descarga de la célula (trazo negro).

También estudiamos la relación entre el umbral, la C_m y la expresión de la $I_{K,M}$. Para realizar estos experimentos fijamos el potencial de membrana en -60 mV y aplicamos pulsos variables de corriente. Las células que expresaron $I_{K,M}$ tuvieron menor resistencia de membrana que las células que no expresaron $I_{K,M}$ (R_m = 230 ± 15 MΩ, *n* = 69; versus R_m = 411 ± 28 MΩ, *n* = 28; *P* < 0.001; Figura 15 B). Debido a la diferencia en la Rm y la influencia de la misma en las propiedades de cable de las neuronas, determinamos de dos maneras el umbral en el primer potencial de acción; primero, como el valor mínimo de corriente necesaria para generar un potencial de acción y como el valor de voltaje umbral del potencial de acción (ver material y métodos). Cuando el umbral fue medido como la corriente necesaria para provocar un potencial de acción, las células que expresaron $I_{K,M}$ fueron menos excitables ya que tuvieron mayor umbral (835 ± 70 pA; *n* = 55) comparado con las células que no expresaron $I_{K,M}$ (470 ± 95 pA; *n* = 22; *P* = 0.005). Cuando el umbral fue medido en función del voltaje, las células que expresaron la $I_{K,M}$ (*n* = 54) mostraron un umbral de 4 mV por debajo de las que no tuvieron $I_{K,M}$ (*n* = 17; *P* = 0.04).

6.7 Inhibición de la corriente $I_{K,M}$ por la activación de la PLC y depleción de la concentración de PIP_2.

Para evaluar si la activación de la PLC (fosfolipasa C) participa en la inhibición de la corriente $I_{K,M}$ por activación de los mAChr, colocamos en la pipeta de registro, un inhibidor de la PLC, el U73122 3 μM y 10 μM. Después de 10 minutos de haber obtenido la configuración de célula completa, obtuvimos

inmediatamente los trazos control y cuando la corriente se mantuvo estable, observamos que la aplicación de oxo-M 10 μM disminuyó la amplitud de la corriente $I_{K,M}$ un 40 ± 6 % (*n* = 4) y en un 23 ± 3 % (*n* = 7) respectivamente (Figuras 16A y B). El efecto inhibidor de oxo-M en estos experimentos, se comparó con el efecto de oxo-M previamente obtenido (en ausencia del inhibidor de la PLC) que fue de 58 ± 12%. Se consideró como control de estos experimentos, aquellos descritos en la figura 13A, donde la pipeta de registro no contenía inhibidor de la PLC. No obtuvimos diferencia significativa entre ambas condiciones (*P* = 0.24) cuando se usó el U73122 3 μM, pero si fue significativa (*P* = 0.006) cuando se usó el U73122 10 μM.

Como control adicional luego de aplicar la oxo-M 10 μM se coaplico XE-991 1 μM, la corriente disminuyó adicionalmente un 12 ± 5% (*n* = 4) para el primer caso y 35 ± 3% (*n* = 4) para el segundo corroborando la presencia de la $I_{K.M}$ en estas células.

En condiciones de fijación de corriente, en presencia de U73122 10 μM, la aplicación de oxo-M 10 μM despolarizó el potencial de membrana 1 ± 1 mV y después de la coaplicación de oxo-M y 1 μM XE-991 el potencial de membrana se despolarizó 7 ± 2 mV y en una de dos células registradas provocó el disparo de un potencial de acción más (*n* = 4) (Figura 16C).

Como control del efecto observado con U73122, incluimos en la pipeta de registro su análogo inactivo, el U73343 3 μM. Encontramos que luego de la aplicación de oxo-M 10 μM la corriente $I_{K,M}$ disminuyó 50 ± 11% (*n* = 3) (Figura 17A). Con 10 μM U73343, la perfusion de 10 μM oxo-M redujo la $I_{K,M}$ 51 ± 3 % (*n* = 10) (Figura 17A). En estos experimentos el efecto inhibidor de oxo-M fue significativamente mayor que el obtenido en presencia de U73122 10 μM (*P* = 0.01). No observamos diferencia significativa con el efecto de oxo-M en condición

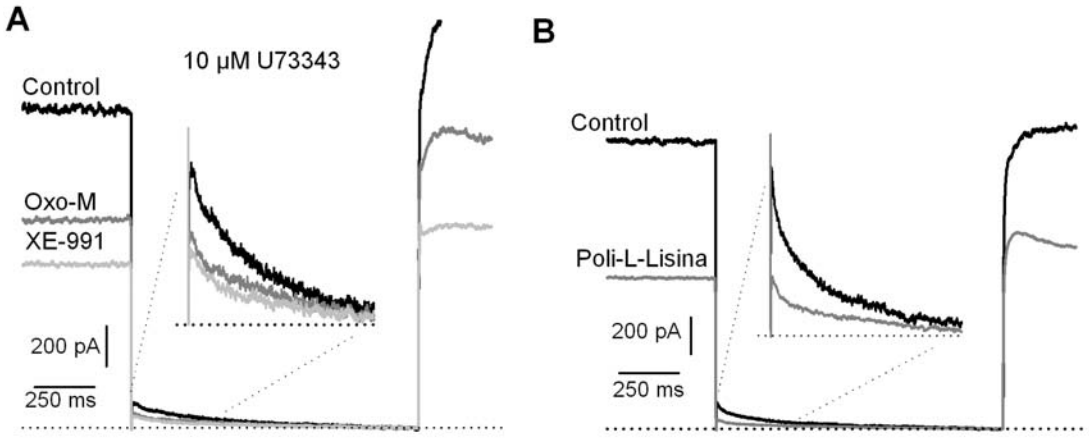

Figura 17. Efecto del análogo inactivo de la PLC, U73343 y del secuestrador de PIP_2, Poli-L-lisina. En A, registro de corriente en condiciones control (trazo negro), se reduce significativamente después de la perfusión de 10 μM oxo-M (trazo gris claro) en presencia de 10 μM U73343. Adicionalmente se perfundio XE-991 10 μM (trazo gris oscuro) el cual produce un ligera reducción adicional de la corriente. En B, el uso de Poli-L-lisina en la solución intracellular provocó una disminución de la corriente $I_{K,M}$ después de 3 minutos de haber establecido la condición de registro de célula completa (trazo gris), en negro se muestra el trazo control. La linea punteada muestra el cero de corriente

control (58 ± 12%; *P* = 0.65). La coaplicación de 10 μM oxo-M y 1 μM XE-991 disminuyó de manera adicional la amplitud de la corriente $I_{K,M}$ 9 ± 3 % (*n* = 7) (Figura 17A).

Finalmente realizamos otra serie experimental para estudiar el efecto de la depleción intracelular del PIP_2 sobre la amplitud de la corriente $I_{K,M.}$ Para llevar a cabo estos experimentos aplicamos Poli-L-lisina 100 μg/mL en la pipeta de registro (un secuestrador de PIP_2), observamos que después de aproximadamente 1 minuto la corriente $I_{K,M}$ empezó a disminuir, finalmente obtuvimos una disminución del 64 ± 4% (*n* = 4) (Figura 17B).

7. DISCUSION

Nuestros resultados indican que las NAV de alrededor de 42 pF de capacitancia de membrana expresan de manera funcional la $I_{K,M}$. Encontramos que bajas concentraciones de linopirdina y XE-991, bloqueadores selectivos de canales de potasio KCNQ (Costa y Brown, 1997; Romero y cols., 2004) inhiben un componente de la corriente saliente, el cual está presente en las NAV y que el bloqueador de canales erg, E-4031 inhibe un componente entrante transitorio. Además el agonista muscarínico oxo-M, inhibe el mismo componente de la corriente saliente cuya sensibilidad al voltaje y sus características durante la desactivación coinciden con las reportadas para la $I_{K,M}$ (Brown y Adams, 1980; Constanti y Brown, 1981; Wang y cols., 1998). La inhibición de $I_{K,M}$ por linopirdina, XE-991, u oxo-M despolarizó el valor del potencial de membrana, redujo la amplitud de la AHP y modificó el patrón de descarga, aumentando el número de potenciales de acción, indicando la importancia funcional de la $I_{K,M}$ en el control de la excitabilidad de las NAV.

En las NAV, el efecto inhibidor de la linopirdina sobre la corriente $I_{K,M}$ (CI_{50} de 3.5 μM) coincide con el valor reportado para heteromultímeros KCNQ2+3 (CI_{50} = 4 μM), y es similar a la CI_{50} reportada en neuronas del ganglio cervical superior (Lamas y cols., 1997; Selyanko y cols., 1999). Aunque la linopirdina tiene mayor selectividad para $I_{K,M}$ (10 a 20 veces) en comparación con otras corrientes activadas por voltaje, puede bloquear canales activados por ligando tales como GABA y receptores nicotínicos (Gómez-Casati y cols., 2004). A pesar de esto, en células aisladas la linopirdina ha demostrado ser una útil herramienta en el estudio de la $I_{K,M}$ (Costa y Brown, 1997).

En nuestros experimentos, XE-991 mostró mayor potencia para inhibir la corriente M que la linopirdina (CI_{50} = 30 nM). Este CI_{50} es un orden de magnitud menor que la CI_{50} de XE-991 que se ha reportado es necesaria para incrementar la liberación de [3H] ACh en rebanadas de hipocampo de rata (Zaczek, 1998) e inhibir la $I_{K,M}$ en neuronas del ganglio dorsal de la rata (Passmore y cols., 2003) y menor que la CI_{50} (0.6 μM) para las subunidades KCNQ2+KCNQ3 expresadas en ovocitos de Xenopus (Wang y cols., 1998).

Nuestros resultados son consistentes con la idea de que los heteromultímeros KCNQ2+3 son las subunidades involucradas en la expresión de la corriente $I_{K,M}$ en las NAV. Además, la inactivación lenta de la $I_{K,M}$ que encontramos en nuestras células es semejante a la descrita para los canales con la subunidad KCNQ3 (Wang y cols., 1998; Passmore y cols., 2003). Sin embargo, la desactivación de $I_{K,M}$ en las NAV se ajustó con dos funciones exponenciales, lo cual sugiere que pudiera participar otro tipo de canal en la generación de dicha corriente. Se ha demostrado que la familia de canales de potasio ERG contribuye

a la expresión de la corriente $I_{K,M}$ en células neuronales de mamífero (Selyanko y cols., 1999). En este trabajo estudiamos la presencia de los canales tipo ERG utilizando el bloqueador E-4031. Encontramos que todas las células que estudiamos expresan la corriente $I_{K(ERG)}$. Sin embargo la aplicación de E-4031 no modificó la amplitud de la corriente M durante su desactivación, esto significa que en las NAV los canales ERG no participan de forma significativa en la generación de la corriente M.

Evidencias recientes han implicado a los canales KCNQ en la función del oído interno: en los órganos vestibulares del ratón, las células ciliadas tipo I y sus terminales en forma de cáliz son específicamente inmunoreactivas a la subunidad KCNQ4 (Kharkovets y cols., 2000; Lysakowski y Price, 2003); sin embargo, mutaciones en la subunidad KCNQ4 que eliminan la funcionalidad del canal no producen trastornos vestibulares (Trussell, 2000; Kharkovets y cols., 2000), aunque existen reportes que indican un incremento en la suceptibilidad a sufrir vértigo y enlentecimiento del reflejo vestíbulo-ocular en personas que padecen sordera tipo DFNA2, por mutación en la subunidad KCNQ4 (De Leenheer y cols., 2002).

7.1 Sistema vestibular eferente

El estudio de la expresión de los receptores a acetilcolina muscarínicos (mAChR) subtipos (m1– m5) en los órganos vestibulares y en el ganglio vestibular de humano y de rata utilizando la técnica de RT-PCR, ha mostrado que en humanos se expresan los subtipos m1, m2, y m5, mientras que en la rata se expresan los cinco subtipos de receptores (Wackym y cols., 1996; Safieddine y

cols., 1996). Estos resultados indican que las sinapsis eferentes colinérgicas axo-dendrítica y axo-somática tienen un componente muscarínico (Lysakowski y Goldberg, 1997; Ross, 1997).

Utilizamos un modelo experimental basado en neuronas de rata P7-P10 en cultivo primario durante 24h. En este periodo del desarrollo, la población de células ciliadas tipo I y tipo II en el ratón aún no están completamente diferenciadas (Dechesne y cols., 1986). En la edad P5, las terminales en botón y cáliz ya están diferenciadas, en P8 las conductancias iónicas que muestran las células ciliadas maduras ya están presentes (Rüsch y cols., 1998), y en P10 el patrón de inervación y la sensibilidad de las fibras aferentes a corrientes galvánicas aplicadas externamente son similares a las que presentan animales adultos (Desmadryl y Sans, 1990; Desmadryl, 1991). Sin embargo la inervación eferente en la rata se establece durante las primeras dos semanas después del nacimiento (Demêmes y cols., 2001). En nuestros experimentos con células obtenidas de rata P25 – P30 el porcentaje de células sensibles a XE-991 fue mayor que en células P7-P10, lo cual indica que existe algún cambio en el grupo de canales expresados durante la maduración celular. Por ejemplo, observamos un claro incremento en la magnitud de la corriente rectificadora de entrada presente en neuronas P25 – P30.

Desde un punto de vista funcional, el hallazgo más consistente es que la estimulación eferente produce un incremento de la descarga aferente en mamíferos (Goldberg y Fernández, 1980), a pesar de que se han observado respuestas heterogéneas en reptiles y anfibios (Rossi y Martini 1991; Guth y Norris, 1996; Sugai y cols., 1991; Brichta y Goldberg, 2000). Nuestros resultados

indican que la inhibición de la corriente $I_{K,M}$ mediante la aplicación de linopirdina o XE-991 y por el agonista muscarínico oxo-M produce un incremento en la excitabilidad celular. Esto constituye un posible mecanismo postsináptico por el cual el sistema eferente produce una respuesta excitadora en las neuronas aferentes (Marlinski y cols., 2004). Para las terminales en forma de cáliz, la influencia directa de las fibras eferentes es importante, pues determina las propiedades de su respuesta. Aunque se ha descrito que algunas neuronas eferentes contactan fibras aferentes en botón (Lysakowski y Goldberg, 1997), no existen datos cuantitativos de este tipo de inervación que probablemente corresponden a las fibras aferentes dimórficas. Basados en el hecho de que las neuronas que expresan $I_{K,M}$ son las de mayor tamaño, suponemos que las neuronas resistentes a linopirdina, XE-991 u oxo-M probablemente son las que inervan en forma de botón y que no reciben inervación colinérgica por parte de las fibras eferentes. Sin embargo, en neuronas del ganglio simpático de ratón, la aplicación de XE-991 no disminuye la adaptación de la frecuencia de disparo, a pesar de que estas neuronas expresan corriente M. Además las subunidades KCNQ poseen diferente sensibilidad a sus bloqueadores (Schoeder y cols., 2000) y es posible que la composición de los canales KCNQ difiera entre las neuronas aferentes vestibulares.

7.2 Participación de la PLC en la inhibición de la corriente $I_{K,M}$

En neuronas del ganglio simpático la vía de señalización responsable del decremento de la corriente $I_{K,M}$ es resultado de la activación de la proteína Gq/11 acoplada al receptor M1 (Brown y Adams, 1980; Selyanko y cols., 2001;

Hernandez y cols., 2008). La subunidad α activa a la PLCβ, la cual hidroliza PIP_2 y es la depleción de este último la que provoca el cierre del canal KCNQ (Suh y cols., 2006; Jensen y cols., 2009). Además se requiere de ATP intracelular para que la corriente generada por KCNQ2-KCNQ3 se recupere después de la supresión muscarínica (Suh y Hille, 2002). En nuestros experimentos el efecto de oxo-M fue similar tanto en condiciones de parche perforado como en célula completa, esto sugiere que el efecto es mediado por un mensajero no difusible asociado a la membrana celular (Zhang y cols., 2003). Además la recuperación de la corriente $I_{K,M}$, después de la aplicación de oxo-M en ambas condiciones fue semejante (> 20 min), esto implica que en nuestras condiciones experimentales existe una depleción del fosfolípido de membrana PIP_2 o algún otro fosfolípido relacionado, ya que estos han sido asociados con la recuperación de las corrientes generadas por canales KCNQ después de la aplicación de oxo-M (Zhang y cols., 2003).

Debido a lo antes mencionado realizamos experimentos para estudiar la participación de la PLC en la inhibición de la $I_{K,M}$, nuestros resultados mostraron que en las neuronas aferentes vestibulares, la inhibición de la PLC atenúa el efecto de oxo-M sobre la corriente $I_{K,M,}$ sin embargo obtuvimos diferencia significativa sólo con 10 μM del inhibidor U73122, a diferencia de lo reportado en neuronas simpáticas de la rana toro y en células tsA en las que con 3 μM del inhibidor obtienen atenuación significativa del efecto de oxo-M (Suh y Hille, 2002; Ford y cols., 2003). Esta diferencia podría deberse a que el U-73122 ha sido reportado como un agonista débil de la PLC (Horowitz y cols., 2005).

Consideramos que el efecto observado con U73122 fue específico ya que con el análogo inactivo no obtuvimos reducción significativa en el efecto de oxo-M. También mostramos que la depleción intracelular de PIP_2 reduce la amplitud de la corriente $I_{K,M,}$ mediante la aplicación de Poli-L-lisina, tal y como se ha reportado en células tsA y en sistemas de expresión heterólogos (Suh y Hille, 2008; Zhang y cols., 2003).

Nuestros resultados demuestran que la activación de receptores muscarínicos inhibe la corriente $I_{K,M}$ en una gran proporción de las neuronas aferentes incrementando su ganancia. Esto contribuirá significativamente al estudio de la acción farmacológica de drogas anticolinérgicas utilizadas en transtornos relacionados con el sistema vestibular. Estos resultados abren la posibilidad del uso terapéutico de moduladores de la corriente M como el retigabine y linopirdina (Romero y cols., 2004; Rivera-Arconada y López-García, 2005; Surti y Jan, 2005) en el tratamiento de padecimientos del sistema vestibular.

8. CONCLUSIÓN

Las neuronas aferentes vestibulares aisladas de la rata, presentaron una corriente de potasio tipo M sensible a linopirdina y XE-991, mostrando de esta manera que son los canales de la familia KCNQ los que generan esta corriente. La amplitud de la corriente $I_{K,M}$ disminuyó con la activación de receptores muscarínicos utilizando el agonista oxo-M. En experimentos de fijación de corriente, la inhibición de la corriente $I_{K,M}$ aplicando linopirdina, XE-991 y oxo-M incrementó la frecuencia de descarga en un grupo específico del total de neuronas registradas. Este grupo correspondió a las neuronas de mayor tamaño. El estudio del mecanismo intracelular que participa en la inhibición de la corriente mostró que es mediado por la actividad de la PLC y la depleción de PIP_2.

Consideramos, que la inhibición de la corriente $I_{K,M}$ por activación de los receptores muscarínicos, la subsecuente estimulación de la PLC y depleción del PIP_2 constituyen una de las vías que subyacen a la respuesta excitadora de las neuronas aferentes vestibulares ante la influencia del sistema eferente colinérgico.

9. BIBLIOGRAFIA

Adams PR, Brown DA, Constanti A (1982) M-currents and other potassium currents in bullfrog sympathetic neurones. J Physiol 330: 537-572.

Almanza A, Vega R, Naverrete F, Soto E (2007) Nitric oxide modulation of L type Ca current in sensory hair cells. Journal of Neurophysiology 97: 1188-1195.

Angelaki DE, Cullen KE (2008) Vestibular System: The Many Facets of a Multimodal Sense. Annu Rev Neurosci 31: 125-150.

Anniko M (1988) Functional morphology of the vestibular system. In: Physiology of the ear, (Eds.), Jhan, A.F. y Sacchi, S. Raven Press, New York, 457 472.

Annoni JM, Cochran SL, Precht W (1984) Pharmacology of the vestibular hair cell-afferent fibre synapse in the frog. J Neurosci 4: 2106-2116.

Aiken SP, Lampe BJ, Murphy PA, Brown BS (1995) Reduction of spike frequency adaptation and blockade of M-current in rat CA1 pyramidal neurones by linopirdine (DuP 996), a neurotransmitter release enhancer. Br J Pharmacol 115: 1163-1168.

Baird R, Desmadryl G, Fernández C, Goldberg JM (1988) The vestibular nerve of the chinchilla. II. Relation between afferent response properties and peripheral innervation patterns in the semicircular canals. J Neurophysiol 60: 182-203.

Bauer CK, Engeland B., Wulfsen I., Ludwing J., Pongs O., Schwarz JR (1998) RERG is a molecular correlate of the inward-rectifying K^+ current in clonal rat pituitary cells. Receptors Channels 6: 19-29.

Bäurle J, Kleine J, Grüsser O, Güldin W (1997) Co-localization of glycine and calbindin D-28K in the vestibular ganglion of the rat. Neuroreport 8: 2443-2447.

Bäurle J, Gulding W (1998) Unbiased number of vestibular ganglion neurons in the mouse. Neurosci Lett 246: 89-92.

Belluzzi O, Sacchi O, Wanke E (1985a) Identification of delayed potassium and calcium currents in the rat sympathetic neurone under voltage clamp. J Physiol 358: 109-129.

Belluzzi O, Sacchi O, Wanke E (1985b) A fast transient outward current in the rat sympathetic neurone studied under voltage-clamp conditions. J Physiol 358: 91-108.

Bernard C, Cochran SL, Precht W (1985) Presynaptic actions of cholinergic agents upon the hair cell-afferent fiber synapse in the vestibular labyrinth of the frog. Brain Res 338: 225-236.

Bertollini L, Biella G, Wanke E, Avanzini G, de Curtis M (1994) Fluoride reversibly blocks HVA calcium current in mammalian thalamic neurons. Neuroreport 5: 553-556.

Bofill-Cardona E, Vartian N, Nanoff C, Freissmuth M, Boehm S (2000) Two different signaling mechanisms involved in the excitation of rat sympathetic neurons by uridine nucleotides. Mol Pharmacol 57: 1165-1172.

Brichta AM, Goldberg JM (2000) Responses to efferent activation and excitatory response-intensity relations of turtle posterior-crista afferents. J Neurophysiol 83: 1224-1242.

Bridgeman D, Hoffman L, Wackym PA, Micevych PE, Popper P (1996) Distribution of choline acetyltransferase mRNA in the efferent vestibular neurons of the chinchilla. J Vestib Res 6: 203-212.

Brontë-Stewart H, Lisberg S (1994) Physiological properties of vestibular primary afferents that mediate motor learning and normal performance of the vestibuloocular reflex in monkeys. J Neurosci 14: 1290-1308.

Brown DA, Adams PR (1980) Muscarinic suppression of a novel voltage-sensitive K+ current in a vertebrate neurone. Nature 283: 673-676.

Brown BS, Yu SP (2000) Modulation and genetic identification of the M channel. Prog Biophys Mol Biol 73: 135-166.

Caulfield MP, Jones S, Vallis Y, Buckley NJ, Kim GD, Milligan G, Brown DA (1994) Muscarinic M-current inhibition via Gαq/11 and α-adrenoceptor inhibition of Ca^{2+} current via Gαo in rat sympathetic neurones. J Physiol 477: 415-422.

Carrillo E (2005) Efecto de cannabinoides sobre la actividad eléctrica de las neuronas aferentes de los canales semicirculares. Tesis de Licenciatura. Facultad de Medicina de la Universidad Autónoma de Puebla.

Clapp LH, Sims SM, Singer JJ, Walsh JV (1992) Role for diacylglycerol in mediating the actions of ACh on M-current in gastric smooth muscle cells. Am J Physiol 263: C1274-C1281.

Constanti A, Brown DA (1981) M-currents in voltage-clamped mammalian sympathetic neurones. Neurosci Lett 24: 289-294.

Constanti A, Sim JA (1987) Muscarinic receptors mediating suppression of the M-current in guinea-pig olfactory cortex neurones may be of the M2-subtype. Br J Pharmac 90: 3-5.

Costa AM, Brown BS (1997) Inhibition of M-current in cultured rat superior cervical ganglia by linopirdine: mechanism of action studies. Neuropharmacol 36:1747-1753.

Curthoys IS (1982) The response of primary horizontal semicircular canal neurons in the rat and guinea pig to angular acceleration. Exp Brain Res 47: 286-294.

Cruzblanca H, Koh DS, Hille B (1998) Bradykinin inhibits M current via phospholipase C and Ca^{+2} release from IP_3-sensitive Ca^{+2} stores in rat sympathetic neurons. Proc Natl Acad Sci USA 95:7151–7156.

Chabbert C, Chambard J, Valmier J, Sans A, Desmadryl G (1997) Voltage activated sodium currents in acutely isolated mouse vestibular ganglion neurones. Neuroreport 8: 1253-1256.

Chabbert C, Chambard J, Sans A, Desmadryl G (2001a) Three types of depolarization-activated potassium currents in acutely isolated mouse vestibular neurons. J Neurosci 85: 1017-1026.

Chabbert C, Chambard JM, Valmier J, Sans A, Desmadryl G (2001b) Hyperpolarization-activated (I_h) current in mouse vestibular primary neurons. Neuroreport 12: 2701-2704.

Chambard J, Chabbert C, Sans A, Desmadryl G (1999) Developmental changes in low and high voltage-activated calcium currents in acutely isolated mouse vestibular neurons. J Physiol 518: 141-149.

Chávez H, Vega R, Soto E (2005) Histamine (H3) receptors modulate the excitatory amino acid receptor response of the vestibular afferents. Brain Res 1064: 1-9.

Dechesne CJ, Mbiene JP, Sans A (1986) Postnatal development of vestibular receptor surfaces in the rat. Acta Otolaryngol 101: 11-18.

Dechesne CJ, Desmadryl G, Dememes D (1987) Myelination of the mouse vestibular ganglion. Acta Otolaryngol 103: 18-23.

Dechesne CJ, Hampson DR, Goping G, Wheaton KD, Wenthold RJ (1991) Identification and localization of a kainate binding protein in the frog inner ear by electron microscopy immunocytochemistry. Brain Res 545: 223-233.

De Leenheer EM, Huygen PL, Coucke PJ, Admiraal RJ, van Camp G, Cremers CW (2002) Longitudinal and cross-sectional phenotype analysis in a new, large Dutch DFNA2/KCNQ4 family. Ann Otol Rhinol Laryngol 111: 267-274.

Del Río E, Bevilacqua JA, Marsh SJ, Halley P, Caulfield MP (1999) Muscarinic M1 receptors activate phosphoinositide turnover and Ca^{2+} mobilisation in rat sympathetic neurones, but this signalling pathway does not mediated M-current inhibition. J Physiol 520: 101-111.

Demêmes D, Raymond J, Atger P, Grill C, Winsky L, Dechesne C (1992) Identification of neuron subpopulations in the rat vestibular ganglion by calbindin-D 28 K, calretinin and neurofilament proteins immunoreactivity. Brain Res 582: 168-172.

Demêmes D, Lleixa A, Dechesne CJ (1995) Cellular and subcellular localization of AMPA-selective glutamate receptors in the mammalian peripheral vestibular system. Brain Res 671: 83-94.

Demêmes D, Dechesne CJ, Venteo S, Gaven F, Raymond J (2001) Development of the rat efferent vestibular system on the ground and in microgravity. Dev Brain Res 128: 35-44.

Derbenev AV, Linn CL, Guth PS (2005) Muscarinic ACh receptor activation causes transmitter release from isolated frog vestibular hair cells. J Neurophysiol 94: 3134–3142.

Desmadryl G, Sans A (1990) Afferent innervation patterns in crista ampullaris of the mouse during ontogenesis. Dev Brain Res 52: 183-189.

Desmadryl G (1991) Postnatal developmental changes in the response of mouse primary vestibular neurons to externally applied galvanic currents. Dev Brain Res 64: 137-143.

Desmadryl G, Chambard JM, Valmier J, Sans A (1997) Multiple voltage-dependent calcium currents in acutely isolated mouse vestibular neurons. Neuroscience 78: 511 522.

Eatock R, Hutzler M (1992) Ionic currents of mammalian vestibular hair cell. Ann NY Acad Sci 656: 58-74.

Elgoyhen A (2001) Cloning and functional properties of hair cells nAChRs. 24th Annual Midwinter Research Meeting of the Association for Research in Otolaryngology, C469.

Elgoyhen AB, Jhonson DS, Boulter J, Vetter DE, Heinemann S (1994) Alpha 9: an acetylcholine receptor with novel pharmacological properties expressed in rat cochlea hair cells. Cell 79: 705-715.

Ernfors P, Van de Water T, Loring J, Jaenish R (1995) Complementary Roles of BDNF and NT-3 in Vestibular and Auditory Development. Neuron 14: 1153-1164.

Eróstegui C, Norris CH, Bobbin RP (1994) In vitro pharmacological characterization of a cholinergic receptor on outer hair cells. Hearing Res 74: 135-147.

Estes MS, Blanks RH, Markham CH (1975) Physiologic characteristics of vestibular first-order canal neurons in the cat. I. Response plane determination and resting discharge characteristics. J Neurophysiol 38: 1232-1249.

Ezure K, Cohen M, Wilson V (1983) Response of cat semicircular canal afferents to sinusoidal polarizing currents: implication for input-output properties of second-order neurons. J Neurophysiol 49: 639-648.

Fernández C, Baird RA, Goldberg JM (1988) The vestibular nerve of the chinchilla. I. Peripheral innervation patterns in the horizontal and superior semicircular canals. J. Neurophysiol 60: 167-181.

Flores A, León-Olea M, Vega R, Soto E (1996) NADPH histochemistry and role in the amphibian inner ear. Neurosci Lett 205: 131-134.

Flores A, Soto E, Vega R (2001) Nitric oxide in the afferent synaptic transmission of the axolotl vestibular system. Neurosci 103: 457-464.

Ford CP, Stemkowski PL, Light PE, Smith PA (2003) Experiments to test the role of phosphatidylinositol 4,5-bisphosphate in neurotransmitter-induced M-channel closure in bullfrog sympathetic neurons. J Neurosci, 23:4931- 4941.

Fritzsch B, Silos-Santiago I, Bianchi LM, Fariñas I (1997) The role of neurotrophic factor in regulating the development of inner ear innervation. TINS 20: 159-164.

Gamper N, Stockand JD, Shapiro MS (2003) Subunit-specific modulation of KCNQ potassium channels by Src tyrosine kinase. J Neurosci 23: 84-95.

Gacek R (1980) Neuroanatomical correlates of vestibular function. Ann Otol Rhinol Laryngol 89: 2-5.

Goldberg JM, Fernández C (1971) Physiology of peripheral neurons innervating semicircular canals of the squirrel monkey III. Variations among units in their discharge properties. J. Neurophysiol 34: 676-684.

Goldberg JM, Fernández C (1977) Conduction times and background discharge of vestibular afferents. Brain Res 122: 545-550.

Goldberg JM, Fernández C (1980) Efferent vestibular system in the squirrel monkey: anatomical localization and influence on afferent activity. J Neurophysiol 43: 986-1025.

Goldberg JM, Smith C, Fernández C (1984) Relation between discharge regularity and responses to externally applied galvanic currents in vestibular nerve afferents of the squirrel monkey. J Neurophysiol 51:1236-1256.

Goldberg JM, Highstein S, Moschovakis A, Fernández C (1987) Inputs from regularly and irregularly discharging vestibular nerve afferents to secondary neurons in the vestibular nuclei of the squirrel monkey. I. An electrophysiological analysis. J Neurophysiol 58: 700-718.

Goldberg JM, Desmadryl G, Baird RA, Fernández C (1990a) The vestibular nerve of the chinchilla. IV. Discharge properties of utricular afferents. J Neurophysiol 63: 781-790.

Goldberg JM, Desmadryl G, Baird RA, Fernández C (1990b) The vestibular nerve of the chinchilla. V. Relation between afferent discharge properties and peripheral innervation patterns in the utricular macula. J Neurophysiol 63: 791-804.

Gómez-Casati ME, Katz E, Glowatzki E, Lioudyno MI, Fuchs P, Elgoyhen AB (2004) Linopirdine blocks α9,α10-containing nicotinic cholinergic receptors of cochlear hair cells. J Assoc Res Otolaryngol 5: 261-269.

Guevara JM (1995) Análisis de la estructura fina de las relaciones sinápticas en el sistema vestibular del axolotl (Ambystoma tigrinum). Tesis de Maestria. Instituto de Fisiología de la Universidad Autónoma de Puebla.

Guth PS, Dunn A, Kronomer K, Norris CH (1994) The cholinergic pharmacology of the frog saccule. Hear Res 75: 225-232.

Guth PS, Norris CH (1996) The hair cell acetylcholine receptors: a synthesis. Hear Res 98:1-8.

Gutman GA, Chandy KG, Adelman JP, Aiyar J, Bayliss DA, Clapham DE, Covarriubias M, Desir GV, Furuichi K, Ganetzky B, Garcia ML, Grissmer S, Jan LY, Karschin A, Kim D, Kupeschmidt S, Kurachi Y, Lazdunski M, Lesage F, Lester HA, McKinnon D, Nichols CG, O'Kelly I, Robbins J, Robertson GA, Rudy B, Sanguinetti M, Seino S, Stuehmer W, Tamkun MM, Vandenberg CA, Wei A, Wulff H, Wymore RS (2003) International Union of Pharmacology. XLI. Compendium of voltage-gated ion channels: potassium channels. Pharmacol Rev 55: 583-586.

Hadley JK, Noda M, Selyanko AA, Wood IC, Abogadie FC, Brown DA (2000) Differential tetraethylammonium sensitivity of KCNQ1-4 potassium channels. Br J Pharmacol 129: 413-415.

Haley JE, Abogadie PC, Delmas P, Dayrell M, Vallis Y, Milligan G, Caulfield MP, Brown DA, Buckley NJ (1998) The α subunit of Gq contributes to muscarinic inhibition of the M-type potassium current in sympathetic neurons. J Neurosci 18: 4521-4531.

Hernandez CC, Zaika O, Tolstykh GP, Shapiro MS (2008) Regulation of neural KCNQ channels: signalling pathways, structural motifs and functional implications. J Physiol 586: 1811-1821.

Hiel H, Elgoyhen A, Drescher D, Morley B (1996) Expression of nicotinic acetylcholine receptor mRNA in the adult rat peripheral vestibular system. Brain Res 738: 347-352.

Highstein SM, Baker R (1985) Action of the efferent vestibular system on primary afferents in the toadfish, Opsanus tau. J Neurophysiol 54: 370-384.

Holt JC, Stauffer EA, Abraham D, Géléoc SG (2007) Dominant-negative inhibition of M-like potassium conductance in hair cells of the mouse inner ear. J Neurosci 27: 8940-8951.

Hong SH, Park SK, Cho YS, Lee HS, Kim KR, Kim MG, Chung WH (2006) Gentamicin induced nitric oxide-related oxidative damages on vestibular afferents in the guinea pig. Hear Res 211: 46-53.

Honrubia V, Sitko S, Lee R, Kuruvilla A, Schwartz IR (1984) Anatomical characteristics of the anterior vestibular nerve of the bullfrog. Laryngoscope 94: 464-474.

Horowitz LF, Hirdes W, Suh BC, Hilgemann DW, Mackie K, Hille B (2005) Phospholipase C in living cells: activation, inhibition, Ca^{+2} requirement, and regulation of M current. J Gen Physiol 126: 243-262.

Hoshi N, Zhang JS, Omaki M, Takeuchi T, Yokoyama S, Wanaverbecq N, Langeberg LK, Yoneda Y, Scott JD, Brown DA, Higashida H (2003) AKAP150 signaling complex promotes suppression of the M-current by muscarinic agonists. Nat Neurosci 6: 564-571.

Hurley KM, Gaboyard S, Zhong M, Price SD, Wooltorton JR, Lysakowski A, Eatock RA (2006) M-like K^+ currents in type I hair cells and calyx afferent endings of the developing rat utricle. J Neurosci 26: 10253-10269.

Ishiyama G, Lopez I, Williamson R, Acuna D, Ishiyama A (2002) Subcellular immunolocalization of NMDA receptor subunit NR1, 2A, 2B in the rat vestibular periphery. Brain Res 935: 16-23.

Jensen JB, Lyssand JS, Hague C, Hille B (2009) Fluorescence changes reveal kinetic steps of muscarinic receptor–mediated modulation of phosphoinositides and Kv7.2/7.3 K^+ channels. J Gen Physiol 133: 347-359.

Jentsch TJ (2000) Neuronal KCNQ potassium channels: physiology and role in disease. Nat Rev Neurosci 1: 21-30.

Jespersen T, Grunnet M, Olesen SP (2005) The KCNQ1 potassium channel: from gene to physiological function. Physiology 20:408-416.

Kharkovets T, Hardelin JP, Safieddine S, Schweizer M, El-Amraoui A, Petit C, Jentsch TJ (2000) KCNQ4, a K^+ channel mutated in a form of dominant deafness,

is expressed in the inner ear and the central auditory pathway. Proc Natl Acad Sci USA 97: 4333-4338.

Kharkovets T, Dedek K, Maier H, Schweizer M, Khimich D, Nouvian R, Vardanyan V, Leuwer R, Moser T, Jentsch TJ (2006) Mice with altered KCNQ4 K^+ channels implicate sensory outer hair cells in human progressive deafness. EMBO J 25: 642-652.

Kreindler JL, Troyanovskaya M, Wackym PA (2001) Ligand-gated purinergic receptors are differentially expressed in the adult rat vestibular periphery. Ann Otol Rhinol Laryngol 110: 277- 282.

Kubisch C, Schroeder BC, Friedrich T, Lutjohann B, El-Amraoui A, Marlin S, Petit C, Jentsch TJ (1999) KCNQ4, a novel potassium channel expressed in sensory outer hair cells, is mutated in dominant deafness. Cell 96: 437-446.

Kurenny DE, Barnes S (1994) Proton modulation of M-like potassium current (IKx) in rod photoreceptors. Neurosci Lett 170: 225-228.

Kurenny DE, Barnes S (1997) Regulation of M-like K^+ current, IKx, by $Ca(^{2+})$-dependent phosphorylation in rod photoreceptors. Am J Physiol 272: 1844-1853.

Lamas JA, Selyanko AA, Brown DA (1997) Effects of a cognition-enhancer, linopirdine (DuP 996), on M-type potassium currents ($I_{K(M)}$) and some other voltage- and ligand-gated membrane currents in rat sympathetic neurons. Eur J Neurosci 9: 605- 616.

Lerche C, Scherer CR, Seebohm G, Derst C, Wei AD, Busch AE, Steinmeyer K (2000) Molecular cloning and functional expression of KCNQ5, a potassium channel subunit that may contribute to neuronal M-current diversity. J Biol Chem 275: 22395-22400.

Li GQ, Kevetter GA, Leonard RB, Prusak DJ, Wood TG, Correia MJ (2007) Muscarinic acetylcholine receptor subtype expression in avian vestibular hair cells, nerve terminals and ganglion cells. Neurosci 146: 384-402.

Limón A (1998) Ubicación del ganglio vestibular y presencia de NF-160 kDa en neuronas aferentes vestibulares del VIII par craneal del Ambystoma tigrinum. Tesis de Licenciatura. Facultad de Ciencias Químicas de la Universidad Autónoma de Puebla.

Limón A, Pérez C, Vega R, Soto E (2005) Ca^{2+}-activated K^{+} current density is correlated with soma size in rat vestibular- afferent neurons in culture. J Neurophysiol 94: 3751- 3761.

Liu B, Wu D (2004) Analysis of Gprotein-mediated activation of phospholipase C in cultured cells. Methods Mol Biol 237: 99-102.

Lopes CMB, Zhang H, Rohacs T (2002) Alterations in conserved Kir channel-PIP_2 interactions underlie channelopathies. Neuron 34: 933-944.

Ludwing J, Terlau H, Wunder F, Bruggemann A, Pardo LA, Marquardt A, Stuhmer W, Pongs O (1994) Functional expression of a rat homologue of the voltage-gated ether a go-go potassium channel reveals differences in selectivity and activation kinetics between the Drosophila channel and its mammalian counterpart. EMBO J 13: 4451-4458.

Lysakowski A, Minor L, Fernández C, Goldberg J (1995) Physiological identification of morphologically distinct afferent classes innervating the cristae ampullares of the squirrel monkey. J Neurophysiol 73: 1270-1281.

Lysakowski A, Goldberg J (1997) A regional ultrastructural analysis of the cellular and synaptic architecture in the chinchilla cristae ampullares. J Comp Neurol 389: 419–443.

Lysakowski A, Price SD (2003) Ultrastructural localization of potassium channels in the inner ear. FASEB 17: A1228.

Marais-Cabral JH, Lee A, Cohen SL, Chait BT, Li M, MacKinnon R (1998) Crystal structure and functional analysis of the HERG potassium channel N terminus: a eukaryotic PAS domain. Cell 95: 649-655.

Marlinski V, Plotnik M, Goldberg JM (2004) Efferent actions in the chinchilla vestibular labyrinth. J Assoc Res Otolaryngol 5: 126-143.

Marrion NV (1997) Control of M-current. Annu Rev Physiol 59: 483-504.

Matsubara A, Takumi Y, Nakagawa T, Usami S, Shinkawa H, Ottersen OP (1999) Immunoelectron microscopy of AMPA receptor subunits reveals three types of putative glutamatergic synapse in the rat vestibular end organs. Brain Res 819: 58-64.

Mercado F, López IA, Acuna D, Vega R, Soto E (2006) Acid-sensing ionic channels in the rat vestibular endorgans and ganglia. J Neurophysiol 96: 1615-1624.

Meves H, Schwarz JR, Wulfsen I (1999) Separation of M-like current and ERG current in NG108-15 cells. Br J Pharmacol 127: 1213-1223.

Mirshahi T, Jin T, Logothetis DE (2003) G beta gamma and KACh: old story, new insigths. Sci STKE 194: PE32.

Nagata N, Harada N, Chen L, Cho H, Tomoda K, Yamashita T (2000) Extracellular adenosine 5'-ATP-induced calcium signaling in isolated vestibular ganglion cells of the guinea pig. Acta Otolaryngol 120: 704-709.

Niedzielski A, Wenthold R (1995) Expression of AMPA, kainate and NMDA receptor subunits in cochlear and vestibular ganglia. J Neurosci 15: 2338-2353.

Owen DG, Marsh SJ, Brown DA (1990) M-current noise and putative M-channels in cultured rat sympathetic ganglion cells. J Physiol 43: 269-290.

Passmore GM, Selyanko AA, Mistry M, Al-Qatari M, Marsh SJ, Matthews EA, Dickenson AH, Brown TA, Burbidge SA, Main M, Brown DA (2003) KCNQ/M currents in sensory neurons: significance for pain therapy. J Neurosci 23: 7227-7236.

Perachio AA, Kevetter GA (1989) Identification of vestibular efferent neurons in the gerbil: histochemical and retrograde labelling. Exp Brain Res 78:315-326.

Popper P, Cristobal R, Wackym PA (2004) Expression and distribution of mu opioid receptors in the inner ear of the rat. Neurosci 129: 225-233.

Prigioni I, Russo G, Valli P, Masetto S (1990) Pre and postsynaptic excitatory action of glutamate agonists on frog vestibular receptors. Hearing Res 46: 253-260.

Puel JL, Ladrech S, Chabert R, Pujol R, Eybalin M (1991a) Electrophysiological evidence for the presence of NMDA receptors in the guinea pig cochlea. Hearing Res 51: 255-264.

Puel JL, Pujol R, Ladrech S, Eybalin M (1991b) Alpha-amino-3-hydroxy-5-methyl-4-isoxazole propionic acid (AMPA) electrophysiological and neurotoxic effects in the guinea pig cochlea. Neurosci 45: 63-72.

Puyal J, Sage C, Demêmes D, Dechesne CJ (2002) Distribution of α-amino-3-hydroxy-5-methyl-4-isoazolepropionic acid and N-methyl-D-aspartate receptor subunits in the vestibular and spiral ganglia of the mouse during early development. Dev Brain Res 139: 51-57.

Rabejac D, Devau G, Raymond J (1997) AMPA receptors in cultured vestibular ganglion neurons: detection and activation. Eur J Neurosci 9: 221-228.

Rae J, Cooper K, Gates P, Watsky M (1991) Low access resistance perforated patch recordings using amphotericin B. J Neurosci Meth 37: 15-26.

Rennie KJ, Ashmore JF (1993) Effects of extracellular ATP on hair cells isolated from the guinea-pig semicircular canals. Neurosci Lett 160: 185-189.

Risner JR, Holt JR (2006) Heterogeneous potassium conductances contributes to the diverse firing properties of postnatal mouse vestibular ganglion neurons. J Neurophysiol. 96: 2364-2376.

Rivera-Arconada I, López-García JA (2005) Effects of M-current modulators on the excitability of immature rat spinal sensory and motor neurons. Eur J Neurosci 22: 3091-3098.

Robbins J (2001) KCNQ potassium channels: physiology, pathophysiology, and pharmacology. Pharmacol Ther 90: 1-19.

Rocha-Sanchez S M S, Morris K A, Kachar B, Nichols D, Fritzsch B, Beisel K W (2007) Developmental expression of Kcnq4 in vestibular neurons and neurosensory epithelia. Brain Res 1139: 117-125.

Rome C, Luo D, Dulon D (1999) Muscarinic receptor-mediated calcium signaling in spiral ganglion neurons of the mammalian cochlea. Brain Res 846: 196-203.

Romero M, Reboreda A, Sanchez E, Lamas JA (2004) Newly developed blockers of the M-current do not reduce spike frequency adaptation in cultured mouse sympathetic neurons. Eur J Neurosci 19: 2693-2702.

Ross MD (1997) Morphological evidence for local microcircuits in rat vestibular maculae. J Comp Neurol 379: 333-346.

Rossi ML, Martini M (1991) Efferent control of posterior canal afferent receptor discharge in the frog labyrinth. Brain Res 555: 123-134.

Rüsch A, Lysakowski A, Eatock RA (1998) Postnatal development of type I and type II hair cells in the mouse utricle: acquisition of voltage-gated conductances and differentiated morphology. J Neurosci 18: 7487-7501.

Ruel J, ChenC, Pujol R, Bobbin RP, Puel JL (1999) AMPA-preferring glutamate receptors in cochlear physiology of adult guinea-pig. J Physiol 518: 667-680.

Safieddine S, Bartolami S, Wenthold RJ, Eybalin M (1996) Pre- and postsynaptic M3 muscarinic receptor mRNAs in the rodent peripheral auditory system. Mol Brain Res 40: 127-135.

Sanguinetti MC, Jurkiewicz NK (1990) Two components of cardiac delayed rectifier K^+ current. Differential sensitivity to block by class III antiarrhythmic agents. J Gen Physiol 96: 195-215.

Sankaranarayanan S, Simasko SM (1996) Characterization of an M-Like current modulated by thyrotropin-releasing hormone in normal rat lactotrophs. J Neurosci 16: 1668-1678.

Sans A, Etchecopar B, Brehier A, Thomasset M (1986) Immunocytochemical detection of vitamin D- dependent calcium-binding protein (CaBP-28K) in vestibular sensory hair cells and vestibular ganglion neurones of the cat. Brain Res 364: 190-194.

Schnee ME, Brown BS (1998) Selectivity of linopirdine (DuP 996), a neurotransmitter release enhancer, in blocking voltage-dependent and calcium-activated potassium currents in hippocampal neurons. J Pharmacol Exp Ther 286: 709-717.

Schneider LW, Anderson DJ (1976) Transfer characteristics of first and second order lateral canal vestibular neurons in gerbil. Brain Res 112: 61-76.

Schroeder BC, Hechenberger M, Weinreich F, Kubisch C, Jentsch TJ (2000) KCNQ5, a novel potassium channel broadly expressed in brain, mediates M-type currents. J Biol Chem 275: 24089-24095.

Schwake M, Pusch M, Kharkovets T, Jentsch TJ (2000) Surface expression and single channel properties of KCNQ2/KCNQ3, M-type K^+ channels involved in epilepsy. J Biol Chem 275: 13343–13348.

Selyanko AA, Hadley JK, Wood IC, Abogadie FC, Delmas P, Buckley NJ, London B, Brown DA (1999) Two types of K^+ channel subunit, Erg1 and KCNQ2/3, contribute to the M-like current in a mammalian neuronal cell. J Neurosci 19: 7742-7756.

Selyanko AA, Delmas P, Hadley JK, Tatulian L, Wood IC, Mistry M, London B, Brown DA (2002) Dominant-negative subunits reveal potassium channel families that contribute to M-like potassium currents. J Neurosci 19: 7742-7756.

Shapiro MS, Roche JP, Kaftan EJ, Cruzblanca H, Mackie K, Hille B (2000) Reconstitution of muscarinic modulation of the KCNQ2/KCNQ3 K^+ channels that underlie the neuronal M current. J Neurosci 20: 1710-1721.

Shah MM, Migliore M, Valencia I, Cooper EC, Brown DA (2008) Functional significance of axonal Kv7 channels in hippocampal pyramidal neurons. PNAS 105: 7869-7874.

Shen Z, Marcus DC (1998) Divalent cations inhibit IsK/KvLQT1 channels in excised membrane patches of strial marginal cells. Hearing Res 123(1-2): 157-167.

Shi W, Wymore RS, Wang HS, Pan Z, Cohen IS, McKinnon D, Dixon JE (1997) Identification of two nervous system-specific members of the erg potassium channel gene family. J Neurosci 17: 9423-9432.

Shibasaki T (1987) Conductance and kinetics of delayed rectifier potassium channels in nodal cells of the rabbit heart. J Physiol 387: 227-250.

Shigemoto T, Ohmori H (1991) Muscarinic receptor hyperpolarizes cochlear hair cells of chick by activating Ca^{2+}-activated K^+ channels. J Phys 442: 669-690.

Søgaard R, Ljungstrøm T, Pedersen KA, Olesen SP, Jensen BS (2001) KCNQ4 channels expressed in mammalian cells: functional characteristics and pharmacology. Am J Physiol Cell Physiol 280: 859-866.

Soto E, Vega R (1988) Actions of excitatory amino acid agonists and antagonists on the primary afferents of the vestibular system of the axolotl (Ambystoma mexicanum) Brain Res 462: 104-111.

Soto E, Guevara J, Andrade J, Cruz R (1994a) Ultraestructura e inervación del oído interno en el axoltol (Ambystoma tigrinum). Segundo Congreso Mexicano de Microscopía Electrónica. Cancún, México, SSB14-15.

Soto E, Flores A, Eróstegui C, Vega R (1994b) Evidence for NMDA receptor in the afferent synaptic transmission of the vestibular system. Brain Res 633: 289-296.

Soto E, Salceda R, Cruz R, Ortega A, Vega R (2000) Microcomputer program for automated action potential waveform analysis. Computer Methods and Programs in Biomedicine 62: 141-144.

Soto E, Limón A, Ortega A, Vega R (2002) Características morfológicas y electrofisiológicas de las neuronas vestibulares en cultivo. Gac Med Mex 138: 1-13.

Soto E, Cervantes B, Limón A, Vega R (2006) Sodium activated potassium current participates in the action potential repolarization in the vestibular afferent neurons of the rat. Assoc Res Otolaryngol Abs. 454.

Soto E, Vega R, Luis E (2008a) Developmental expression of inward rectifier K^+ currents in vestibular-afferent neurons of the rat. Assoc Res Otolaryngol Abstr 769:99.

Soto E, Ortega A, Vega R (2008b) Betahistine actions on the primary afferent activity in the isolated rodent vestibule. 45th Inner Ear Biology Workshop - Ferrara (Italy) September 21-24. Abstracts P. 43.

Sugai T, Sugitani M, Ooyama H (1991) Effects of activation of the divergent efferent fibers on the spontaneous activity of vestibular afferent fibers in the toad. Jpn J Physiol 41: 217-232.

Suh BC, Hille B (2002) Recovery from muscarinic modulation of M current channels requires phosphatidylinositol 4,5-bisphosphate synthesis. Neuron 35: 507-520.

Suh BC, Hille B (2008) Electrostatic interaction of internal Mg^{2+} with membrane PIP_2 seen with KCNQ K^+ channels. J Gen Physiol 130: 241-256.

Suh BC, Horowitz LF, Hirdes W, Mackie K, Hille B (2004) Regulation of KCNQ2/KCNQ3 current by G protein cycling: the kinetics of receptor-mediated signaling by Gq. J Gen Physiol 123: 663 – 683.

Suh BC, Inoue T, Meyer T, Hille B (2006) Rapid chemically induced changes of PtdIns(4,5) P_2 gate KCNQ ion channels. Science 314: 1454-1457.

Surti TS, Jan LY (2005) A potassium channel, the M-channel, as a therapeutic target. Curr Opin Investig Drugs 6: 704-711.

Takumida M, Anniko M (2001) Nitric oxide in guinea pig vestibular sensory cells following gentamicin exposure in vitro. Acta Otolaryngol 121:346-350.

Titus SA, Warmke JM, Ganetzky B (1997) The *Drosophila* erg K^+ channel polypeptide is encoded by the seizure locus. J Neurosci 17: 875-881.

Toesca A (1996) Central and peripheral myelin in the rat cochlear and vestibular nerves. Neurosci. Lett 221: 21-24.

Tomko DL, Peterka RJ, Schor RH and O' Leary DP (1981) Response dynamics of horizontal canal afferents in barbiturateanesthetized cats. J Neurophysiol 45: 376-396.

Tristani-Firouzi M, Sanguinetti MC (2003) Structural determinants and biophysical properties of HERG and KCNQ channel gating. J Moll Cell Cardiol 35: 27-35.

Trussell L (2000) Mutant ion channel in cochlear hair cells causes deafness. Proc Natl Acad Sci USA 97: 3786-3788.

Valli P, Caston J, Zucca G (1984) Local mechanisms in vestibular receptor control. Effects of curare on the EPSPs and spike discharge recorded from single afferent fibres of the posterior canal nerve of the frog. Acta Otolaryngol 97: 611-618.

Vega R, Soto E (2003) Opioid peptide receptors mediate an inhibitory presynaptic and excitatory postsynaptic input to the vestibular afferent neurons. Neurosci 118: 75-85.

Wackym P, Popper P, Lopez I, Micevych P (1995) Expression of alpha 4 and beta 2 nicotinic acetylcholine receptor subunit mRNA and localization of alpha-bungarotoxin binding proteins in the rat vestibular periphery. Cell Biol Int 19: 291-300.

Wackym PA, Chen CT, Ishiyama A, Pettis RM, López IA, Hoffman L (1996) Muscarinic acetylcholine receptor subtype mRNAs in the human and rat vestibular periphery. Cell Biol Int 20: 187-192.

Wang X, Reynolds ER, Deak P, Hall LM (1997) The seizure locus encodes the *Drosophila* homolog of the HERG potassium channel. J Neurosci 17: 882-890.

Wang HS, Pan Z, Shi W, Brown BS, Wymore RS, Cohen IS, Dixon JE, McKinnon D (1998) KCNQ2 and KCNQ3 potassium channel subunits: molecular correlates of the M-channel. Science 282: 1890-1893.

Warmke J, Drysdale R, Ganetzky B (1991) A distinct potassium channel polypeptide encoded by the *Drosophila eag* locus. Science 252: 1560-1562.

Warmke J, Ganetzky B (1994) A family of potassium channel genes related to eag in Drosophila and mammals. Proc Natl Acad Sci USA 91: 3438-3442.

Wersäll, J (1956) Studies on the structure and innervation on the sensory epithelium of the crista ampullaris in the guinea pig. A light and electron microscopic investigation. Acta Otolaryngol. (Stock) 126(suppl): 1-85.

Wersäll RA, Bagger-Sjöbäck D (1974) Handbook of Sensory Physiology, Vestibular System. Basic Mechanisms. ed. Kornhuber, H.H. (Springer, New York), pp. 123-170.

Yamaguchi K, Ohmori H (1993) Suppression of the slow K^+ current by cholinergic agonists in cultured chick cochlear ganglion neurons. J Physiol 464: 213-228.

Yagi T, Simpson NE, Markham CH (1977) The relationship of conduction velocity to other physiological properties of the cat's horizontal canal neurons. Exp Brain Res 30: 587-600.

Ylikoski J (1983) The fine structure of the sheaths of vestibular ganglion cells in the rat, monkey and man. Acta Otolaringol 95: 486-493.

Young RL (1984) Perception of the body in the space. In: Handbook of physiology (eds) Brook Hart JM and Mouncastle VB section Y, The nervous system, Vol III, (Ed) American Physiological Society, Maryland Bethesda USA. 1023-1062.

Yue C, Yaari Y (2004) KCNQ/M channels control spike afterdepolarization and burst generation in hippocampal neurons. J Neurosci 24:4614-4624.

Yue C, Yaari Y (2006) Axo-somatic and apical dendritic Kv7/M channels differentially regulate the intrinsic excitability of adult rat CA1 pyramidal cells. J Neurophysiol 95: 3480-3495.

Zaczek R, Chorvat RJ, Saye JA, Pierdomenico ME, Maciag CM, Logue AR, Fisher BN, Rominger DH, Earl RA (1998) Two new potent neurotransmitter release enhancers, 10,10-bis(4-pyridinylmethyl)-9(10h)-anthracenone and 10,10-bis(2-fluoro-4-pyridinylmethyl)-9(10h)-anthracenone: comparison to linopirdine. J Pharmacol Exp Ther 285: 724-730.

Zhang H, Craciun LC, Mirshahi T, Rohács T, Lopes CM, Jin T, Logothetis DE (2003) PIP_2 activates KCNQ channels, and its hydrolysis underlies receptor-mediated inhibition of M currents. Neuron 37: 963-975.

APÉNDICE

J Neurophysiol 94: 3751–3761, 2005.
First published August 17, 2005; doi:10.1152/jn.00177.2005.

Ca^{2+}-Activated K^+-Current Density Is Correlated With Soma Size in Rat Vestibular-Afferent Neurons in Culture

Agenor Limón,[1] Cristina Pérez,[1,2] Rosario Vega,[1] and Enrique Soto[1]
[1]*Institute of Physiology, Autonomous University of Puebla, Puebla and* [2]*Institute of Cellular Physiology, National Autonomous University of Mexico, Mexico City, Federal District, Mexico*

Submitted 18 February 2005; accepted in final form 14 August 2005

Limón, Agenor, Cristina Pérez, Rosario Vega, and Enrique Soto. Ca^{2+}-activated K^+-current density is correlated with soma size in rat vestibular- afferent neurons in culture. *J Neurophysiol* 94: 3751–3761, 2005. First published August 17, 2005; doi:10.1152/jn.00177.2005. Vestibular-afferent neurons (VANs) transmit information about linear and angular accelerations during head movements from vestibular end organs to vestibular nuclei. In situ, these neurons show heterogeneous discharge patterns that may be produced by differences in their intrinsic properties. However, little is known about the ionic currents underlying their different firing patterns. Using the whole cell patch-clamp technique, we analyzed the expression of Ca^{2+} and Ca^{2+}-activated K^+ currents (I_{KCa}) in primary cultured neurons isolated from young rats (p7–p10). We found two overlapping subpopulations of VANs classified according to low-threshold Ca^{2+}-current [low-voltage–activated (LVA)] expression; LVA (−) neurons, formed by small cells, and LVA (+) neurons composed of medium to large cells. The I_{KCa} in both cell-groups was carried through channels of high (BK), intermediate (IK), and low conductance (SK), besides a resistant channel to classical blockers (IR). BK was expressed preferentially in LVA (+) cells, whereas IR expression was preferentially in LVA (−) cells. No correlation between SK and IK expression with the soma size was found. Current-clamp experiments showed that BK participates in the adaptation of discharge and in the duration of the action potential, whereas SK and IK did not show a significant contribution to electrical discharge of cultured VANs. However, because of the low number of VANs in culture with repetitive firing it is difficult to interpret our results in terms of discharge patterns. Our results demonstrate that vestibular-afferent neurons possess different Ca^{2+}-activated K^+ (K_{Ca}) channels and that their expression, heterogeneous among the cells, would contribute to explain some of the differences in the electrical-firing properties of these neurons.

INTRODUCTION

The vestibular system transforms mechanical stimuli from linear and angular accelerations during head movements into spike trains that are transmitted to the vestibular nuclei through bipolar-afferent neurons. Vestibular-afferent neurons (VANs) have a resting discharge in the absence of any stimuli that depend on the spontaneous release of a neurotransmitter from the sensory hair cells (Annoni et al. 1984; Soto and Vega 1988; Starr and Sewell 1991). Based on the coefficient of variation of their resting discharge, VANs have been classified into regular and irregular cells. However, there is no clear separation into two neuronal subgroups because the regularity of the discharge varies from the most irregular to regular cells forming a continuum among all cells (Goldberg and Fernández 1971; Honrubia et al. 1989). VAN morphology has been correlated with the regularity of the resting discharge. Calyx-ending neurons, with the largest somas and thick afferent dendrites that innervate type I hair cells mainly located in the central zones of the sensory neuroepithelia, have an irregular resting discharge. The smallest neurons, with thin dendrites that establish bouton synapses with type II hair cells in the peripheral zones of sensory epithelia, have a regular resting discharge. Dimorphic neurons, with medium soma size innervating both type I and type II hair cells, are distributed throughout the sensory epithelia and have intermediate electrical properties (Fernández et al. 1988, 1995; Kevetter and Leonard 2002; Leonard and Kevetter 2002; Lysakowski et al. 1995; Si et al. 2003).

Besides this, vestibular neurons exhibit differences in their dynamic spike response to mechanical (Baird et al. 1988; Curthoys 1982; Goldberg and Fernández 1971; Lysakowski et al. 1995) and electrical stimulation (Brontë-Stewart and Lisberger 1994; Ezure et al. 1983; Goldberg et al. 1987) of the membranous labyrinth. Differences in the firing properties of VANs cannot be explained solely by their synaptic input (Smith and Goldberg 1986) nor by the type of hair cells they innervate because vestibular neurons from animals lacking type I hair cells can also be grouped into irregular and regular types with a similar regional distribution of their terminals within the neuroepithelia (Honrubia et al. 1989; Myers and Lewis 1990). Thus as suggested (Goldberg 2000; Smith and Goldberg 1986), ionic conductance of vestibular neurons may vary depending on the location of the cells within the neuroepithelia that these neurons innervate. However, there is little information about the ionic conductance expressed by vestibular neurons in mammals. Studies in embryonic and neonatal mice have shown that VANs express a tetrodotoxin (TTX)-sensitive Na^+ current (Chabbert et al. 1997), a hyperpolarization-activated inward current (Chabbert et al. 2001b), three voltage-dependent K^+ currents (Chabbert et al. 2001a), and a voltage-dependent Ca^{2+} current composed of L-, N-, P/Q-, R-, and T-type channels (Chambard et al. 1999; Desmadryl et al. 1997). Only the T-type current has been shown to have a heterogeneous distribution among afferent neurons (Chambard et al. 1999; Desmadryl et al. 1997), leaving unsolved the question of a putative differential expression of ionic conductance that in turn could be correlated with the differences in the firing pattern observed in VANs.

In mathematical models, interspike-interval statistics, sensitivity to galvanic currents, and the relation between discharge

Address for reprint requests and other correspondence: A. Limón, Universidad Autónoma de Puebla, Apartado Postal 406, Puebla, Pue, C.P. 72000, Mexico (E-mail: alimonru@uci.edu).

The costs of publication of this article were defrayed in part by the payment of page charges. The article must therefore be hereby marked "*advertisement*" in accordance with 18 U.S.C. Section 1734 solely to indicate this fact.

VAN regularity and galvanic sensitivity can be accounted for by interactions between the synaptic noise and the slope of the afterhyperpolarization (AHP) (Smith and Goldberg 1986), which is in part dependent on the Ca^{2+}-activated K^+ current (I_{KCa}) characteristics (Cloues and Sather 2003; Sah 1996). At present, there is only one report of big conductance current (BK) channels in the sacular nerve of goldfish, in which it was shown that BK current is selectively expressed in a population of cells innervating the caudal portion of the saccular macula (Davis 1996). In this work, we report for the first time that in the primary afferent neurons of the vestibular system the Ca^{2+}-activated K^+ current (I_{KCa}) is composed of four components: *1*) big conductance current (BK), sensitive to iberiotoxin (IbTx); *2*) small conductance current (SK), sensitive to apamin; *3*) intermediate conductance current (IK), sensitive to clotrimazole (CLT) and charibdotoxin (ChTx); and *4*) a resistant current (IR) that is not sensitive to any of the drugs used in this work and that is activated by extracellular Ca^{2+}. In addition we found that the current density of total I_{KCa}, the BK, and the IR were correlated with soma size and with the expression of a low-voltage–activated (LVA) Ca^{2+} current. Current-clamp experiments using the perforated-patch technique indicate that the BK current participates in the adaptation of discharge and in the repolarization of the action potential of cultured VANs.

Some of these results were previously presented in abstract form (Limón et al. 2003).

METHODS

Young Wistar rats of either gender were used for the experiments. Animal care and procedures were in accordance with the National Institutes of Health Guide for the Care and Use of Laboratory Animals and the *Reglamento de la Ley General de Salud en Materia de Investigación para la Salud* of the Secretaría de Salud de México. All experimental procedures were done after approval by an appropriate committee within the institution. All efforts were made to minimize animal suffering and to reduce the number of animals used, as outlined in the "Guide to the Care and Use of Laboratory Animals" issued by the National Academy of Sciences.

Cell somata of rat VANs initiate their myelinization around the eighth day after birth (p8) (Toesca 1997). To maintain accessibility to neuronal plasmalemma with patch pipettes, we decided to use rats at ages between p7 and p10, a time at which we can obtain isolated neurons without a myelin sheath. Some of the experiments were done in acutely dissociated vestibular neurons as indicated. However, because enzymatic dissociation could alter properties of K_{Ca} channels (Spreadbury et al. 2004) and produce soma size changes caused by cell swelling (Emgard et al. 2002), we decided to use primary cultured (18–24 h) VANs to allow cells to recover from possible alterations of membrane ionic channels. Also, some of the acutely isolated cells have a thin myelin sheet covering the cell body. Because of the culturing procedure, this myelin sheet disappears, facilitating patch-clamping procedures (Santos-Sacchi 1993). Because the culture procedure also removes the myelin in some adult neurons, a small experimental sample was done in VANs from rats p23 to p26. Soma size of neurofilament (NF)-immunoreactive cultured VANs follows a Gaussian distribution [21.8 ± 5 μm (mean ± SD); Soto et al. 2002] similar to the distribution of NF-immunoreactive VANs in the rat vestibular ganglion in situ (19 ± 4 μm; Demêmes et al. 1992), indicating that morphologically they are representative of the in vivo conditions.

Cell culture

Young Wistar rats (p7–p10) were anesthetized with ether and decapitated. The head was cleaned with 70% alcohol, the inferior maxillary was removed, and the cranium immersed in L-15 medium (Gibco, Grand Island, NY). The upper part of the skull and the brain were removed and both the otic capsule and the vestibular ganglia were identified by using a stereoscopic microscope (Nikon, Tokyo, Japan). The superior vestibular ganglion was dissected and placed in fresh L-15 with added collagenase 1A at 1.25 mg/mL (Sigma-Aldrich, St. Louis, MO) and porcine trypsin 1.25 mg/mL (USB, Cleveland, OH) for 30 min at 37°C. Tissue pieces were then washed three times in L-15 medium. After each wash, tissue was centrifuged 5 min at 4,000 rpm, after which the tissue was suspended in incubated feeding medium. The feeding medium contained L-15, 10% fetal bovine serum, 100 IU/mL penicillin (Lakeside, Toluca, Mexico), 2.5 μL/mL Fungizone (Gibco), 15.7 mM $NaHCO_3$ (Merck, Naucalpan, Mexico), and 15.8 mM HEPES (Sigma-Aldrich), and was adjusted with NaOH to pH 7.7 (medium was incubated 30 min in a CO_2 tissue-culture incubator for it to reach pH 7.4). The cells were mechanically dissociated from the tissue by gently sucking it back and forth with a flame-narrowed Pasteur pipette. The cell suspension was diluted with incubated feeding medium and seeded into 35-mm Nunclon tissue-culture petri dishes (Nunc Denmark, Roskilde, Denmark) previously treated with 100 μg/mL poly-D-lysine (Sigma-Aldrich). The petri dishes were transferred to a 5% CO_2 tissue-culture incubator (Nuaire, Plymouth, MN) and maintained there at 37°C until the electrophysiological recording (2 h for acutely dissociated neurons and 18 to 24 h for cultured cells). Three vestibular ganglia per dish were used in each experiment.

Soma size measurements

Although the electrical capacitance of a membrane depends on the membrane area of the cells, and it is an indirect measurement of soma size, we decided to analyze the correlation between soma diameter and membrane capacitance to ensure that there were no differences in cellular-membrane characteristics between small and large cells, such as differences in the membrane folding (García-Pérez et al. 2004) that could prevent the use of membrane capacitance as an indicator of soma size. For this, cell images were acquired with a CCD camera (TI-24A, NEC, Elk Grove Village, IL) mounted in a triocular microscope (Diaphot, Nikon) and digitized with a frame-grabber board DT2867-LC (Data Translation, Marlboro, MA). The soma diameter was calculated as the average of major and minor longitudinal axes using the Global Lab Image (Data Translation) software tools.

Electrophysiological recording

The culture dish with attached neurons was mounted on the stage of an inverted phase-contrast microscope (TMS, Nikon). Membrane ionic currents and voltage changes in the cell membrane were studied by standard protocols of whole cell voltage-clamp and current-clamp techniques at room temperature (23–25°C) using an Axopatch 200B amplifier (Axon Instruments, Foster City, CA). Some of the current-clamp experiments, as indicated in RESULTS, were done at temperatures of 35 to 37°C using the perforated-patch technique with 260 μM amphotericin B (Sigma-Aldrich). Command-pulse generation and data sampling were controlled by pClamp 7.0 software (Axon Instruments) using a 12-bit data-acquisition system (Digidata 1200, Axon Instruments). Signals were low-pass filtered at 5 or 2 kHz and digitized at 20 or 10 kHz depending on the ionic current under study. Patch pipettes were pulled from borosilicate glass capillaries (TW120-3; WPI, Sarasota, FL) using a Flaming–Brown electrode puller (80/PC; Sutter Instruments, San Rafael, CA); they typically had a resistance of 1 to 3 MΩ when filled with internal solutions. Cells were bathed with different solutions depending on the experimental protocol (Table 1). To isolate the Ca^{2+} current (I_{Ca}), Cs^+, tetraethylammonium (TEA), and 4-aminopyridine (4-AP) were used to eliminate outward K^+ currents (Table 1, external and internal Cs^+ solutions) and TTX was used to block Na^+ currents. For the analyses of

TABLE 1. *Solutions*

Sol	NaCl	Choline Cl	KCl	CsCl	$CaCl_2$	$MgCl_2$	TEA	4-AP	EGTA	HEPES
I_{Ca} External Cs^+*				5	3.6	1.2	130	10		10
I_{Ca} Internal Cs^+				140	0.134		10		2	5
I_{KCa} External choline*		130	5.4		3.6	1.2		10		10
I_{KCa} Ca^{2+} free choline solution*		130	5.4		0	1.2		10	5	10
I_{KCa} Internal choline		10	140		0.134				2	5
External CC	140		5.4		1.8	1.2		10		10
Internal CC	18		140		0.134				2	5

The leftmost column indicates the ionic current that each solution was used for. External and internal CC solutions were used for current-clamp experiments. *Added with TTX 200 nM.

the Ca^{2+}-activated K^+ current (I_{KCa}), Na^+ and 4-AP–sensitive K^+ currents were blocked. The outward current elicited using internal and external choline solutions consisted of the I_{KCa} and a voltage-dependent, Ca^{2+}-independent outward current resistant to 4-AP. To evaluate the total I_{KCa} component, cells were perfused with a Ca^{2+}-free, 5 mM EGTA external choline solution (Table 1) and the I_{KCa} was obtained by subtraction. The free Ca^{2+} concentration in the internal solutions using 2 mM EGTA was about 4 nM estimated with the Maxc software (from Chris Patton, Hopkins Marine Station, Stanford University). In current-clamp experiments, internal and external solutions were the same as those used to analyze I_{KCa} except that choline-Cl was replaced by NaCl 18 (internal) and by 140 mM (external) and the $CaCl_2$ in the external solution was set to 1.8 mM (Table 1, external and internal CC). All internal solutions also contained 2 mM ATP-Mg and 0.5 mM GTP-Na. The pH was adjusted for the external solution to 7.4 and for the internal solution to 7.2. Osmolarity was monitored by a vapor pressure osmometer (Wescor, Logan, UT) and was around 300 mOsm for internal solutions and adjusted with dextrose to 310 mOsm for external solutions.

The analysis of the pharmacological properties of K_{Ca} channels underlying the I_{KCa} was made with 100 nM IbTx, 100 nM ChTx, 100 nM apamin, and 1 μM CLT (Sigma-Aldrich) added to the corresponding external solution. A gravity-driven perfusion system maintained the external solution flowing into the culture dish at a rate of around 2 mL/min. Additionally a three-barrel array of square borosilicate-glass capillaries connected to a SF-B77 perfusion system (Warner Instruments, Hamden, CT) was placed approximately 50 μm from the neuron under study. Each capillary was coupled to an independent syringe driven by a Baby Bee pump (BAS, West Lafayette, IN). Through this system, the neuron was continuously microperfused (20 μL/min) with external solution alone or with the selected drug added. Drugs were perfused until the current amplitude was nearly stable. The stability of membrane properties was evaluated periodically during the course of the experiment and data were discarded where there was ostensible variation in the access or seal resistance. Steady-state properties of the membrane and series resistance were measured on-line using pClamp 7.0 software (Axon Instruments) and calculated off-line by measuring the transient current induced by a −10 mV step from a V_H of −70 mV (Amstrong and Gilly 1992). Cells that showed instability of I_{Ca} or I_{KCa} were eliminated from the analysis. For current-clamp experiments, only cells with a membrane potential at rest above −35 mV were considered.

The residual series resistance after 80% of compensation in whole cell patch-clamp experiments was 2.6 ± 0.3 MΩ (n = 107; range 0.8–5.9 MΩ). Measured liquid junction potentials were 3 mV for solutions used to study I_{Ca} and 2 mV for solutions for I_{KCa}. Solutions with Na^+ used to analyze membrane voltage responses in current clamp had a liquid junction potential of 1 mV. To plot the current density versus membrane capacitance, the inward Ca^{2+} current was measured at the peak of the current. The K^+ currents were measured at 800 ms after the onset of depolarizing pulses. The maximum current density of total I_{KCa} and of its components was estimated from their respective I–V plots, which were obtained by subtraction of I–V relationships (corrected for residual series resistance and liquid junction potential) before and during perfusion of pharmacological agents or external free Ca^{2+} solution. This was done instead of constructing I–V curves from isolated currents to avoid possible errors that could emerge because of an uncompensated series resistance when large currents with different kinetics are subtracted from one another (Marcotti et al. 2004).

Action potential analysis

Some of the current-clamp experiments as indicated in RESULTS were done at temperatures of 35 to 37°C using the perforated-patch technique with 260 μM amphotericin B. In these experiments, action-potential variables were measured. For this, the voltage value of the threshold level was used as a reference point. Threshold was defined in two forms: *1*) as the point where the time course of a voltage response to a suprathreshold pulse diverts from a single exponential fit to the electrical charging of the membrane [the exponential fit was of the form $V(t) = \exp(-t/\iota) + C$, where V is the voltage, t is time, and ι is the time constant of the cell membrane]; *2*) as the point where the first-order derivative dV/dt of membrane potential reached a value higher than the noise 5 ms before spike onset (Leger et al. 2005), there were no significant differences using both methods. The amplitude of the action potential was defined as the peak action-potential value minus the threshold voltage. The action-potential duration was measured at 75% of the spike amplitude.

Data analysis

Recordings were analyzed off-line using Clampfit in the pClamp 7.0 suite and Origin software (Microcal Software, Northampton, MA). Statistical differences of means were determined using a Student's t-test, considering significant those with a $P < 0.05$. Curve-fitting routines were made by using a nonlinear least-squares method. Pooled data are presented as means ± SE unless otherwise stated.

RESULTS

Vestibular-afferent neurons in culture were identified by their birefringent round or ovoid soma when viewed under phase-contrast optics (Fig. 1*A*). The relationship between membrane capacitance and neuronal size showed a linear correlation (r = 0.92), indicating that membrane capacitance can be used as an indirect measure of soma size (Fig. 1*B*).

Previous reports indicate that in acutely dissociated VANs from embryonic mice, the largest cells express a LVA-Ca^{2+} current, whereas the high-voltage–activated (HVA) Ca^{2+} current is expressed homogeneously in all cells (Chambard et al. 1999; Desmadryl et al. 1997). Thus we analyzed the Ca^{2+} current to define whether cultured rat VANs have the same relationship between soma size and Ca^{2+} current expression.

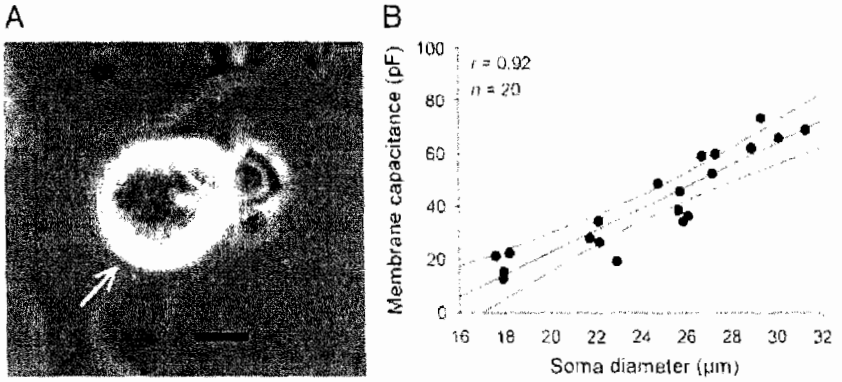

FIG. 1. Membrane capacitance and soma diameter are linearly correlated. *A*: isolated vestibular neuron after 19 h in culture (arrow) viewed under phase-contrast optics. Calibration bar represents 10 μm. *B*: correlation between membrane capacitance and soma size (n = 20). Diameter of the neuron cell bodies was calculated as the mean of major and minor longitudinal axes. Dashed lines represent the 95% confidence intervals.

Voltage-dependent calcium current I_{Ca}

The isolated Ca^{2+} current (I_{Ca}) was studied in 35 neurons. In 26% of the cells (n = 35), I_{Ca} was formed exclusively by HVA components, whereas in the remaining cells (74%) both LVA and HVA components were identified (Fig. 2, *A* and *B*). The I_{Ca} in LVA-lacking [LVA (−)] cells activated near −45 mV has its maximum amplitude around −10 mV, inactivating partially during the 800-ms pulse (n = 9). The maximum peak current density in these cells was −30 ± 6 pA/pF. In the LVA-expressing [LVA (+)] neurons, the Ca^{2+} current activated around −60 mV and completely inactivated with a single time constant of 31 ± 2 ms for pulses at −40 mV (n = 26). The HVA current in LVA (+) cells was evident around −30 mV and partially inactivated during the 800-ms pulse. The maximum peak current density around −10 mV in LVA (+) neurons was −49 ± 8 pA/pF.

To analyze whether there was any correlation between HVA current density and membrane capacitance, the current density at the end of an 800-ms pulse to −10 mV was calculated in both neuronal subtypes. This allowed us to compare HVA current between LVA (−) and LVA (+) cells because at 800 ms the contribution of a T-type current in LVA (+) cells was negligible. The HVA current density between LVA (−) (17.5 ± 4 pA/pF; n = 9) and LVA (+) cells (12.5 ± 2 pA/pF; n = 26) was not significantly different ($P > 0.05$). In experiments made to study the I_{KCa} in which the Ca^{2+} current was not isolated, it was also possible to identify the LVA (−) and LVA (+) neurons by analyzing the current caused by a test pulse to −53 mV from a V_H of −113 mV (Fig. 2*C*, *insets*). Membrane capacitances of cells identified using this procedure or by analysis of isolated I_{Ca} were pooled according to LVA expression (Fig. 2*C*). Cell capacitance had a normal distribu-

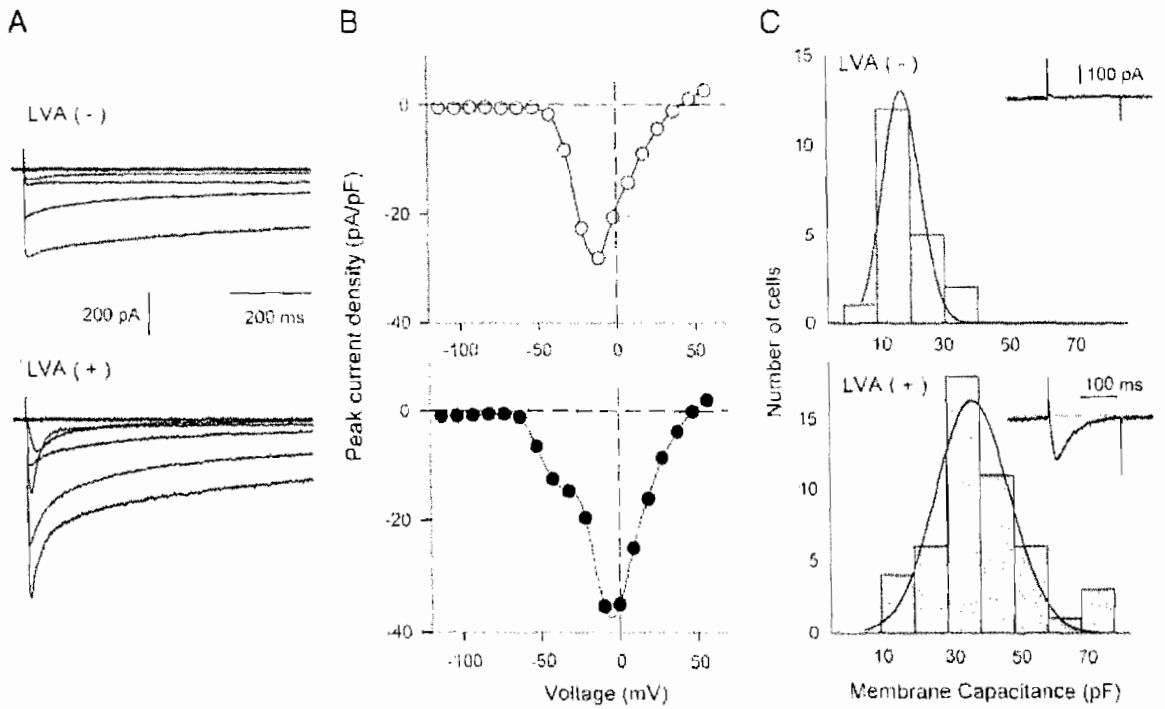

FIG. 2. I_{Ca} expression in vestibular-afferent neurons (VANs). *A*: families of isolated Ca^{2+} currents obtained from 2 representative cells. Currents were elicited with voltage pulses in nominal increments of 10 mV from a V_H of −93 mV (some traces were omitted for clarity). Above, a cell expressing only the high-voltage–activated (HVA)–Ca^{2+} current [low-voltage–activated (LVA) (−)]. Below, a cell expressing both LVA- and HVA-Ca^{2+} currents [LVA (+)]. *B*: peak current density–voltage relationship for the cells shown in *A*. *C*: histograms of the membrane capacitance of cells according to LVA expression. *Insets*: currents (calibrations apply for both inserts) elicited with a pulse to −53 mV from a V_H of −113 mV. LVA (−) cells had a mean membrane capacitance significantly lower (18.5 ± 7 pF) than that of LVA (+) cells (39 ± 15 pF; $P < 0.0005$). Continuous line is the Gaussian fit to data; r = 0.98 for both histograms.

tion of 18.5 ± 7 pF (mean ± SD; n = 19/68) for LVA (−) and 39 ± 15 pF (n = 49/68) for LVA (+). The statistical difference in capacitance (soma size) between these subgroups was significant ($P < 0.0005$). Experiments made in VANs isolated from p23 to p26 rats indicate that the separation of LVA (−) and LVA (+) cells is still present in the mature vestibular system. The mean ± SD of membrane capacitance for LVA (−) cells was 12 ± 2 pF (n = 5) and for LVA (+) it was 29 ± 1 pF (n = 10; $P < 0.0005$).

Calcium-activated potassium current I_{KCa}

The expression of I_{KCa} in VANs was analyzed by recording outward currents in external and internal choline solutions and during perfusion with Ca^{2+}-free external choline solution (Table 1). The control current was composed of I_{Ca}, I_{KCa}, and a voltage-dependent, 4-AP–insensitive K^+ current. The perfusion with Ca^{2+}-free external choline solution reversibly reduced the outward current, leaving the Ca^{2+}-independent components. The I_{KCa} component of the outward current was obtained by subtraction of the current remaining after perfusion with the Ca^{2+}-free external solution from the control current (Fig. 3*A*). The I_{KCa} component of the outward currents was observed in 100% of acutely dissociated (n = 6) and cultured neurons (n = 47). The I_{KCa} activated above −40 mV reached its maximum around 10 mV, followed by a decline in the current amplitude for more depolarized values (Fig. 3*B*). Total I_{KCa} current density was 87 ± 7 pA/pF and it was not significantly different ($P > 0.05$) in cultured or acutely dissociated neurons.

The analysis of correlation between membrane capacitance and I_{KCa} shows that small LVA (−) cells express three times higher I_{KCa} current density (171 ± 32 pA/pF; n = 8) than larger LVA (+) cells (54 ± 5 pA/pF; n = 17; $P < 0.01$) (Fig. 3*C*). Two cell groups are evident based on the expression of the LVA-Ca^{2+} current. Without this association, the analysis of correlation between the membrane capacitance and I_{KCa} has a continuous pseudoexponential form.

I_{KCa} was also observed in the 100% of cells obtained from adult p23 to p26 rats (n = 15). The total I_{KCa} current density in VANs from p23 to p26 rats was 318 ± 75 (range 105 to 968 pA/pF). The difference in I_{KCa} current density between young and adult VANs was considerably significant ($P < 0.0001$), indicating an increase in I_{KCa} expression during the postnatal development. The I_{KCa} current density of LVA (−) cells (681 ± 99 pA/pF; n = 5) was also significantly higher than that found in LVA (+) cells (137 ± 10 pA/pF; n = 10) ($P < 0.001$) (Fig. 3*D*).

The correlation between current density and membrane capacitance shows that I_{KCa} decreased as the cell membrane capacitance increased (r = 0.92), indicating a qualitatively similar relationship between p7 to p10 and p23 to p26 VANs. The range and the mean of membrane capacitance of the p23 to p26 cells were smaller because of a smaller culturing time (5 h for p23–p26 compared with 18 h in p7–p10 neurons).

The outward current that remains during perfusion with Ca^{2+}-free solution showed a significant difference ($P < 0.05$) between LVA (−) (58 ± 7 pA/pF; n = 8) and LVA (+) (38 ± 4 pA/pF; n = 17) cells. No efforts to characterize that current were made.

Calcium-activated potassium current components SK, BK, IK, and IR

To analyze I_{KCa} components in cultured vestibular-afferent neurons from p7 to p10 rats, the pharmacological agents used

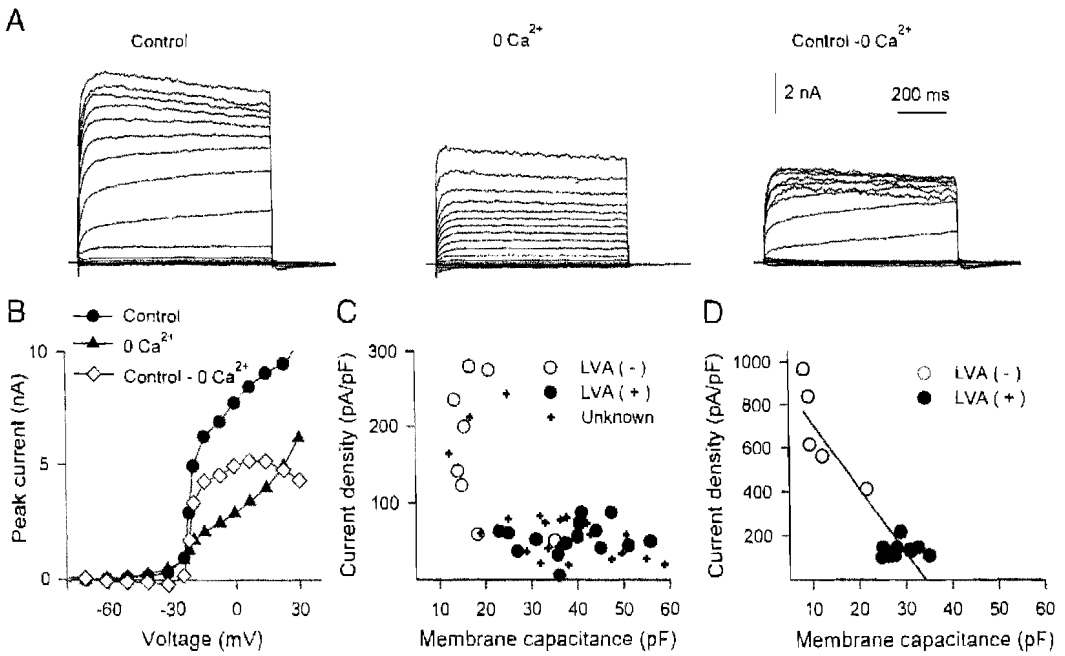

FIG. 3. Ca^{2+}-dependent outward current expression in VANs. *A*: currents obtained from a representative neuron in external and internal choline solutions (*left*) and during application of Ca^{2+}-free external choline solution (*middle*). At right, the I_{KCa} obtained by digital subtraction. Ionic currents were elicited with nominal pulses of 10 mV from a V_H of −61 mV. *B*: *I–V* curves from the outward current of the cell shown in *A*, before and after Ca^{2+} removal. *I–V* relationship of I_{KCa} was obtained by subtraction of *I–V* curves before and after Ca^{2+} removal. *C*: plot of maximum current density vs. membrane capacitance for LVA (−) (n = 8) and LVA (+) (n = 17) cells from p7 to p10 rats. Also, neurons in which the expression of LVA-Ca^{2+} current was not evaluated (n = 22) were included. *D*: plot of maximum current density vs. membrane capacitance for LVA (−) (n = 5) and LVA (+) (n = 10) from p23 to p26 rats. Continuous line is the linear fit to the whole data set (r = 0.92).

were specific blockers for BK (100 nM IbTx) (Galvez et al. 1990; Giangiacomo et al. 1992), SK (100 nM apamin) (Hugues et al. 1982), and IK (1 μM CLT) (Grissmer et al. 1993; Jensen et al. 2001; Kaczorowski and Garcia 1999). In some experiments, ChTx was also used to isolate the IK current. Because ChTx blocks both BK and IK channels (Jensen et al. 2001; Kaczorowski and Garcia 1999), BK channels were first blocked with IbTx and then cells were subsequently perfused with an external solution with ChTx + IbTx added. IK was obtained by the subtraction of the current during IbTx perfusion minus the current elicited with IbTx + ChTx. We found a Ca^{2+}-activated K^+ current that was resistant to classical I_{KCa} blockers (100 nM IbTx, 100 nM ChTx, 100 nM apamin, and 1 μM CLT). Because no specific blockers for this current exist, we obtained the resistant current (IR) by removal of external Ca^{2+} after IbTx + apamin + ChTx/CLT application.

The cells used to study I_{KCa} components extend within all the range of capacitances. Values (mean ± SD) of the initial total outward current (Ca^{2+}-independent K^+ current + I_{KCa}) of the cells used to analyze each I_{KCa} component before drug application were 115.4 ± 83.8 pA/pF for SK (n = 35), 117.2 ± 86.8 pA/pF for IK (n = 15), 114.1 ± 87.7 pA/pF for BK (n = 30), and 148.7 ± 130.3 for IR (n = 15). There were no statistical differences between these data ($P > 0.05$), indicating that the cell sample used to make the analyses of I_{KCa} components was not biased.

The perfusion of 100 nM apamin reduced the outward current in 86% of the cells (n = 30/35) (Fig. 4*A*). Subtraction of the current during apamin perfusion from control current gave the SK current. The SK component activates for voltages positive to −30 mV and reaches its maximum amplitude between 5 and 10 mV (data not shown). The SK current had a slow activation and did not decay during the 800-ms pulse, indicating a minimal, if any, inactivation. The maximum current density of SK was classified according to LVA expression. The SK current density was not different between LVA (−) and LVA (+) cells (8.3 ± 3.8 vs. 13.6 ± 3.5 pA/pF; $P > 0.05$). No significant correlation between SK expression and cell membrane capacitance was found (r = 0.21), indicating that the SK current is expressed independently of VAN size (Fig. 5, *A* and *B*).

The perfusion of 100 nM IbTx reduced the outward current in 73% of the cells (n = 22/30) (Fig. 4*B*). Digital subtraction of the outward current before and during IbTx perfusion yielded the BK current. The BK current activated at voltages positive to −60 mV in 64% of the cells (n = 14/22). In the remaining cells BK activated around −40 mV. The maximum amplitude was observed around 20 mV (data not shown). The plot of BK current density versus cell membrane capacitance (r = 0.66) indicates that small LVA (−) cells have a smaller BK than that of larger LVA (+) cells, which have higher BK

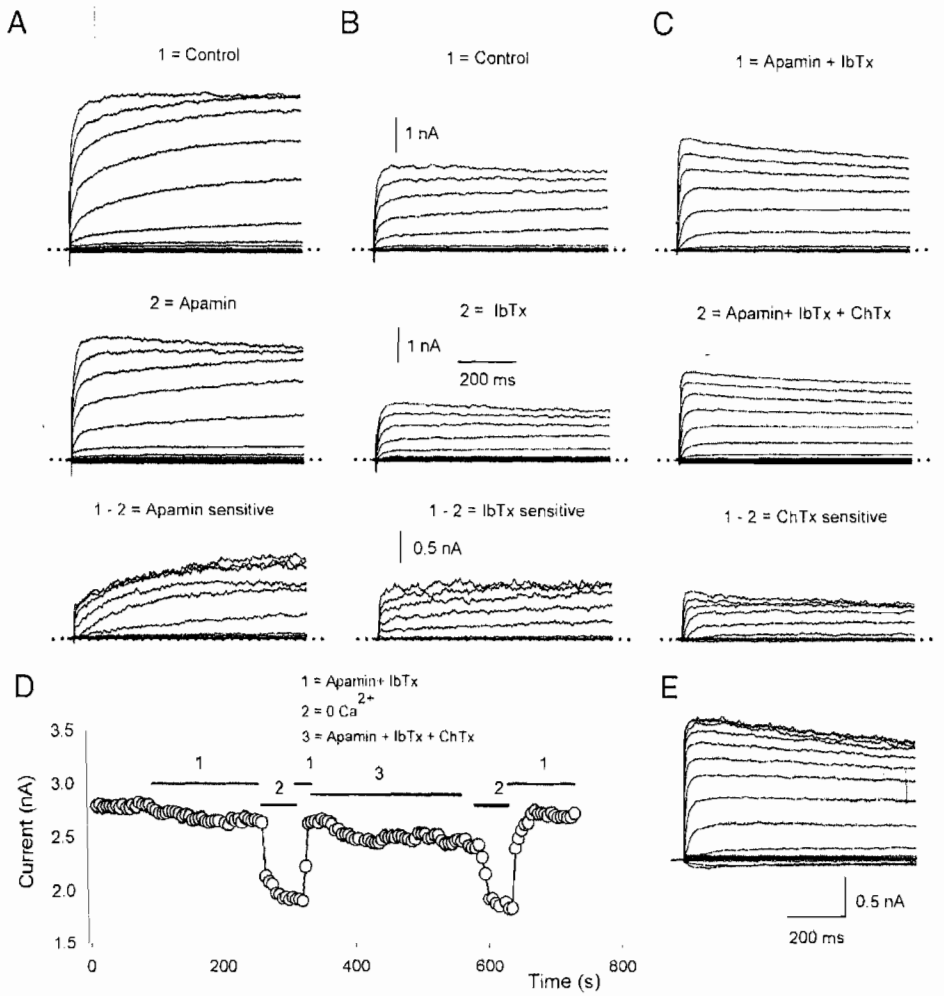

FIG. 4. Subtypes of Ca^{2+}-activated K^+ currents. Currents were recorded in external and internal choline solutions. *A* and *B*: effect of apamin and iberiotoxin (IbTx, 100 nM each) on outward current elicited with pulses in nominal increments of 10 mV from a V_H of −61 mV. Outward current in control conditions (*above*), during toxin perfusion (*middle*), and toxin-sensitive current obtained by digital subtraction (*below*). *C*: effect of 100 nM charibdotoxin (ChTx) on apamin- and IbTx-resistant current. ChTx perfusion after big conductance current (BK) and small conductance current (SK) channel blockade with IbTx and apamin allows isolation of ionic current through intermediate conductance current (IK) channels. Current calibration bars shown in *B* apply for the same row in *A* and *C*. Timescale is for all recording traces. *D*: time course of outward current in control conditions (elicited with a pulse test to 25 mV from a V_H of −61 mV) and during application of indicated toxins at a concentration of 100 nM each. *E*: resistant current (IR) in a LVA (−) cell, obtained by external Ca^{2+} removal and after apamin + IbTx + clotrimazole (CLT) perfusion. Ionic currents were generated with pulses in nominal increments of 10 mV from a V_H of −61 mV.

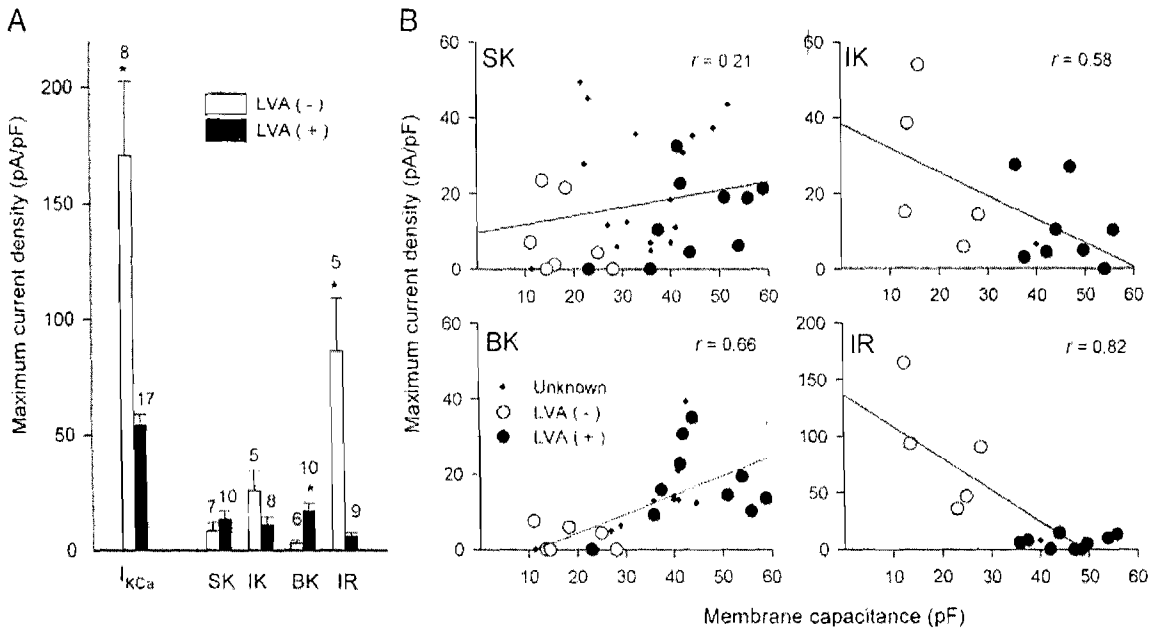

FIG. 5. Expressions of I_{KCa} subtypes are correlated with membrane capacitance and with expression of LVA-Ca^{2+} current. *A*: I_{KCa} and IR maximum current densities were significantly higher in LVA (−) than in LVA (+) cells. On the contrary the expression of BK was significantly larger in LVA (+) when compared with LVA (−) cells (*$P < 0.01$). SK and IK did not show significant differences between subgroups. Difference of total I_{KCa} current density between LVA (−) and LVA (+) cells is mainly caused by the IR current that is the principal component of I_{KCa} in LVA (−) cells. *B*: plots of maximum current density for each I_{KCa} subtype vs. membrane capacitance. Cross symbols indicate cells in which the presence of LVA-Ca^{2+} current was not evaluated. Continuous line is the linear fit to the whole data set. *r* is the correlation coefficient for each linear fit. Number of cells in SK, IK, BK, and IR plots were 35, 15, 30, and 15.

current density (3 ± 1.4 vs. 17 ± 3.3 pA/pF; $P < 0.01$; Fig. 5, *A* and *B*).

Perfusion of 100 nM ChTx (after BK blockade with IbTx) reduced the outward current in 86% of the cells ($n = 6/7$; Fig. 4*C*). The perfusion of 1 μM CLT ($n = 8$) allowed us to isolate an outward current whose characteristics were indistinguishable from the ChTx-sensitive current. Therefore for IK analysis, data obtained from ChTx- and CLT-sensitive currents were pooled. The IK did not inactivate during 800-ms voltage pulses. The IK activated above −40 mV, reaching its maximum amplitude at 10 mV (data not shown). The mean IK current density was higher in LVA (−) than in LVA (+) cells, although because of its large variability this difference was not statistically significant (26 ± 9 vs. 11 ± 3.8 pA/pF; $P > 0.05$). The analysis of correlation between IK current density and membrane capacitance gave a weak correlation ($r = 0.58$) (Fig. 5, *A* and *B*).

In 80% of the cells ($n = 12/15$), the application of I_{KCa} blockers (100 nM IbTx, 100 nM ChTx, 100 nM apamin, and 1 μM CLT) did not remove a Ca^{2+}-dependent outward current (Fig. 4*D*). This resistant current (IR) was evident by removal of external Ca^{2+} after IbTx + apamin + ChTx/CLT application (Fig. 4*E*). The IR current density in LVA (−) cells was significantly higher than that in LVA (+) cells (86 ± 3 vs. 6.2 ± 1.8 pA/pF; $P < 0.01$). The plot of IR current density versus membrane capacitance shows a significant correlation ($r = 0.82$) and confirms the existence of two separated cell groups (Fig. 5, *A* and *B*). The first was composed of LVA (−) cells with higher IR current density dispersed in a wide range from 36 to 165 pA/pF. The second was composed of LVA (+) cells that did not express a significant IR component, with a range of IR current density from 0 to 14 pA/pF. Note that the IR current density is always underestimated because it is contaminated with I_{Ca}. This is because removal of Ca^{2+} from the external solutions used to obtain IR simultaneously abolishes the Ca^{2+} current. The range of I_{Ca} current density at 800 ms (time at which IR was measured) was between −4 and −43 pA/pF, so the IR could be underestimated within this range. Because HVA-Ca^{2+} current density was not different between LVA (−) and LVA (+) subgroups, the difference observed in IR current density between LVA (−) and LVA (+) cells is produced exclusively by differences in IR expression.

Effect of I_{KCa} blockers on the voltage response to current pulses

To analyze the influence of I_{KCa} components on the discharge of the cultured vestibular neurons, the effect of I_{KCa} channel blockers on the electrical response of VANs was studied. For this, the perforated patch-clamp technique was used to avoid dialysis of internal constituents of VANs. Recordings were done at temperatures between 35 and 37°C to approximate to more physiological conditions. Voltage responses were recorded using external and internal CC solutions (Table 1), and with holding membrane potential of −60 mV (close to the zero current potential of VANs). In these conditions, 60% of VANs fired one or two action potentials (APs) during 200-ms and 2-s pulses of suprathreshold current injection ($n = 21$). The remaining 40% of the cells showed a slowly adapting response, firing no more than eight action potentials with long-duration pulses (2 s). The threshold of the first AP in control conditions was −36 ± 1 mV ($n = 21$). AP amplitude from the threshold to the maximum peak was 53 ± 3 mV. The AP duration (measured at 75%) was 4 ± 0.4 ms (note that external CC solution contains 10 mM 4-AP).

The perfusion of 100 nM apamin or 1 μM CLT did not significantly modify any of these variables (Fig. 6, *A* and *B*).

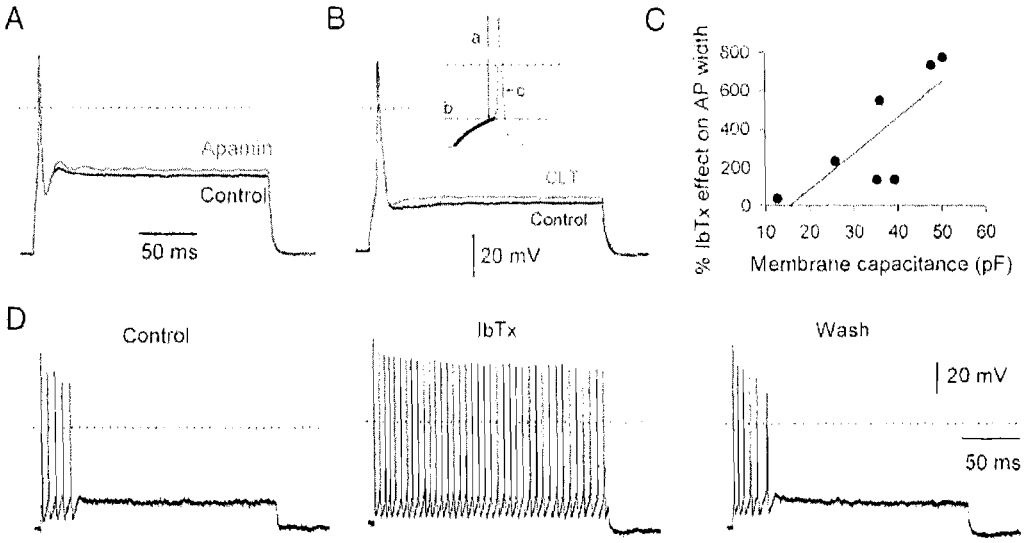

FIG. 6. Effect of K_{Ca} channels blockers on the electrical discharge of VANs. Records were made using a perforated patch in the current-clamp mode. *A* and *B*: current-clamp recordings showing the effects of 100 nM apamin and 1 μM CLT. Voltage responses were elicited with 0.6 and 0.4 nA current injections for *A* and *B*. *B*, *inset*: morphological variables of the action potentials (APs) that were measured: a, AP amplitude; b, threshold; and c, AP duration at 75%. Dotted lines indicate the zero voltage. Darker traces indicate the exponential fit to the electrical charge of the membrane. *C*: summary of drug effects on the AP duration as a function of cell capacitance. *D*: IbTx 100 μM removes the adaptation of the response to 0.4-nA current pulse in a reversible form.

However, in 38% of the cells, either apamin or CLT perfusion produced a slight (5–10 mV) oscillatory behavior in the voltage response after the first action potential. This oscillatory response continuously decreased and vanished within 150 ms.

The effect of IbTx was variable among cells as expected from correlation analysis between I_{KCa} current density and membrane capacitance. The perfusion of IbTx in small cells did not significantly modify AP waveform, whereas in large cells the AP duration increase was ≤770% ($r = 0.78$, $n = 7$) (Fig. 6*C*). In those cells with repetitive discharge, the perfusion of 100 nM IbTx removed the adaptation of the response during 200-ms and 2-s current pulses (Fig. 6*D*).

These results indicate that the BK current contributes to repolarization of the action potential and to discharge adaptation, and this contribution is correlated with the membrane capacitance of VANs.

Voltage-clamp experiments indicate that the IR is the principal I_{KCa} component expressed by small LVA (−) cells and its contribution is correlated with the membrane capacitance. Because of the lack of a specific channel blocker for this current, there is no possibility of making a pharmacological analysis of its contribution to the VANs' discharge.

DISCUSSION

Calcium-activated current expression

Rat VANs in primary culture expressed a Ca^{2+} current formed by LVA and HVA components. Whereas the HVA-Ca^{2+} current was present in 100% of VANs, the expression of LVA-Ca^{2+} was heterogeneous among cells and preferentially polarized to medium and large neurons. Correlation between T-type Ca^{2+}-current expression and diameter has been reported in vestibular-ganglion neurons of mice (Chambard et al. 1999; Desmadryl et al. 1997) and in the dorsal root and nodosus-ganglion neurons of rat (Fedulova et al. 1985; Lambert et al. 1997). The percentage of cells expressing the LVA-Ca^{2+} current in this study (74%) was greater than that reported in newborn mice (20%). The differences are because in mice only the largest cells express the LVA-Ca^{2+} current, whereas in the rat, medium and large cells express this current. This may be an interspecies difference or caused by distinct culturing times of isolated neurons (2–8 h as compared with 18–24 h in the present study). Another possible source for the differences could arise from the distinct age of the animals used (p4–p8 compared with p7–p10 in the present study). In mice, the separation of VANs into two groups on the basis of T-type current starts around E17, and at p4 it is possible to observe two completely separated groups (Chambard et al. 1999). As shown in this work, in rats this separation is still present in the nearly mature (p23 to p26) neurons. The expression of the LVA-Ca^{2+} current in medium to large cells suggests that the T-type current could contribute to discharge differences between small and large cells in situ. The T-type current is preferentially expressed in dendrites of central neurons and participates in the threshold for action-potential generation, in synaptic integration, and in the configuration of spike discharge (Gauck et al. 2001; Perez-Reyes 2003; Pouille et al. 2000). Therefore as proposed for mice (Desmadryl et al. 1997), the presence of an LVA-Ca^{2+} current in large cells may decrease the threshold for spike generation, which could explain the increased sensitivity of thick axons that innervate central zones of the neuroepithelium compared with thinner axons that innervate peripheral zones.

For the HVA-Ca^{2+} currents, although we did not perform a pharmacological dissection, its characteristics were similar to those reported in mice (Desmadryl et al. 1997), where it has been found that the HVA-Ca^{2+} current is composed of L-, P/Q-, N-, and R-type currents (Chambard et al. 1999; Desmadryl et al. 1997). The whole HVA-Ca^{2+} current was found in 100% of the rat VANs, and no correlation between its current density and soma size (membrane capacitance) was observed. However, we cannot discard the possibility that some of the ionic channels that make up the HVA-Ca^{2+} current have a polarized distribution or are coupled differently with

some of the K_{Ca} channels reported in this work. Therefore further studies focused on the characterization of channels underlying the HVA-Ca^{2+} current and its functional coupling with K_{Ca} channels are needed to determine its particular role in the electrical firing of VANs.

Calcium-activated potassium current expression

The removal of Ca^{2+} from the external solution decreased the outward current, indicating the presence of an outward current that is activated by the influx of extracellular Ca^{2+}.

The I_{KCa} current was found in 100% of the studied cells. Current-density analysis showed that small LVA (−) neurons had up to four times higher current density than that of larger LVA (+) cells. Our results indicate that in both cell groups four different currents compose the I_{KCa}—SK, IK, BK, and IR—although in different proportions. Of these, only BK and IR have a clear correlation with soma size (membrane capacitance) and with the expression of the LVA-Ca^{2+} current.

The BK current was preferentially expressed in LVA (+) cells, whereas the IR was strongly expressed in LVA (−) cells. In 60% of the cells, BK was activated at voltages below the AP threshold, indicating its physiological coupling with LVA-Ca^{2+} channels, similar to data reported in central-vestibular neurons (Smith et al. 2002). If the correlation between soma diameter and BK expression and the functional coupling with T-type currents are present in VANs in situ, it might have important functional consequences. The T-type current decreases the AP threshold, but the major contribution of BK may tend to repolarize the cells, thus producing failures in the AP generation and irregularity of discharge. Actually, the participation of BK in the adaptation of the response to current pulses, revealed by IbTx effects, indicates that BK inhibition converts the firing pattern from phasic to tonic. Furthermore, the BK participates in the repolarization of the action potential and contributes to the spike duration, supporting the hypothesis that the expression of BK significantly contributes to determination of the discharge properties of VANs in situ.

Our current-clamp experiments with the perforated-patch technique, which should maintain endogenous intracellular buffers, reveal that SK and IK have an insignificant participation in the discharge of VANs caused by constant-current pulses, despite the fact that electrical firing was recorded using external solutions with 4-AP, which enhances the excitability of sensory neurons (Sculptoreanu et al. 2004; Soto et al. 2002; Stansfeld et al. 1986). However, the possibility that SK and IK currents participate in the more dynamic and complex conditions in situ cannot be discarded.

SK as well as IK activity depends largely on the concentration of intracellular Ca^{2+}. However, the *I–V* relationships of SK and IK did not follow the expected decrease for voltages >0 mV (at which the inward Ca^{2+} current decreases). This can be attributable to contamination with voltage-dependent channels (such as BK currents), although this is unlikely because ChTx and CLT inhibit similar currents and to date there are no reports about nonspecific effects of CLT and apamin on voltage-dependent channels at the concentrations used in this work. Another possibility is that Ca^{2+} may accumulate by an incomplete clearance by mechanisms of extrusion or sequestration of Ca^{2+} between voltage pulses. In dorsal root ganglion neurons (Thayer and Miller 1990) and in chromaffin cells of the rat (Herrington et al. 1996) large Ca^{2+} loads (1–2 μM) produce a rapid initial Ca^{2+} uptake by mitochondria, but intracellular [Ca^{2+}] decay to resting levels can last >2 min. The modulation of I_{KCa} currents by Ca^{2+} released from intracellular stores will also be taking place in our system and that particular issue should be addressed in future studies.

The identity of the K_{Ca} channels underlying the IR current will require further studies. However, the electrophysiological properties of the IR current are similar to drug-resistant currents from oocytes expressing BK channels coupled with the β4 subunit (Meera et al. 2000) and astrocytes expressing the β4 subunit (Gebremedhin et al. 2003). The β4 subunit has been reported to confer resistance to IbTx to the BK channels (Gebremedhin et al. 2003; Meera et al. 2000). Unfortunately, the lack of selective blockers of the IR current deters an adequate analysis of its contribution to the firing discharge of VANs. The IR has current densities ≤160 pA/pF, which are considerably greater than those of other currents reported in this study. Thus the differences found in outward current among cells seems to be caused by the expression of IR.

In mathematical models of VAN, it has been proposed that the AHP slope accounts for differences in sensibility and regularity of discharge (Smith and Goldberg 1986). According to this, the irregular discharge of large neurons innervating type I hair cells may be caused by a smaller slope of postspike voltage trajectory compared with small regular neurons innervating type II hair cells. Although the AP duration did not have a significant linear correlation with total outward current, there is a tendency of small cells to have shorter APs, as observed in VANs in situ innervating the peripheral zones of chick vestibular-neuroepithelium (Yamashita and Ohmori 1990).

It is worth noting that the electrophysiological properties of VANs in situ are changing during the first weeks after the birth until reaching a stable phenotype around p23 (Curthoys 1979). Therefore because most of our results were obtained from rats between p7 and p10, our conclusions are mainly circumscribed by this time window in the development of the vestibular system. However, at this age irregular neurons almost show a mature phenotype except for the presence of firing, bursting, and silent neurons at rest (Curthoys 1979). The percentage of regular neurons between p7 and p10 is in the range of 10 to 15%, which is nearly half of those in the adult animal (32%). Regular neurons at p7 to p10 have an electrical discharge at rest of about 20 spikes/s, which is around one third of the rate in the adult rat (Curthoys 1979, 1982). The inability of our cultured VANs to fire tonically during sustained pulses in current clamp suggests that they are in an intermediate stage of maturity or the spatial relationships of ionic channels is not the same as that in the vestibular system in situ. That total I_{KCa} increases in adult p23 to p26 rats reinforces the idea of the immaturity of VANs at p7 to p10 and is in agreement with studies of vestibular-nucleus neurons, which show that electrical properties of vestibular-nucleus neurons change during the embryonic ages (Peusner and Giaume 1997) and beyond birth (Dutia and Johnston 1998). Despite the increase in I_{KCa} current density, the correlation between total I_{KCa} and membrane capacitance in p23 to p26 adult VANs indicates that the differences in the expression of I_{KCa} are maintained in the mature vestibular system. However, the individual contribution of each I_{KCa} subtype to total I_{KCa} in p23 to p26 neurons was not defined. It is also possible that some of the kinetic and elec-

trophysiological properties of I_{KCa} change during the development as previously reported in central neurons (Kang et al. 1996).

The I_{KCa} has been shown to significantly contribute to the shaping of the action potential waveform and to the firing-discharge pattern of neurons (Dutia and Johnston 1998; Faber and Sah 2002; Johnston et al. 1994; Sah and Faber 2002; Smith et al. 2002). In lamprey motoneurons, blockade of the SK current increased the variation coefficient of the spike discharge (El Manira et al. 1994). The heightened contribution of the I_{KCa} in small LVA (−) cells could determine a faster AHP slope, thus significantly influencing discharge regularity of VANs (Smith and Goldberg 1986).

The functional role of K_{Ca} channels is not restricted to the modulation of the electrical firing but also may participate at the central synapse controlling neurotransmitter release (Hu et al. 2001; Robitaille et al. 1993). The particular role of K_{Ca} channels at central terminals should be analyzed in experimental models keeping intact the synapses between primary afferents and second-order neurons. It is worth noting that our results are limited to analysis of the K_{Ca} currents expressed in specific developmental stages and that there is no evidence indicating whether the complement of these currents is also expressed in afferent dendrites or central terminals of the mature VAN. Our results indicate that cultured VANs express an I_{KCa} carried by several channel subtypes. As shown in other systems I_{KCa} may participate in determining the threshold, latency, repolarization rate, and afterhyperpolarization of the action potential. Its differential expression among VANs may have important functional implications in the coding of vestibular sensory information. Future studies to analyze the expression and distribution of I_{KCa} subtypes within the primary sensory neuron in the mature vestibular system, including recordings in the vestibular nerve in situ, would contribute to our understanding of the role of the intrinsic properties of VANs in the coding of the vestibular information.

ACKNOWLEDGMENTS

The authors thank Dr. Ellis Glazier for editing the English-language text.

GRANTS

This research was partially supported by Consejo Nacional de Ciencia y Tecnología (CONACyT) Grant 35525-N to E. Soto and Grant VIEP-II84G01 to R. Vega. During this work A. Limón and C. Pérez were recipients of CONACyT fellowships 124156 and 185855.

REFERENCES

Adamson CL, Reid MA, Mo ZL, Bowne-English J, and Davis RL. Firing features and potassium channel content of murine spiral ganglion neurons vary with cochlear location. *J Comp Neurol* 447: 331–350, 2002.

Akita T and Kuba K. Functional triads consisting of ryanodine receptors, Ca^{2+} channels, and Ca^{2+}-activated K^+ channels in bullfrog sympathetic neurons, plastic modulation of action potential. *J Gen Physiol* 116: 697–720, 2000.

Armstrong CM and Gilly WF. Access resistance and space clamp problems associated with whole-cell patch clamping. *Methods Enzymol* 207: 100–122, 1992.

Annoni JM, Cochran SL, and Precht W. Pharmacology of the vestibular hair cell afferent fiber synapse in frog. *J Neurosci* 4: 2106–2116, 1984.

Baird RA, Desmadryl G, Fernández C, and Goldberg JM. The vestibular nerve of the chinchilla. II. Relation between afferent response properties and peripheral innervation patterns in the semicircular canals. *J Neurophysiol* 60: 182–203, 1988.

Brontë-Stewart HM and Lisberger SG. Physiological properties of vestibular primary afferents that mediate motor learning and normal performance of the vestibuloocular reflex in monkeys. *J Neurosci* 14: 1290–1308, 1994.

Chabbert C, Chambard JM, Sans A, and Desmadryl G. Three types of depolarization-activated potassium currents in acutely isolated mouse vestibular neurons. *J Neurophysiol* 85: 1017–1026, 2001a.

Chabbert C, Chambard JM, Sans A, and Desmadryl G. Voltage-activated sodium currents in acutely isolated mouse vestibular neurones. *Neuroreport* 8: 1253–1256, 1997.

Chabbert C, Chambard JM, Valmier J, Sans A, and Desmadryl G. Hyperpolarization-activated (I_h) current in mouse vestibular primary neurons. *Neuroreport* 12: 2701–2704, 2001b.

Chambard JM, Chabbert C, Sans A, and Desmadryl G. Developmental changes in low and high voltage-activated calcium currents in acutely isolated mouse vestibular neurons. *J Physiol* 518: 141–149, 1999.

Cloues RK and Sather WA. Afterhyperpolarization regulates firing rate in neurons of the suprachiasmatic nucleus. *J Neurosci* 23: 1593–1604, 2003.

Curthoys IS. The development of function of horizontal semicircular canal primary neurons in the rat. *Brain Res* 167: 41–52, 1979.

Curthoys IS. Postnatal developmental changes in the response of rat primary horizontal semicircular canal neurons to sinusoidal angular accelerations. *Exp Brain Res* 47: 295–300, 1982.

Davies PJ, Ireland DR, and Mc Lachlan EM. Sources of Ca^{2+} for different Ca^{2+}-activated K^+ conductances in neurones of the rat superior cervical ganglion. *J Physiol* 495: 353–366, 1996.

Davis RL. Differential distribution of potassium channels in acutely demyelinated primary-auditory neuron in vitro. *J Neurophysiol* 76: 438–447, 1996.

Demêmes D, Raymond J, Atger P, Grill C, Winsky L, and Dechesne C. Identification of neuron subpopulations in the rat vestibular ganglion by calbindin-D 28 K, calretinin and neurofilament proteins immunoreactivity. *Brain Res* 582: 168–172, 1992.

Desmadryl G, Chambard JM, Valmier J, and Sans A. Multiple voltage-dependent calcium currents in acutely isolated mouse vestibular neurons. *Neuroscience* 78: 511–522, 1997.

Dopico AM, Widnier H, Wang G, Lemos JR, and Treistman SN. Rat supraoptic magnocellular neurones show distinct large conductance, Ca^{2+}-activated K^+ channel subtypes in cell bodies versus nerve endings. *J Physiol* 519: 101–114, 1999.

Duncan RK and Fuchs PA. Variation in large-conductance, calcium-activated potassium channels from hair cells along the chicken basilar papilla. *J Physiol* 547: 357–371, 2003.

Dutia MB and Johnston AR. Development of action potentials and apamin sensitive after-potentials in mouse vestibular nucleus neurones. *Exp Brain Res* 118: 148–154, 1998.

El Manira A, Tegner J, and Grillner S. Calcium-dependent potassium channels play a critical role for burst termination in the locomotor network in lamprey. *J Neurophysiol* 72: 1852–1861, 1994.

Emgard M, Blomgren K, and Brundin P. Characterization of cell damage and death in embryonic mesencephalic tissue: a study on ultrastructure, vital stains and protease activity. *Neuroscience* 115: 1177–1187, 2002.

Ezure K, Cohen M, and Wilson V. Response of cat semicircular afferents to sinusoidal polarizing currents: implications for input–output properties of second-order neurons. *J Neurophysiol* 49: 639–648, 1983.

Faber ES and Sah P. Physiological role of calcium-activated potassium currents in the rat lateral amygdala. *J Neurosci* 22: 1618–1622, 2002.

Fedulova SA, Kostyuk PG, and Veselovsky NS. Two types of calcium channels in the somatic membrane of new-born rat dorsal root ganglion neurones. *J Physiol* 359: 431–446, 1985.

Fernández C, Baird RA, and Goldberg JM. The vestibular nerve of the chinchilla. I. Peripheral innervation patterns in the horizontal and superior semicircular canals. *J Neurophysiol* 60: 167–181, 1988.

Fernández C, Lysakowski A, and Goldberg JM. Hair-cell counts and afferent innervation patterns in the cristae ampullares of the squirrel monkey with comparison to the chinchilla. *J Neurophysiol* 73: 1253–1269, 1995.

Galvez A, Gimenez-Gallego G, Reuben JP, Roy-Contancin L, Feigenbaum P, Kaczorowski GJ, and Garcia ML. Purification and characterization of a unique potent peptidyl probe for the high conductance calcium activated potassium channel from the venom of the scorpion *Buthus talamus*. *J Biol Chem* 265: 11083–11090, 1990.

García-Pérez E, Vargas-Caballero M, Velazquez-Ulloa N, Minzoni A, and De-Miguel FF. Synaptic integration in electrically coupled neurons. *Biophys J* 86: 646–655, 2004.

Gauck V, Thomann M, Jaeger D, and Borst A. Spatial distribution of low- and high-voltage-activated calcium currents in neurons of the deep cerebellar nuclei. *J Neurosci* 21: RC158, 2001.

Gebremedhin D, Yamaura K, Zhang C, Bylund J, Koehler RC, and Harder DR. Metabotropic glutamate receptor activation enhances the activities of two types of Ca^{2+}-activated K^+ channels in rat hippocampal astrocytes. *J Neurosci* 23: 1678–1687, 2003.

Giangiacomo KM, Garcia ML, and McManus OB. Mechanism of iberiotoxin block of the large-conductance calcium-activated potassium channel from bovine aortic smooth muscle. *Biochemistry* 31: 6719–6727, 1992.

Goldberg JM. Afferent diversity and the organization of central vestibular pathways. *Exp Brain Res* 130: 277–297, 2000.

Goldberg JM and Fernández C. Physiology of peripheral neurons innervating semicircular canals of the squirrel monkey. 3. Variations among units in their discharge properties. *J Neurophysiol* 34: 676–684, 1971.

Goldberg JM, Highstein SM, Moschovakis AK, and Fernández C. Inputs from regularly and irregularly discharging vestibular nerve afferents to secondary neurons in the vestibular nuclei of the squirrel monkey. I. An electrophysiological analysis. *J Neurophysiol* 58: 700–718, 1987.

Golding NL, Jung H, Mickus T, and Spruston N. Dendritic calcium spike initiation and repolarization are controlled by distinct potassium channel subtypes in CA1 pyramidal neurons. *J Neurosci* 18: 8789–8798, 1999.

Grissmer S, Nguyen A, and Cahalan MD. Calcium-activated potassium channels in resting and activated human T lynfocytes. Expression levels, calcium dependence, ion selectivity and pharmacology. *J Gen Physiol* 102: 601–630, 1993.

Herrington J, Park YB, Babcock DF, and Hille B. Dominant role of mitochondria in clearance of large Ca^{2+} loads from rat adrenal chromaffin cells. *Neuron* 16: 219–228, 1996.

Honrubia V, Hoffman LF, Sitko S, and Schwartz IR. Anatomic and physiological correlates in the bullfrog vestibular nerve. *J Neurophysiol* 61: 688–701, 1989.

Hu H, Shao LR, Chavoshy S, Gu N, Trieb M, Behrens R, Laake P, Pongs O, Knaus HG, Ottersen OP, and Storm JF. Presynaptic Ca^{2+}-activated K^+ channels in glutamatergic hippocampal terminals and their role in spike repolarization and regulation of neurotransmitter release. *J Neurosci* 21: 9585–9597, 2001.

Hugues M, Romey G, Duval D, Vincent JP, and Lazdunski M. Apamin as a selective blocker of the calcium-dependent potassium channel in neuroblastoma cells: voltage-clamp and biochemical characterization of the toxin receptor. *Proc Natl Acad Sci USA* 79: 1308–1312, 1982.

Jensen BS, Strøbæck D, Olesen SP, and Christophersen P. The Ca^{2+}-activated K^+ channel of intermediate conductance: a molecular target for novel treatments? *Curr Drug Targets* 2: 401–422, 2001.

Johnston AR, MacLeod NK, and Dutia MB. Ionic conductances contributing to spike repolarization and afterpotentials in rat vestibular nucleus neurones. *J Physiol* 15: 61–77, 1994.

Kaczorowski GJ and Garcia ML. Pharmacology of voltage gated and calcium-activated potassium channels. *Curr Opin Chem Biol* 3: 448–458, 1999.

Kang J, Huguenard JR, and Prince DA. Development of BK channels in neocortical pyramidal neurons. *J Neurophysiol* 76: 188–198, 1996.

Kevetter GA and Leonard RB. Molecular probes of the vestibular nerve. II. Characterization of neurons in Scarpa's ganglion to determine separate populations within the nerve. *Brain Res* 928: 18–29, 2002.

Koyama S, Kanemitsu Y, and Weight FF. Spontaneous activity and properties of two types of principal neurons from the ventral tegmental area of rat. *J Neurophysiol* 93: 3282–3293, 2005.

Lambert RC, Maulet Y, Mouton J, Beattie R, Volsen S, De Waard M, and Feltz A. T-type Ca^{2+} current properties are not modified by Ca^{2-} channel β subunit depletion in nodosus ganglion neurons. *J Neurosci* 17: 6621–6628, 1997.

Leger JF, Stern EA, Aertsen A, and Heck D. Synaptic integration in rat frontal cortex shaped by network activity. *J Neurophysiol* 93: 281–293, 2005.

Leonard RB and Kevetter GA. Molecular probes of the vestibular nerve. I. Peripheral termination patterns of calretinin, calbindin and peripherin containing fibers. *Brain Res* 928: 8–17, 2002.

Limón A, Pérez C, Vega R, and Soto E. Intrinsic properties of vestibular primary afferent neurons in culture. *Soc Neurosci Abstr* 702.7, 2003.

Lysakowski A, Minor LB, Fernández C, and Goldberg JM. Physiological identification of morphologically distinct afferent classes innervating the crista ampullares of the squirrel monkey. *J Neurophysiol* 73: 1270–1281, 1995.

Marcotti W, Johnson SL, and Kros CJ. Effects of intracellular stores and extracellular Ca^{2+} on Ca^{2+}-activated K^+ currents in mature mouse inner hair cells. *J Physiol* 557: 613–633, 2004.

Meera P, Wallner M, and Toro L. A neuronal β subunit (KCNMB4) makes the large conductance, voltage- and Ca^{2+}-activated K^+ channel resistant to charybdotoxin and iberiotoxin. *Proc Natl Acad Sci USA* 97: 5562–5567, 2000.

Myers SF and Lewis ER. Hair cell tufts and afferent innervation of the bullfrog crista ampullaris. *Brain Res* 534: 15–24, 1990.

Perez-Reyes E. Molecular physiology of low-voltage-activated T-type calcium channels. *Physiol Rev* 83: 117–161, 2003.

Peusner KD and Giaume C. Ontogeny of electrophysiological properties and dendritic pattern in second-order chick vestibular neurons. *J Comp Neurol* 384: 621–633, 1997.

Pouille F, Cavelier P, Desplantez T, Beekenkamp H, Craig PJ, Beattie RE, Volsen SG, and Bossu JL. Dendro-somatic distribution of calcium-mediated electrogenesis in Purkinje cells from rat cerebellar slice cultures. *J Physiol* 527: 265–282, 2000.

Ricci AJ, Gray-Keller M, and Fettiplace R. Tonotopic variations of calcium signaling in turtle auditory hair cells. *J Physiol* 524: 423–436, 2000.

Robitaille R, Garcia ML, Kaczorowski GJ, and Charlton MP. Functional colocalization of calcium and calcium-gated potassium channels in control of transmitter release. *Neuron* 11: 645–655, 1993.

Sah P. Ca^{2+}-activated K^+ currents in neurones: types, physiological roles and modulation. *Trends Neurosci* 19: 150–154, 1996.

Sah P and Faber ES. Channels underlying neuronal calcium-activated potassium currents. *Prog Neurobiol* 66: 345–353, 2002.

Santos-Sacchi J. Voltage-dependent ionic conductances of type I spiral ganglion cells from the guinea pig inner ear. *J Neurosci* 13: 3599–3611, 1993.

Sculptoreanu A, Yoshimura N, and de Groat WC. KW-7158[(2s)-(+)-3,3,3-trifluoro-2-hydroxy-2-methyl-N-(5,5,10-trioxo-4,10-dihydrothienol[3,2-c][1]benzothiepin-9-yl) propanamide] enhances A-type K^+ currents in neurons of the dorsal root ganglion of the adult rat. *J Pharmacol Exp Ther* 310: 159–168, 2004.

Si X, Zakir M, and Dickman JD. Afferent innervation of the utricular macula in pigeons. *J Neurophysiol* 89: 1660–1677, 2003.

Smith CE and Goldberg JM. A stochastic afterhyperpolarization model of repetitive activity in vestibular afferents. *Biol Cybern* 54: 41–51, 1986.

Smith MR, Nelson AB, and DuLac S. Regulation of firing response gain by calcium dependent mechanisms in vestibular nucleus neurones. *J Neurophysiol* 87: 2031–2042, 2002.

Soto E, Limón A, Ortega A, and Vega R. Características morfológicas y electrofisiológicas de las neuronas del ganglio vestibular en cultivo. *Gac Med Mex* 138: 1–13, 2002.

Soto E and Vega R. Actions of excitatory amino acids agonists and antagonists on the primary afferents of the vestibular system of the axolotl (*Ambystoma mexicanum*). *Brain Res* 462: 104–111, 1988.

Spreadbury IC, Kros CJ, and Meech RW. Effects of trypsin on large-conductance Ca^{2+}-activated K^+ channels of guinea-pig outer hair cells. *Hear Res* 190: 115–127, 2004.

Stansfeld CE, Marsh SJ, Halliwell JV, and Brown DA. 4-Aminopyridine and dendrotoxin induce repetitive firing in rat visceral sensory neurons by blocking a slowly inactivating outward current. *Neurosci Lett* 64: 299–304, 1986.

Starr PA and Sewell WF. Neurotransmitter release from hair cells and its blockade by glutamate-receptor antagonists. *Hear Res* 52: 23–41, 1991.

Thayer SA and Miller RJ. Regulation of the intracellular free calcium concentration in single rat dorsal root ganglion neurones in vitro. *J Physiol* 425: 85–115, 1990.

Toesca A. Central and peripheral myelin in the rat cochlear and vestibular nerves. *Neurosci Lett* 221: 21–24, 1997.

Yamashita M and Ohmori H. Synaptic responses to mechanical stimulation in calyceal and bouton type vestibular afferents studied in an isolated preparation of semicircular canal ampullae of chicken. *Exp Brain Res* 80: 475–488, 1990.

Neuroscience 158 (2009) 1662–1674

THE MUSCARINIC INHIBITION OF THE POTASSIUM M-CURRENT MODULATES THE ACTION-POTENTIAL DISCHARGE IN THE VESTIBULAR PRIMARY-AFFERENT NEURONS OF THE RAT

C. PÉREZ, A. LIMÓN,[1] R. VEGA AND E. SOTO*

Instituto de Fisiología, Universidad Autónoma de Puebla, BUAP, Apartado Postal 406, Puc. 72000, Puebla, Mexico

Abstract—There is consensus that muscarinic and nicotinic receptors expressed in vestibular hair cells and afferent neurons are involved in the efferent modulation of the electrical activity of the afferent neurons. However the underlying mechanisms of postsynaptic control in neurons are not well understood. In our work we show that the activation of muscarinic receptors in the vestibular neurons modulates the potassium M-current modifying the activity of afferent neurons.

Whole-cell patch-clamp recordings were made on vestibular-afferent neurons isolated from Wistar rats (postnatal days 7–10) and held in primary culture (18–24 h). The M-current was studied during its deactivation after depolarizing voltage-clamp pulses. In 68% of the cells studied, those of larger capacitance, the M-current antagonists linopirdine and XE-991 reduced the amplitude of the M-current by 54%±7% and 50%±3%. The muscarinic-receptor agonist oxotremorine-M also significantly reduced the M-current by 58%±12% in the cells. The action of oxotremorine-M was blocked by atropine, thus indicating its cholinergic nature. The erg-channel blocker E-4031 did not significantly modify the M-current amplitude. In current-clamp experiments, linopirdine, XE-991, and oxotremorine-M modified the discharge response to current pulses from single spike to multiple spiking, reducing the adaptation of the electrical discharge. Our results indicate that large soma-size cultured vestibular-afferent neurons (most probably calyx-bearing neurons) express the M-current and that the modulation of this current by activation of muscarinic-receptor reduces its spike-frequency adaptation.

Key words: efferent synapse, KCNQ, linopirdine, XE-991, E4031, muscarinic receptors.

Vestibular-afferent neurons have significant differences in their intrinsic properties, producing heterogenous electrical response patterns and coding properties. Outward potassium currents play a significant role in determining the electrical properties in these neurons. Vestibular neurons express at least three different types of voltage-gated K^+ currents and a calcium-dependent K^+ current (I_{KCa}) characterized in the rat vestibule and that is composed of four conductance subtypes; 1) big conductance current (BK) sensitive to iberiotoxin (IbTx), 2) small conductance current (SK) sensitive to apamin, 3) intermediate conductance current (IK) sensitive to clotrimazole (CLT) and charibdotoxin (ChTx), and 4) a resistant current (IR) (Limón et al., 2005). The three voltage-gated K^+ currents were characterized in postnatal-mouse vestibular neurons on the basis of their pharmacology as a tetraethylammonium (TEA) sensitive current, 4-aminopyridine (4-AP)-(0.5 mM) and α-dendrotoxin sensitive current, and 4-AP-(2 mM) and blood-depressing-substance sensitive current (Chabbert et al., 2001a; Risner and Holt, 2006).

Outside the vestibule, the M-current ($I_{K,M}$) has been characterized as a low-threshold, voltage-gated K^+ current that is active around the resting membrane-potential and constitutes an important regulator of neuronal excitability by tuning the membrane potential about the threshold level and participating in the spike-frequency adaptation (Brown and Adams, 1980; Constanti and Brown, 1981; Aiken et al., 1995). The $I_{K,M}$ is produced by K^+ channel subunits, particularly KCNQ2-KCNQ3 and KCNQ3-KCNQ5 heteromers (Schroeder et al., 2000; Lerche et al., 2000) and KCNQ4 homomers (Søgaard et al., 2001). The ether-a-go-go-related gene (erg) particularly erg1–erg2 heteromers (Meves et al., 1999; Selyanko et al., 2002) may also give rise to M-like currents. Typically, the $I_{K,M}$ is modulated by the activation of G protein–coupled receptors, including muscarinic receptors (hence its name $I_{K,M}$) (Brown and Adams, 1980; Robbins, 2001).

In rodents the KCNQ1 channels are expressed on the apical surface of the dark cells of the vestibular system (Shen and Marcus, 1998). The KCNQ3 and KCNQ5 subunits are present in hair cells and KCNQ5 is also expressed in supporting cells and in calyceal afferents (Hurley et al., 2006). KCNQ4 subunits seem to be highly expressed in the inner ear structures and are present in afferent calyx-bearing vestibular-ganglion neurons and in type I and type II hair cells (Kharkovets et al., 2000; Hurley et al., 2006; Rocha-Sánchez et al., 2007; Holt et al., 2007). PCR products for all three erg subunits (erg1, erg2, and erg3) and for KCNQ3, KCNQ4, and KCNQ5 subunits in both the utricular epithelium and vestibular ganglion have also been reported; no KCNQ2 signal was detected in that study (Hurley et al., 2006). Herg immunoreactivity has been found in hair cells and on maturing calyces (after P4).

[1] Present address: Neurobiology and Behavior Department, University of California Irvine, 2205 McGaugh Hall, Irvine, CA 92617, USA.
*Corresponding author. Tel: +52-222-2295500x7316; fax: +52-222-2295500x7301.
E-mail address: esoto@siu.buap.mx or esoto2424@yahoo.com (E. Soto).
Abbreviations: AChE, acetylcholinesterase; AHP, afterhyperpolarization; E-4031, N-[4-[[1-[2-(6-methyl-2-pyridinyl)ethyl]-4-piperidinyl]carbonyl]phenyl] methanesulfonamide dihydrochloride; $I_{K(erg)}$, erg K^+ current; $I_{K,M}$, M-current; mAChR, muscarinic acetylcholine receptor; oxo-M, oxotremorine-M; P, postnatal day; R_m, cell-membrane resistance; XE-991, 10,10-bis(4-pyridinylmethyl)-9(10H)-anthracenone dihydrochloride; 4-AP, 4-aminopyridine.

0306-4522/09 © 2009 IBRO. Published by Elsevier Ltd. All rights reserved.
doi:10.1016/j.neuroscience.2008.11.023

Erg1 appeared more concentrated on afferent endings than on hair cells (Hurley et al., 2006). Because the KCNQ4 channels are highly expressed in calyx endings (Kharkovets et al., 2000, Hurley at al., 2006) and in the vestibular ganglia (Rocha-Sánchez et al., 2007), the possibility of KCNQ4-channel subunits being involved in producing an M-like potassium conductance remains open (Kubisch et al., 1999; Søgaard et al., 2001; Holt et al., 2007). Supporting this result, the deletion of KCNQ4 subunit resulted in loss of a low-voltage-activated potassium conductance ($G_{K,n}$) in the cochlear outer hair cells (Kharkovets et al., 2006).

Because the vestibular-system efferent synapses are thought to be cholinergic (Goldberg and Fernández, 1980; Kong et al., 1998) and the expression of nicotinic and muscarinic receptors has been reported in efferent synapses (Ishiyama et al., 1995, 1997; Wackym et al., 1996; Anderson et al., 1997), the expression of a M-like potassium conductance in hair cells and in afferent endings suggests that muscarinic acetylcholine receptors (mAChRs) may modulate the M-conductance by activation of signaling cascades, thereby regulating the gain of afferent neurons and hair cells (Hurley et al., 2006). In the vestibule the efferent terminals make synaptic contacts with the calyx-afferent endings and also with bouton endings (Lysakowski and Goldberg, 1997) and directly with type-II hair-cell bodies, thus influencing the afferent activity at the postsynaptic and presynaptic level (Goldberg and Fernández, 1980; Lysakowski and Goldberg, 1997; Holt et al., 2006). Although this work focuses on the $I_{K,M}$, the importance of the nicotinic receptors in the efferent modulation should be acknowledged (Anderson et al., 1997; Holt et al., 2006).

An important step toward elucidating modulatory mechanisms in the afferent neuron is to determine the functional expression and to study the characteristics of the $I_{K,M}$ that may participate in the cholinergic-efferent input to the vestibular-afferent neurons. To this end, we used primary cultures of vestibular-ganglion-afferent neurons from the rat and studied the $I_{K,M}$ and its participation in determining the discharge pattern of the afferent neurons.

Part of this work has been presented in abstract form (Soto et al., 2004; Pérez et al., 2005).

EXPERIMENTAL PROCEDURES

Experiments were made on young Wistar rats (postnatal days (P) 7–10) before myelinization of the cell body was established (Dechesne et al., 1987) and P25 to P30 rats, all of them supplied by the "Claude Bernard" animal house of the University of Puebla. Animal care and procedures were in accordance with the National Institutes of Health Guide for the Care and Use of Laboratory Animals and the Reglamento de la Ley General de Salud en Materia de Investigación para la Salud of the Secretaría de Salud of México. All experiments and procedures were reviewed and approved by the appropriate committee of the Institution. All efforts were made to minimize animal suffering and the number of animals used, as outlined in the "Guide to the Care and Use of Laboratory Animals" issued by the National Academy of Science, USA.

Isolation and culture of afferent neurons

Primary culture of the afferent neurons was previously described (Soto et al., 2002a; Limón et al., 2005). Briefly, the vestibular ganglia were dissected and placed in fresh L-15 tissue-culture medium, with added collagenase IA at 1.25 mg/mL (Sigma Chemicals, St. Louis, MO, USA) and porcine trypsin 1.25 mg/mL (USB, Cleveland, OH, USA) for 30 min at 37 °C. Then the tissue was mechanically dissociated and isolated cells were plated in 35-mm Nunclon™ tissue-culture Petri dishes (Nunc, Roskilde, Denmark) and maintained at 37 °C for 18–24 h in a 5% CO_2 tissue-culture incubator. All procedures were done in a tissue-culture room under a laminar flow hood (Nuaire, Plymouth, MN, USA) while maintaining strict aseptic procedures.

Voltage-clamp recording and data analysis of afferent neurons

Experiments were done at room temperature (23–25 °C) and cells were perfused with the corresponding extracellular solution (Table 1). Neurons maintained in culture for 18–24 h were recorded using the patch-clamp technique in the whole-cell voltage-clamp configuration. Patch-clamp pipettes were fabricated from 1.2-mm outside diameter borosilicate-glass capillary tubing (WPI, Sarasota, FL, USA) using a horizontal Flaming Brown micropipette puller (P80/PC Sutter Instruments, San Rafael, CA, USA). Patch-pipette resistance was 1–3 MΩ when filled with the intracellular solution. In some experiments (indicated), the perforated patch-clamp technique was used. For this, 260 μM amphotericin-B was added to the intracellular solution.

Data were recorded with an Axopatch 200B amplifier (Molecular Devices, Union City, CA, USA), the output of which was led to a 12-bit digital-analog converter (Digidata 1200, Molecular Devices) controlled by pClamp 9.0 software (Molecular Devices). The membrane capacitance (C_m) and series resistance (R_s) were measured on-line with the pClamp software. The current response

Table 1. Solution composition (in mM)

	KCl	KF	Choline-Cl	NaCl	$CdCl_2$	$MgCl_2$	$CaCl_2$	4-AP	Hepes	Glucose	EGTA	Mg-ATP	Na-GTP
Extracellular	5.4	—	—	140	—	1.2	3.6	—	10	10	—	—	—
Intracellular	140	—	—	10	—	—	0.134	—	5	—	10	2	1
Modified extracellular	—	5.4	130	—	0.3	1.2	1.8	10	10	30	—	—	—
Modified intracellular	—	140	10	—	—	—	0.134	—	5	—	10	2	1

The pH was adjusted for external solutions to 7.4 and for the internal solutions to 7.2, with osmolarity at 310 (external) and 300 mOsm (internal) measured by a vapor pressure osmometer (Wescor 5500, Logan, UT, USA).

Abbreviations: EGTA, ethylene glycol bis(2-aminoethyl ether)-N,N,N′N′-tetraacetic acid; Hepes, 4-(2-hydroxyethyl)-1-piperazineethanesulfonic acid.

to a −10 mV pulse from a holding potential of −70 mV, filters completely open, was always acquired off-line for the C_m and R_s evaluation of the stability of recordings. During the recordings, C_m and R_s (≈80%) were electronically compensated. Data were low-pass filtered at 2 kHz and sampled at 5 kHz. The junction potential was calculated with the generalized Henderson liquid-junction-potential equation using pClamp software (Molecular Devices). Voltages were not corrected for either liquid-junction potential (less than 3 mV in our experimental conditions) or uncompensated R_s <5 MΩ. Clampfit 9.0 (Molecular Devices) and Origin 6.0 (Microcal Software, Inc., Northampton, MA, USA) were used for the analysis and fitting of ionic currents.

Initially we studied the concentration–response relationships for the $I_{K,M}$ antagonists linopirdine and XE-991. For these experiments we used modified intra- and extracellular solutions (Table 1) and the currents were caused with pulses to 30 mV and a duration of 400 ms departing from a holding potential (V_H) of −60 mV. For the concentration–response relationships, the ionic-current amplitude was normalized as a percent change compared with the control condition, with the mean and the standard error calculated from these values. Results from many cells were pooled because no single cell could be studied at all the concentrations tested.

Concentration–response curves were approximated with the equation

$$f(x)=R_{min}\frac{R_{max}-R_{min}}{1+10^{((\log IC_{50}-C)H}}$$

where R_{max} and R_{min} are the maximum and minimum effect, C is the drug concentration, IC_{50} is the concentration of the drug causing a half-maximum response, and H is the Hill number.

To study the effect of various drugs on the $I_{K,M}$, its amplitude was investigated during its deactivation produced by a 1-s hyperpolarizing step to −60 mV and delivered from a holding potential of −20 mV. This protocol was used to take advantage of the slow deactivation time-course of the $I_{K,M}$. The deactivation-current amplitude was measured at −60 mV as the difference between the average of a 10-ms segment, taken 10–20 ms into the hyperpolarizing step, and the average during the last 20 ms of that step (Brown and Adams, 1980; Shapiro et al., 2000).

The mean chord conductance of the $I_{K,M}$ was calculated by measuring the tail current amplitudes at −60 mV measured after conditioning voltage steps of 10 mV with a duration of 1.6 s from −80 to −10 mV and a holding potential to −70 mV.

The erg K^+ current ($I_{K(erg)}$) was studied using tail currents at −120 mV caused from step potentials of 4 s from −80 to 0 mV. The activation curve of $I_{K(erg)}$ was constructed by plotting the normalized peak amplitude of tail currents against the pulse potential.

Conductances were normalized and approximated by a Boltzmann function

$$g_{ion}/g_{max}=1/\{1+e^{[(Vm-V1/2)/S]}\}$$

where g_{ion} is the conductance, g_{max} is the maximum conductance, V_m is the membrane potential, $V_{1/2}$ is the potential at which the half of the maximum current is reached, and S is the slope factor.

In some of the experiments, cells were also recorded in current-clamp conditions to study their membrane potential (V_m) and their responses to current injection and drug use. For these experiments filters were open to 10 kHz and square current pulses from −0.5 to 1 nA in 0.1 nA steps were generated using pClamp software. The cell-membrane resistance (R_m) was measured by using hyperpolarizing pulses. Because a significant inward current was seen in the majority of the afferent neurons, the measurement of the R_m was done using hyperpolarizing pulses from −60 to −80 mV, which is the most linear range of these neurons. Action-potential characteristics were measured using Clampfit 9.0 software and ad hoc software developed in our laboratory (Soto et al., 2000). For this, the voltage value of the threshold level was used as a reference point. The threshold was defined as the point where the second derivative of the recording is larger than the mean plus two times the standard deviation of the previous 30-ms recording (Soto et al., 2000). The amplitude of the action potential was defined as the peak action-potential value minus the threshold voltage. The action-potential duration was measured at 75% of the spike amplitude. The afterhyperpolarization (AHP) was measured as the difference between the minimum voltage after the action potential and the membrane potential, and the AHP slope was obtained by a linear fit of voltage trajectory after the minimum voltage (Soto et al., 2000).

The Student's *t*-test was used to assess statistical significance, with $P<0.05$ indicating a significant difference. Numerical results are shown as mean±standard error of the mean (S.E.), except where standard deviation (*s*) is stated.

Solutions used

The recording chamber was continuously perfused by gravity-fed normal extracellular solution or modified extracellular solution as indicated (Table 1).

To construct the concentration–response relationship of linopirdine and XE-991, KCl was replaced with KF to block the Ca^{2+} and Ca^{2+}-activated K^+ currents (Bertollini et al., 1994).

Drugs

Cells in the recording chamber were perfused with the corresponding extracellular solution using a system of square tubes mounted in a step motor (Warner SF-77B, Hamden, CT, USA) and connected to a set of mechanical microsyringes (Baby Bee, BAS, West Lafayette, IN, USA). The flow rate was adjusted to 20 μL/min. When more than one drug was used, sufficient time was allowed to wash off the previous drug. No drug was used until the current returned to the control level. Linopirdine, 4-AP, atropine, oxotremorine-M (oxo-M), E-4031, and amphotericine-B were from Sigma Chemicals Co. and XE-991 was from Tocris-Cookson, Inc. (Ellisville, MO, USA). Aliquots of stock solution in deionized water were prepared and stored in a freezer. Linopirdine was diluted in DMSO (final concentration of DMSO was 0.01%). The aliquots were dissolved in the appropriate perfusion solution before the experiment.

RESULTS

Vestibular-afferent neurons of the rat in culture were identified by their birefringent round or ovoid somata under phase-contrast optics. Because there is a linear correlation between the soma diameter and the capacitance of the membrane for neurons maintained in primary culture between 18 and 24 h ($r=0.92$; Limón et al., 2005) we used the capacitance as an indirect measure of the soma diameter. In normal extra- and intracellular solutions (Table 1), the cultured afferent neurons ($n=101$) had a C_m=37 pF (s=13 pF; range=12–72 pF), R_m of 285 MΩ (s=153 MΩ; range=36–980 MΩ), and V_m=−59 mV (s=6 mV; range=−45 to −76 mV).

Actions of linopirdine and XE-991 on the $I_{K,M}$

To determine whether an $I_{K,M}$ conductance was present in the outward current of vestibular-afferent neurons, we used a depolarizing voltage step from −60 mV to 30 mV, with modified extracellular and intracellular solutions (Table 1) used to isolate the $I_{K,M}$, from other K^+ conduc-

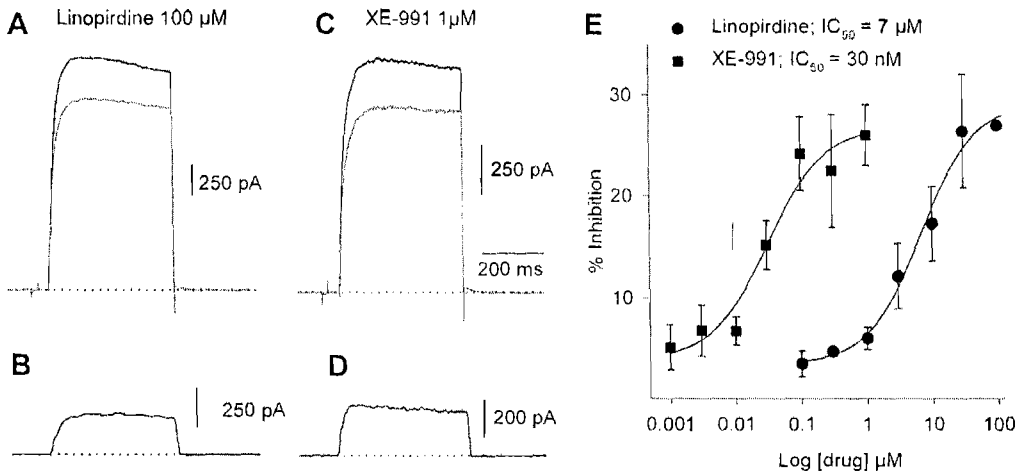

Fig. 1. The linopirdine and XE-991 sensitive current. (A, C) Use of 100 μM linopirdine and 1 μM XE-991 inhibited the outward current by about 20%. (B, D) Linopirdine and XE-991 sensitive currents were obtained by subtraction of the current after drug use from the control current. (E) The concentration–response curve for the linopirdine and XE-991 inhibition of the outward ionic current (linopirdine, n=4–6; XE-991, n=3–8). Currents were recorded using modified solutions (Table 1) and were caused by a 400-ms pulse to 30 mV from a holding potential of −60 mV. In this and the following graphs the points represent the mean±S.E. (standard error of the mean) and the dotted lines represent zero current or 0 mV.

tances. Linopirdine and XE-991 were used as $I_{K,M}$ antagonists (Lamas et al., 1997; Wang et al., 1998). Linopirdine (0.1 μM to 100 μM) and XE-991 (1 nM to 1 μM) caused a concentration-dependent inhibition of the outward current in 78% (n=18, Fig. 1A, B) and in 82% (n=17, Fig. 1C, D) of the cells. In the remaining cells, linopirdine (n=4) and XE-991 (n=3) had no significant effects (P>0.05). The current sensitive to linopirdine or to XE-991 showed no significant inactivation (Fig. 1B, D). The capacitance of the neurons that were sensitive to linopirdine and XE-991 was significantly greater than the capacitance of nonsensitive cells (C_m=38±2 pF, n=28 compared with C_m=26±3 pF, n=7; P=0.005). The inhibitory action of linopirdine and XE-991 on the outward current was fitted to a concentration–response curve with an IC_{50}=7 μM and H=1 and with an IC_{50}=30 nM and H=1 (Fig. 1E). As a control, normal extracellular solution with added 0.01% DMSO (used to dissolve linopirdine) was also ejected from the perfusion system, having no effect in any of the cases studied (n=5, data not shown).

Based on the inhibitory effect obtained for linopirdine and XE-991, we decided to study the action of 10 μM linopirdine and 1 μM XE-991 on the classic $I_{K,M}$-deactivation voltage-clamp protocol using normal extra- and intracellular solutions because no participation of other currents is expected to occur during the deactivation protocol (Brown and Adams, 1980; Adams et al., 1982; Shapiro et al., 2000). The concentration of XE-991 that was used was saturating (1 μM), but for linopirdine it was nonsaturating to avoid potential nonspecific actions on other K^+ currents (Schnee and Brown, 1998). The $I_{K,M}$ density was 4±0.4 pA/pF (n=20). Typically, current traces replicated $I_{K,M}$ deactivation properties (Wang et al., 1998), i.e. the current activation was near −60 mV and the deactivation kinetics were fitted with a double exponential function with time constants at −60 mV of τ_{fast}=76±4 ms and τ_{slow}=789±70 ms (n=20). Double-exponential deactivation kinetics may reflect differences in the KCNQ subunit composition of the $I_{K,M}$ or that it is formed by KCNQ and erg channels (Meves et al., 1999; Selyanko et al., 1999, 2002; Wang et al., 1998).

Perfusion with 10 μM linopirdine inhibited the $I_{K,M}$ amplitude measured during its deactivation by 54%±7% in six cells (n=10) with a mean capacitance of 44±4 pF (Fig. 2A). In the remaining cells, with a mean capacitance of 24±4 pF the inhibition was 19%±2%. The difference in sensitivity between cells and the difference in capacitance were both significant (P=0.04 and P=0.02).

The conductance-voltage curve was calculated from tail currents at −60 mV after depolarizing voltage steps from a holding potential of −70 mV before and after using 10 μM linopirdine. A Boltzmann fit to the linopirdine-sensitive current records had a $V_{1/2}$=−47±2 mV and S=7±1 mV (n=5) (Fig. 2B).

The effect of XE-991 was similarly studied during the $I_{K,M}$ deactivation. Perfusion with 1 μM XE-991 inhibited its amplitude by 50%±3% in 12 cells (n=14) which have a mean capacitance of 45±3 pF (Fig. 3A). The two remaining cells showed smaller capacitance (C_m=24±8 pF) and the current measured in the deactivation was reduced by 10%±3% after perfusion of XE-991. The conductance-voltage curve for XE-991 was fitted with a Boltzmann function with $V_{1/2}$=−47±2 mV and S=8±2 mV (n=5) (Fig. 3B).

Actions of E-4031 on the $I_{K,M}$

It has been suggested that erg K^+ channels could also contribute to the $I_{K,M}$ (Selyanko et al., 1999). To determine if these channel subunits were present in the vestibular-afferent neurons, we used the methanesulfonanilide E-4031, a selective blocker of erg K^+ channels in submicromolar concentrations (Sanguinetti and Jurkiewicz, 1990; Shi et al., 1997; Meves et al., 1999).

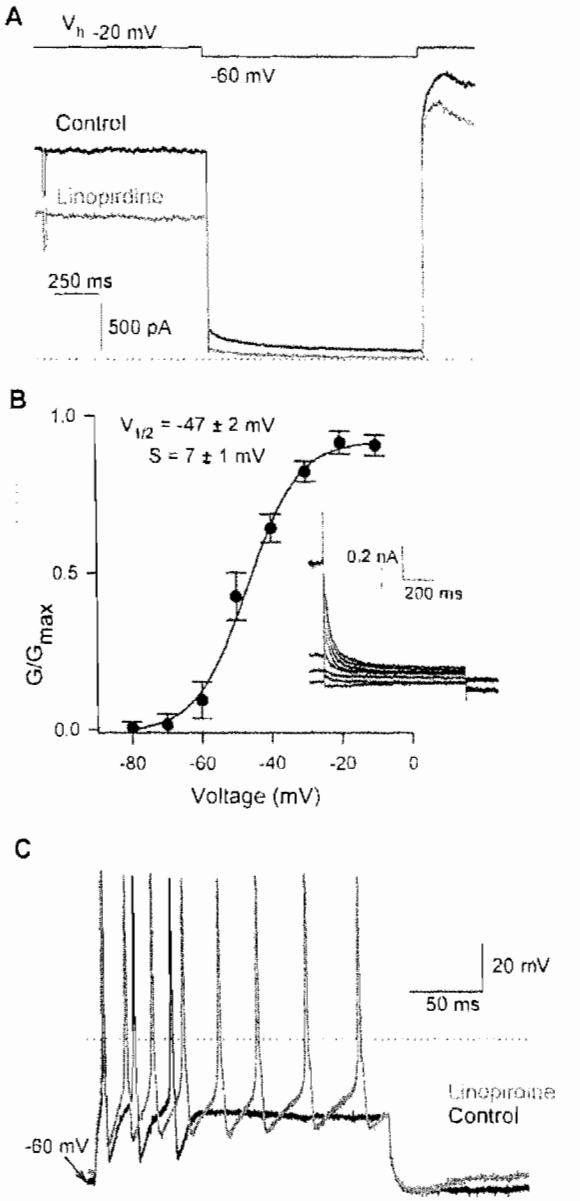

Fig. 2. The effect of linopirdine on the current deactivation, conductance, and firing frequency of vestibular-afferent neurons. (A) Current inhibition by 10 μM linopirdine was 55% (gray line) compared with the control (black line). (B) The normalized conductance of the 10 μM linopirdine-sensitive current. Inset recording shows a typical family of $I_{K,M}$ tails. (C) The response of an afferent neuron to a 0.3 nA, 200-ms current-pulse injection under control conditions (black line) and after 10 μM linopirdine use (gray line). The use of linopirdine converted the firing of afferent neurons from single-action potential discharge to multiple-action potential discharge (V_m = −60 to −56 mV) and also decreased the AHP.

The $I_{K(erg)}$ in vestibular-afferent neurons was identified and studied in normal solutions. Because of its rapid inactivation, the erg current $I_{K(erg)}$ was studied using tail currents at −120 mV caused from step potentials of 4 s from −80 to 0 mV. We observed a transient current mediated by erg channels (see below) and a slowly developing inward current most probably mediated by an I_h or I_{K1} current (Chabbert et al., 2001b; Soto et al., 2008). The erg-selective blocker E-4031 (100 nM) significantly inhibited the transient component without affecting the sustained one. The E-4031 sensitive current was obtained by subtraction (Fig. 4A). The E-4031 also inhibited the outward current, which could be generated by erg1 and erg2 subunits that give rise to a slowly activating, delayed rectifier

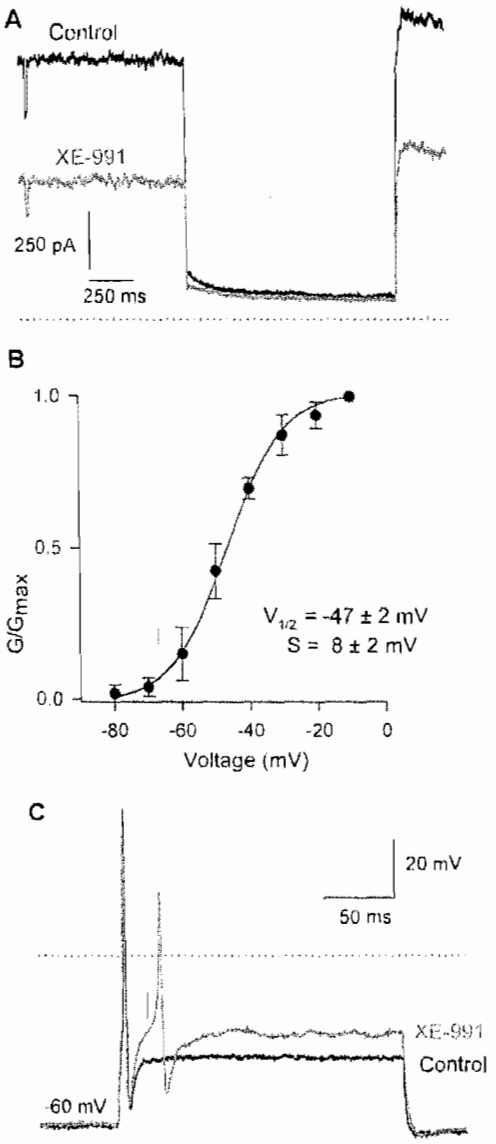

Fig. 3. The effect of XE-991 on the current deactivation, conductance, and firing frequency of the vestibular-afferent neurons. (A) The current deactivation under control conditions (black) and after use of 1 μM XE-991 (gray). XE-991 produced a 47% decrease of the current amplitude. (B) The conductance-voltage curve of the 1 μM XE-991-sensitive current. (C) The response of an afferent neuron (V_m = −60 mV) to a 0.3 nA, 200-ms current pulse injection under control conditions (black) and during the use of 1 μM XE-991 (gray).

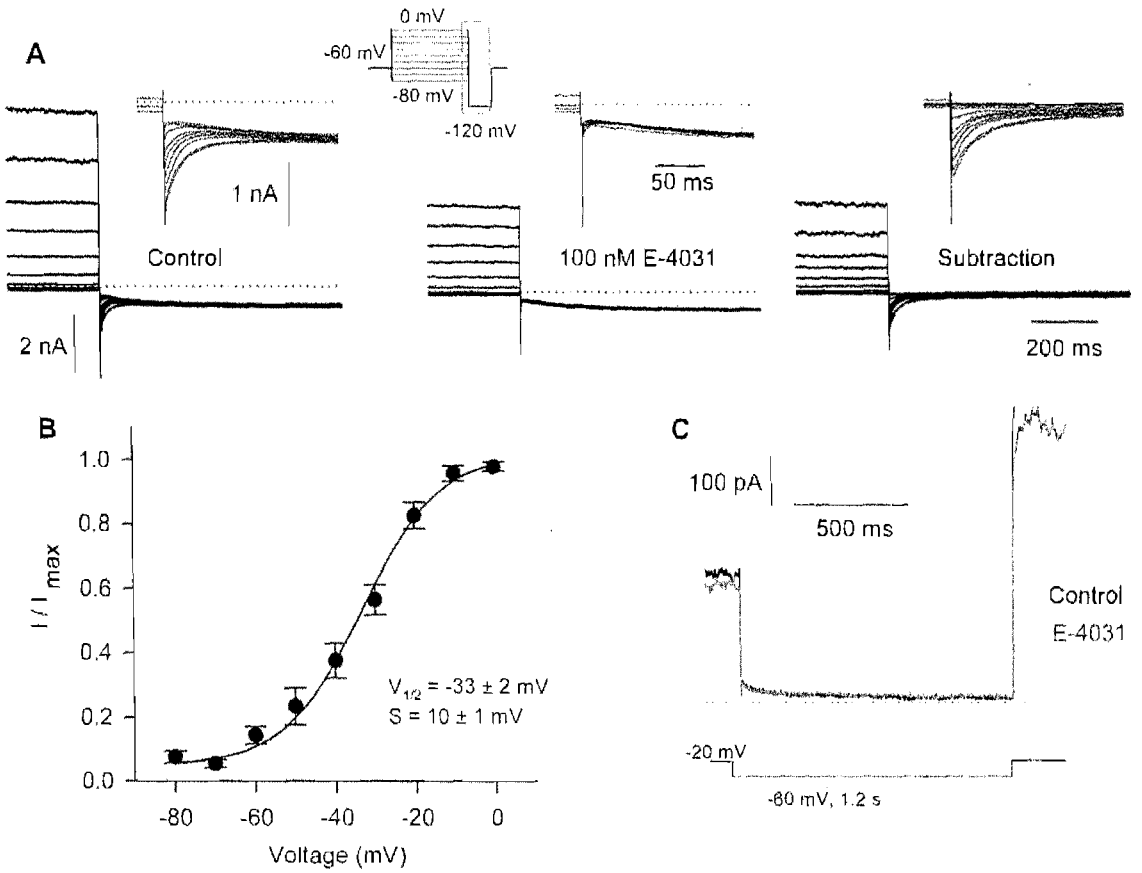

Fig. 4. The effect of the erg channel blocker E-4031. (A) The tail currents under control conditions (left), after 100 nM E-4031 (middle), and the E-4031-sensitive current obtained by subtraction (right). The voltage-clamp protocol used for obtaining tail currents is shown in the inset. (B) The activation curve of the E-4031-sensitive current. The current was measured in the tail currents. The continuous line represents the Boltzmann fit to the data with a $V_{1/2}=-33\pm2$ mV and an $S=10\pm1$ mV. (C) E-4031 did not significantly modify the current amplitude during deactivation.

current in *Xenopus* ovocytes (Shi et al., 1997). The activation curve of the $I_{K(erg)}$ was constructed by plotting the normalized peak amplitude of tail currents against the pulse potential. A Boltzmann function with a $V_{1/2}=-33\pm2$ mV and $S=10\pm1$ mV ($n=9$) best describes the relationship between activation of the $I_{K(erg)}$ and voltage (Fig. 4B). The $I_{K(erg)}$ was found in all the cells that were recorded. Its current density was not significantly different in cells expressing $I_{K,M}$ (erg current density $=24\pm2$ pA/pF; $C_m=46\pm5$ pF; $n=6$) and in those in which $I_{K,M}$ was low if expressed (erg current density $=32\pm12$ pA/pF; $C_m=28\pm1$ pF; $n=3$; $P=0.39$). Although the E-4031 blocked an outward current, the use of 100 nM E-4031 during the $I_{K,M}$ deactivation did not significantly modify the current amplitude ($n=4$) (Fig. 4C).

Effects of linopirdine, XE-991, and E-4031 on the response of afferent neurons to current pulses

The cultured vestibular-afferent neurons of the rat fire almost phasically, discharging one, and at most two, action potentials in response to sustained current injection (Limón et al., 2005; Mercado et al., 2006). This is in contrast with reports of vestibular-ganglion neurons in mice that have been shown to fire more than two action potentials in response to current injection (Risner and Holt, 2006). In five cells ($n=14$) with $C_m=49\pm4$ pF, 10 μM linopirdine reversibly converted the neuron's firing from a single-action potential discharge to a multiple-spike discharge with a mean spike discharge of 3.4 ± 1 action potentials (range 2–7) during a 200-ms current pulse (mean rate of 17 ± 5 impulses per second), slowly adapting during the whole current pulse. Linopirdine depolarized the membrane potential by 2 mV ($P=0.007$) without significantly affecting action-potential variables such as threshold, AHP amplitude, or duration (Fig. 2C). In another four cells, of this experimental series, with $C_m=34\pm4$ pF, linopirdine did not cause repetitive spiking but it depolarized the membrane potential from -60 ± 0.03 mV to -55 ± 2 mV ($P=0.042$) and reduced the AHP amplitude by 7 ± 2 mV. It also uncovered a postdepolarization after the first potential (not shown), but this was not great enough to generate a tonic discharge. In the remaining five cells with $C_m=28\pm2$ pF no significant effect of linopirdine was observed. The difference in the capacitance between cells sensitive and not sensitive to linopirdine was significant with $P=0.02$.

In 9 of 23 neurons (C_m=44±4 pF), 1 μM XE-991 converted the firing from a phasic, single-action potential discharge to a slowly-adapting repetitive discharge with a mean of 5±1 action potentials (range 2–13) during the 200-ms current pulse (mean rate of 26±7 impulses per second). XE-991 reduced the membrane potential from −59±0.4 mV to −52±2 mV, the AHP amplitude 5±1 mV, the action-potential amplitude 10±3 mV, and shifted the threshold from −28±1 mV to −24±1 mV without significantly affecting other action-potential parameters such as the AHP slope or duration. The actions of XE-991 on the spike discharge of afferent neurons were reversible after washout of the drug. In another six cells (C_m=41±2 pF), although XE-991 did not modify the neuron-discharge pattern, it depolarized the cells from −60±1 mV to −57±2 mV and decreased the action potential amplitude by 7±3 mV. In the remaining eight cells (C_m=28±4 pF) no significant effect of XE-991 was noted (Fig. 3C). The difference in the capacitance between cells sensitive and not sensitive to XE-991 was significant with P=0.006. Pooling together all the current-clamp experiments we found that cells responding to linopirdine and XE-991 have a C_m=43±2 pF (n=21), and cells not sensitive to these substances have a C_m=27±2 pF (n=12; P<0.001).

Under current-clamp conditions the perfusion of 100 nM E-4031 (n=7) did not modify the discharge rate, the membrane potential, the threshold voltage, or the action potential duration, although E-4031 decreased the AHP by 2±1 mV and the slope of AHP recovery by 0.4±0.1 ms. We consistently observed that 100 nM E-4031 significantly decreased the amplitude of the action potential from 50±4 mV to 42±5 mV (n=7; P=0.002; data not shown). This last effect is not related to the erg-blocking action of E-4031 and can be caused by a nonspecific action of E-4031 that was not further studied.

$I_{K,M}$ in mature cells

The efferent innervation in the rat vestibule develops during the first 2 weeks after birth (Demêmes et al., 2001). For this reason we made an experimental series in P25 to P30 rats to corroborate whether the $I_{K,M}$ is still present in mature cells. These experiments were limited because of the myelin sheet that at this developmental stage surrounds the majority of afferent neurons. However, in culture some of them lose their myelin sheet and were voltage clamped. These neurons had a C_m=30±2 pF, an R_m=276±27 MΩ, and a V_m=−59±2 mV (n=24). The perfusion of 1 μM XE-991 (n=9) decreased the $I_{K,M}$ amplitude by 36%±9% in eight of the recorded cells (with C_m=34±4 pF as compared with C_m=15 pF in the cell in which no effect was found). Incidentally, we observed that adult neurons showed a large hyperpolarization-activated inward current, which was not so evident in young rats (data not shown). The mean inward-current density in neurons from young P7 to P10 rats was 7±1 pA/pF (n=24), whereas that in neurons from adult P25 to P30 rats was 19±2 pA/pF (n=24). The difference in the inward-current density was significant with a P=0.0007. For the purpose of this study we did not further investigate the characteristics of this current.

In current clamp experiments, the use of 1 μM XE-991 significantly decreased the membrane potential from −57±0.2 to −54±1 mV, the threshold from −26±2 to −22±2 mV, the action-potential amplitude from 47±6 to 29±6 mV, and the AHP by 3±1 mV (n=6; P<0.05).

The oxo-M significantly hyperpolarized the membrane potential from −60±1 to −63±1 mV, reduced the action-potential amplitude from 57±3 to 50±3 mV, and increased the action-potential duration from 1±0.1 to 1.1±0.1 ms and the AHP by 2±2 mV. Additionally we observed that the oxo-M significantly decreased the membrane resistance from 145±22 to 80±17 MΩ (n=9; P=0.001), increased an instantaneous inward current from −0.69±0.2 to −1.6±0.3 nA, and decreased the inward component that activates slowly from −0.43±0.1 to −0.26±0.05 (n=8; P=0.001, data not shown).

Muscarinic inhibition of the $I_{K,M}$

We evaluated the sensitivity of the $I_{K,M}$ to oxo-M, a broad spectrum muscarinic-receptor agonist (Shapiro et al., 2000). Oxo-M (10 μM) inhibited, in a partially reversible fashion, the total outward current by 15%±2% in 7 of 10 cells (n=7; C_m=42±3 pF), having no significant effect in the remaining three cells (C_m=22±2 pF; P=0.001 for the capacitance differences). The oxo-M-sensitive current was obtained by subtraction of the current, after use of oxo-M, from the control current (Fig. 5A, B). The $I_{K,M}$ inhibition by oxo-M was prevented by 1 μM atropine (n=5; Fig. 5C). As expected, atropine by itself had no action on the current amplitude or kinetics (Fig. 5C). The effect of oxo-M was also studied in the $I_{K,M}$ deactivation protocol. In four of five cells (C_m=39±3 pF), 10 μM oxo-M reduced the current amplitude by 58%±12% (Fig. 5D). The conductance-voltage curve for the oxo-M-sensitive current was fitted with a Boltzmann function with $V_{1/2}$=−45±3 mV and S=7±2 mV. The action of oxo-M on the deactivation was completely blocked by the prior application of 1 μM atropine (n=4, data not shown). The action of oxo-M (10 μM) was also studied in perforated patch experiments (n=3). The time course, percentage of current inhibition, and current recovery were not significantly different than values observed with whole-cell experiments.

In current-clamp experiments, the use of 10 μM oxo-M increased the excitability in 3 of 16 cells (C_m=52±6 pF) converting the firing from single action potential discharge to a repetitive discharge with a mean discharge of 5±2 action potentials (range 2–8) during the 200-ms current pulse (mean rate of 23±8, n=3 impulses per second), slowly adapting during the whole current pulse (Fig. 5E) and moving the threshold by 6 mV (from −34 to −28 mV). In another four cells, oxo-M depolarized the membrane potential from −60±1 to −57±3 mV and decreased the AHP peak from −57±4 to −53±4 mV (P=0.04). In six cells the oxo-M hyperpolarized the membrane potential from −60±1 to −61±1 mV, the AHP peak decreased from −58±4 to −56±4 mV, and the AHP slope from 9±2 to 8±2 ms (P=0.048). The oxo-M sensitive cells had a C_m=36±4 pF (n=13). Oxo-M had no effect in 3 of 16 cells (C_m=28±5 pF; P=0.41 for the C_m differences). The sole

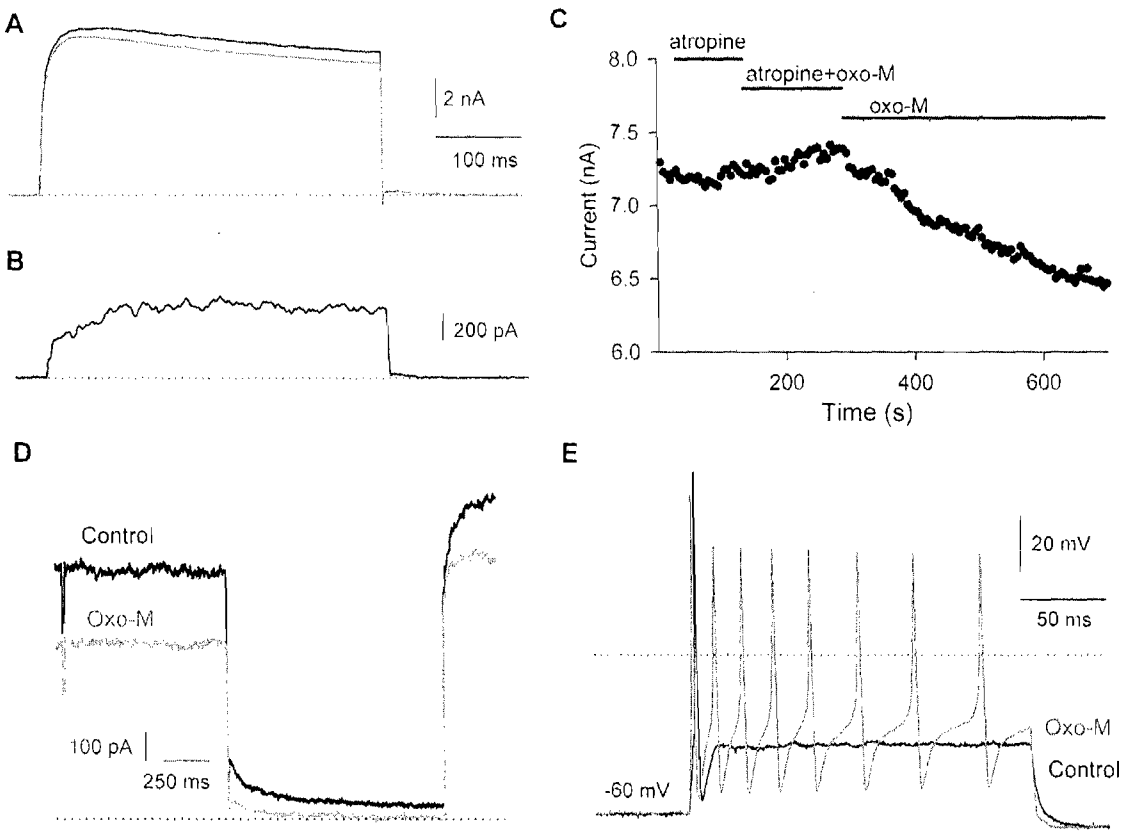

Fig. 5. Effects of oxo-M. (A) The outward current was caused by a 400-ms pulse to +30 mV from a holding potential of −60 mV. Oxo-M (10 μM) inhibited the outward current 8% (gray). (B) The oxo-M-sensitive current obtained by subtraction. (C) The time-course of current amplitude under control conditions, after use of 1 μM atropine, after coapplication of 1 μM atropine and 10 μM oxo-M, and after washout of atropine while oxo-M is still being perfused. (D) The current deactivation under control conditions (black) and after 10 μM oxo-M (gray). Oxo-M caused a 57% decrease of the current amplitude. (E) The response of an afferent neuron (V_m=−60 mV) to a 0.6 nA, 200-ms current pulse injection under control conditions (black) and after the use of 10 μM oxo-M (gray).

application of 10 μM oxo-M caused an action-potential discharge in two of nine cells. The coapplication of 1 μM atropine (n=7) prevented, in a reversible fashion, the generation of an action potential by oxo-M, with a depolarization of 5±2 mV detected in five cells and no effect in two cells (data not shown).

To define whether XE-991 and oxo-M target the same channels the deactivation of the $I_{K,M}$ was measured during the sequential co-application of oxo-M and XE-991. The initial perfusion of 1 μM XE-991 reduced the current amplitude by 51%±4% (n=5; P=0.03). The co-application of 10 μM oxo-M and XE-991 after 2 min of XE-991, produced non-significant additional effect (n=5; P=0.1) (data not shown). The application of 1 μM XE-991 also decreased the sustained current (at −20 mV) by 47%±9% (n=5; P=0.04). The co-perfusion of 10 μM oxo-M and XE-991 decreased the current by an additional 7%±2%, although this additive effect was not significant (n=5; P=0.08, compared with XE-991 effect).

In current clamp, 1 μM XE-991 increased the excitability in three of four cells converting the firing from a single action potential discharge to a repetitive discharge with a mean rate of 6±4 action potentials (range 2–13) during the 200-ms current pulse and depolarized the membrane potential from −60±0.5 to −52±2 mV. The co-application of 10 μM oxo-M and XE-991 after 2 min of XE-991, did not produce significant changes of membrane potential or of spike discharge rate (n=4; P=0.3).

Threshold, body size, and $I_{K,M}$ expression

A correlation analysis between the C_m and sensitivity to linopirdine, XE-991, or oxo-M showed that cells expressing the $I_{K,M}$ had a C_m of 42±1 pF (n=69), which value is significantly different from cells without the $I_{K,M}$ with a C_m of 26±1 pF (n=28; P<0.001; Fig. 6A). We also studied the correlation between the threshold, the C_m, and the expression of the $I_{K,M}$. For these experiments we held the membrane potential to +60 mV and pulses were given at various levels. Cells expressing the $I_{K,M}$ had lower membrane resistance than cells which did not express the $I_{K,M}$ (R_m=230±15 MΩ, n=69; versus R_m=411±28 MΩ, n=28; P<0.001; Fig. 6B). Because of differences in the R_m and the influence of the R_m in the cable properties of the

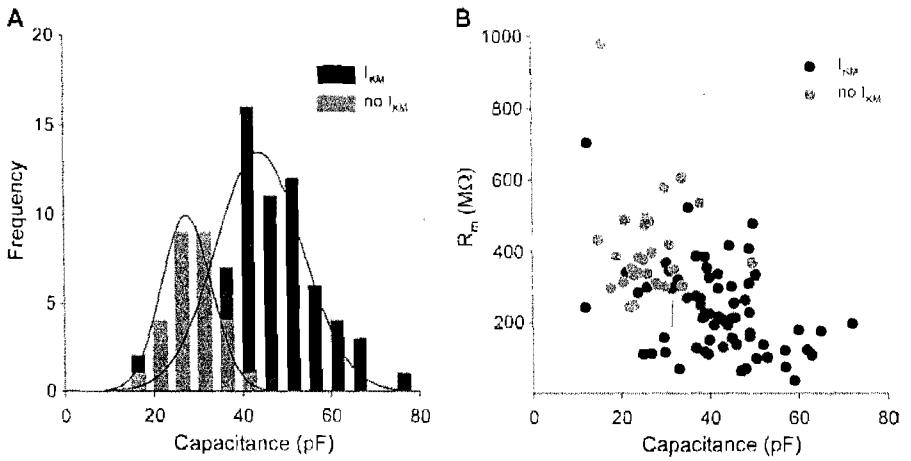

Fig. 6. The expression of the $I_{K,M}$ in vestibular-afferent neurons. (A) Histogram of the membrane capacitance of cells according to the expression of the $I_{K,M}$. Cells without the $I_{K,M}$ had a lower mean capacitance (26±1 pF) than that of cells with the $I_{K,M}$ (42±1 pF; $P<0.001$). The continuous line is the gaussian fit to data; $r=0.9$ and $r=0.99$. (B) Cells expressing the $I_{K,M}$ had a lower membrane resistance than cells that did not ($P=0.0001$, $r=0.13$).

neurons, the threshold to the first action potential was determined in two different ways; as a function of the minimum current needed to generate an action potential and as the voltage for the action-potential threshold (see Experimental Procedures). Though the former evaluation is highly influenced by the R_m, in the second the difference in the R_m between cells has little if any influence on the threshold. When the threshold was measured as current needed to cause an action potential, cells expressing the $I_{K,M}$ had a higher threshold (835±70 pA; $n=55$) than cells not expressing the $I_{K,M}$ (470±95 pA; $n=22$; $P=0.005$). When the threshold was measured as a function of the voltage, cells expressing the $I_{K,M}$ ($n=54$) showed a threshold 4 mV above those lacking the $I_{K,M}$ ($n=17$; $P=0.04$).

DISCUSSION

Our results indicate that vestibular-afferent neurons with larger size somata express a functional $I_{K,M}$. We found that the KCNQ-channel blockers linopirdine and XE-991 inhibit a slowly inactivating component of the outward current, present in the rat vestibular-afferent neurons and that the erg channel blocker E-4031 inhibits a transient inward rectifying component. Also oxo-M, a well-known muscarinic-receptor agonist, modulated this same component of the outward current whose voltage sensitivity and deactivation characteristics coincided with the $I_{K,M}$ properties (Brown and Adams, 1980; Constanti and Brown, 1981; Wang et al., 1998). Inhibition of the $I_{K,M}$ by linopirdine, XE-991, and oxo-M depolarized the membrane potential, reduced the AHP amplitude, reduced the spike-frequency adaptation, and converted the response of cultured vestibular-afferent neurons to current-pulse injection from a single-action potential discharge to a multiple-action potential discharge, indicating the role of the $I_{K,M}$ in the control of excitability of the vestibular-afferent neurons. The $I_{K,M}$ along with the 4-AP-sensitive A-type conductance seems the most influential in determining the repetitive discharge of vestibular-afferent neurons (Chabbert et al., 2001a; Limón et al., 2005; Risner and Holt, 2006).

Linopirdine and XE-991 used during the deactivation protocol reduced the deactivation current by about 50% whereas in other cells the decrease was between 10% and 19%. Notably these two sensitivities were only observed when the protocol of deactivation was used. In the other experiments no effect of the I_{KM} blockers in smaller cells was observed. The reduction of the current observed in the deactivation protocol might be related to changes in the outward currents by the small size of the cells and the long duration of the depolarizing pulses used in the deactivation protocol. Another possibility is that there is a lower participation of muscarinic receptors in small neurons because muscarinic receptors have been described in bouton terminal afferents (Li et al., 2007). Future experiments will clarify the role of muscarinic receptors in small neurons, if any.

Although linopirdine has a greater selectivity for the $I_{K,M}$ (10- to 20-fold) than for other voltage-gated currents, it may also block ligand-gated channels such as GABA and nicotinic receptors (Gómez-Casati et al., 2004). Despite this, in isolated cells linopirdine has been shown to be a useful tool to define the properties of the $I_{K,M}$ (Costa and Brown, 1997). In the vestibular-afferent neurons the inhibitory action of linopirdine on the $I_{K,M}$ ($IC_{50}=7$ μM) coincided with values reported for KCNQ2+3 heteromultimers of about 4 μM and is also similar to the $I_{K,M}$ sensitivity to linopirdine in the superior cervical ganglion (Lamas et al., 1997; Selyanko et al., 1999), compared with more than 200 μM for KCNQ3+4 and 15 μM for KCNQ3+5 (Robbins, 2001).

In our experiments XE-991 showed a greater potency to inhibit the $I_{K,M}$ than linopirdine ($IC_{50}=30$ nM). In general the IC_{50} of XE-991 action that we found is lower than that reported in other preparations such as the rat hippocampal slices and dorsal-root-ganglion neurons (Passmore et al.,

2003) and for KCNQ2+KCNQ3 expressed in *Xenopus* oocytes (Wang et al., 1998). The slow inactivation of the $I_{K,M}$ that we found resembled the one described for KCNQ3-type channels (Wang et al., 1998). These results are coherent with the idea of KCNQ3 heteromultimers as the predominant subunits involved in the expression of the $I_{K,M}$ in vestibular-afferent neurons.

The $I_{K,M}$ deactivation in vestibular-afferent neurons was fitted with two time-constants. This may be a consequence of subunit composition of the channel mediating the $I_{K,M}$ or caused by the participation of other channel subtypes (Marrion et al., 1992). The erg K^+ channels have been shown to shape the slow component of the $I_{K,M}$ in mammalian neuronal cells (Selyanko et al., 1999). In our experiments all the neurons expressed an erg-like component that was sensitive to E-4031. The E-4031 reduced the erg-like current with no significant modification of the $I_{K,M}$-deactivation amplitude and kinetics suggesting that erg channels most probably did not significantly contribute to the $I_{K,M}$ in the vestibular afferents. This coincides with the fact that E-4031 did not increase the spiking frequency in any of the cells studied. Also, probably because of the fast inactivation of erg currents, the E-4031 blockade is not able to increase spike frequency (Shi et al., 1997).

Our experiments were done on isolated neurons that have lost their axonal and dendritic projections. Since the efferent cholinergic synapses are known to contact the afferent dendritic endings under the hair cells (i.e. calyx and bouton afferent endings), our results imply that active muscarinic receptors and KCNQ channels are also co-expressed at the level of the cell body of the neurons after 18 h in culture. This also coincided with the fact that the soma express other voltage-activated ionic currents (i.e. Na^+, Ca^{2+}, Ca^{2+} activated K^+, I_h and I_{k1} inward rectifiers) (Soto et al., 2002a, 2008; Desmadryl et al., 1997; Limón et al., 2005; Chabbert et al., 2001b) and chemically gated currents (i.e. NMDA, AMPA-KA and ASIC) (Rabejac et al., 1997; Dayanithi et al., 2007; Mercado et al., 2006). The functional somatic expression of KCNQ channels has also been reported in hippocampal pyramidal cells (Gu et al., 2005) and interneurons (Lawrence et al., 2006), although previous work has shown that KCNQ is expressed in the calyceal nerve endings of the afferent neurons (Hurley et al., 2006). After dissociation and initial neurite outgrowth the cells may express all their set of conductances, and due to the fact that outgrowing neurites are close to the soma, they may be adequately registered at the soma level without space clamp problems. Preliminary evidence from our laboratory indicates that m1-muscarinic receptor immunoreactivity was evident in practically all the afferent neurons cell bodies of the rat either isolated or in the vestibular ganglion. Also KCNQ4 immunoreactivity can be detected in the cell body of most of the isolated afferent neurons (Tejeda-Muñoz, 2008). More studies are needed to clarify the cellular localization of KCNQ and other conductances in afferent neurons and how they may influence the spiking of these neurons (Lysakowski et al., 2008).

Vestibular efferent system

Studies of the expression of the mAChR subtypes (m1–m5) in the vestibular end organs and in the afferent vestibular-ganglion of the human and the rat using RT-PCR have shown that in humans, the m1, m2, and m5 mAChR subtypes were amplified from the ganglia and the vestibular end organs, whereas in the rat all five mAChR subtypes were expressed (Wackym et al., 1996; Safieddine et al., 1996). These results indicate that the efferent cholinergic axo-dendritic and axo-somatic synapses have a muscarinic component (Lysakowski and Goldberg, 1997). The precise signal-transduction mechanism for the decrease of the $I_{K,M}$ after mAChR activation is not yet known. Inhibition of the $I_{K,M}$ follows the activation of N-ethylmaleimide (NEM) and the pertussis-toxin-insensitive G protein of the Gq-11 class (Caulfield et al., 1994). Intracellular ATP is required for recovery of the KCNQ2-KCNQ3 current from muscarinic suppression (Suh and Hille, 2002). In our experiments the action of oxo-M in perforated and in ruptured whole-cell currents was similar, suggesting that its effect is mediated by a nondiffusible membrane-associated messenger (Zhang et al., 2003). Also, the recovery of the $I_{K,M}$ after use of oxo-M, either in the whole cell or under perforated-patch conditions, was similar (>20 min), thus implying that in our experimental conditions there was a slow replenishment of PIP_2 or a related phosphoinositide that has been shown to mediate the reactivation of KCNQ currents after inhibition by oxo-M (Zhang et al., 2003; Suh and Hille, 2007).

We used an experimental model based on 24-h cultured neurons from P7 to P10 rats. At this developmental stage, type-I and type-II hair-cell populations in the rat are not yet completely differentiated (Dechesne et al., 1986). At P5, bouton and calyx endings are differentiated, at P8 ionic conductances are at mature levels (Rüsch et al., 1998), and at P10 the innervation pattern and sensitivity to externally applied galvanic currents are similar to those in adult animals (Desmadryl, 1991). Efferent innervation in the rat is mature 2 weeks after birth (Demêmes et al., 2001). In our experiments with cells obtained from P25 to P30 rats, the percentage of cells sensitive to XE-991 was greater than in P7–P10 cells, indicating that some changes in the set of channels expressed may have occurred with maturation of the afferent neurons. For example, a significant change in the characteristics of the inward rectifying current was observed in P25 to P30 neurons (Soto et al., 2008).

From a functional point of view, the most consistent finding is that efferent stimulation produces an increase of the afferent firing rate in mammals (Goldberg and Fernández, 1980), although heterogeneous responses were observed in reptiles and anurans (Rossi and Martini, 1991; Brichta and Goldberg, 2000). Our results indicate that the $I_{K,M}$ inhibition, both by channel blockers such as linopirdine or XE-991 and by a muscarinic-receptor agonist such as oxo-M, produced an increase in neuron excitability. This will constitute a postsynaptic mechanism by which the efferent system may mediate its excitatory actions in ves-

tibular afferents (Marlinski et al., 2004). In the cochlea of the chick, the afferent neurons (that receive cholinergic efferent innervation from lateral olivo-cochlear efferent system) express an M-type K^+ current, which is suppressed by the application of ACh and carbamylcholine, presumably via the activation of protein kinase C (Yamaguchi and Ohmori, 1993). In the cochlear neurons isolated from the rat, the activation of mAChR mobilized intracellular Ca^{2+}, probably by interaction with m1 muscarinic receptors (Rome et al., 1999), and the stimulation of mAChR or ATP-receptors, activate a nonselective cationic conductance increasing the neural excitability (Ito and Dulon, 2002).

For vestibular calyx endings, direct, synaptic efferent-influence would be of great significance in determining their response properties. In particular, it has been suggested that the postsynaptic depolarization produced by the afferent neurotransmitter is supplemented by the K^+ ions that accumulate in the synaptic cleft (Goldberg, 1996; Soto et al., 2002b). Thus modifications of a sustained K^+ permeability such as the $I_{K,M}$ might have a significant impact on the calyx-ending neuron-discharge rate under physiological conditions where potential K^+-accumulation mechanisms are preserved (Hurley et al., 2006). Although efferent neurons contacting afferents with no calyx ending (bouton type) have been described (Lysakowski and Goldberg, 1997), there are no quantitative data about the occurrence of this type of synaptic contact that may correspond to dimorphic neuron-pertaining bouton endings. Based on the larger soma size of neurons with the $I_{K,M}$, we hypothesize that neurons resistant to linopirdine, XE-991, or oxo-M most probably are purely bouton-type afferent neurons that do not receive a cholinergic input from efferent fibers, although other possible explanations for the lack of response of smaller neurons are that they express alternative splice variants of KCNQ channels (Beisel et al., 2005; Rocha-Sánchez et al., 2007). It is known that KCNQ subunits have different sensitivities to channel blockers (Schroeder et al., 2000) and it is possible that the subunit composition may vary from large- to small-soma size vestibular-afferent neurons (Howard et al., 2007) or that smaller neurons would have been sensitive to drugs studied, if their terminals had been preserved, indicating a regionalization in channel expression. Alternatively, drugs used in this study may not be universal $I_{K,M}$ blockers. For example, some native $I_{K,M}$s resistant to XE-991 have been reported and XE-991 and linopirdine have been shown to have a voltage-dependent action, which may explain their lack of effect at hyperpolarized voltages (Romero et al., 2004).

In clinics, scopolamine, a competitive muscarinic antagonist, is one of the most effective drugs in preventing motion sickness and physostigmine, an AChE inhibitor, induces a motion sickness–like syndrome in humans (Wood et al., 1986). Whether the efficacy of scopolamine in motion sickness is mediated through peripheral and central pathways, or solely through central mechanisms is yet undetermined (Wackym et al., 1996; Ishiyama et al., 1997). Our results demonstrate that muscarinic-receptor activation inhibits the $I_{K,M}$ in a large proportion of vestibular-afferent neurons by increasing their gain. Then muscarinic receptor antagonists will reduce the afferent-neuron discharge, an effect that might significantly contribute to the clinical action of anticholinergic drugs in the vestibular-system-related symptoms. These results open the need to study the potential use of the $I_{K,M}$ modulators such as retigabine and linopirdine (Romero et al., 2004; Rivera-Arconada and López-García, 2005; Surti and Jan, 2005), which might have potential therapeutic value for the treatment of vestibular disorders.

Acknowledgments—The authors wish to thank Dr. Ellis Glazier for the editing of the English-language manuscript. This work was submitted in partial fulfillment of the requirements for the PhD degree of Cristina Pérez at the Posgrado en Ciencias Biomédicas, Instituto de Fisiología Celular, UNAM. This material is based on work supported by the Consejo Nacional de Ciencia y Tecnología, México (CONACyT) grant 46511 to E.S. and Vicerrectoría de Investigación (VIEP-BUAP)-CONACyT grants 20ISAL06-G and 20ISAL06-I to R.V. and E.S. A.L. and C.P. were supported by CONACyT fellowships 124156 and 185855.

REFERENCES

Adams PR, Brown DA, Constanti A (1982) M-currents and other potassium currents in bullfrog sympathetic neurons. J Physiol 330:537–572.

Aiken SP, Lampe BJ, Murphy PA, Brown BS (1995) Reduction of spike frequency adaptation and blockade of M-current in rat CA1 pyramidal neurons by linopirdine (DuP 996), a neurotransmitter release enhancer. Br J Pharmacol 115:1163–1168.

Anderson AD, Troyanovskaya M, Wackym PA (1997) Differential expression of alpha2-7, alpha9 and beta2-4 nicotinic acetylcholine receptor subunit mRNA in the vestibular end-organs and Scarpa's ganglia of the rat. Brain Res 778(2):409–413.

Beisel KW, Rocha-Sánchez SM, Morris KA, Nie L, Feng F, Kachar B, Yamoah EN, Fritzsch B (2005) Differential expression of KCNQ4 in inner hair cells and sensory neurons is the basis of progressive high-frequency hearing loss. J Neurosci 25:9285–9293.

Bertollini L, Biella G, Wanke E, Avanzini G, de Curtis M (1994) Fluoride reversibly blocks HVA calcium current in mammalian thalamic neurons. Neuroreport 5:553–556.

Brichta AM, Goldberg JM (2000) Responses to efferent activation and excitatory response-intensity relations of turtle posterior-crista afferents. J Neurophysiol 83:1224–1242.

Brown DA, Adams PR (1980) Muscarinic suppression of a novel voltage-sensitive K^+ current in a vertebrate neuron. Nature 283: 673–676.

Caulfield MP, Jones S, Vallis Y, Buckley NJ, Kim GD, Milligan G, Brown DA (1994) Muscarinic M-current inhibition via Gαq/11 and α-adrenoceptor inhibition of Ca^{2+} current via Gαo in rat sympathetic neurons. J Physiol 477:415–422.

Constanti A, Brown DA (1981) M-currents in voltage-clamped mammalian sympathetic neurons. Neurosci Lett 24:289–294.

Costa AM, Brown BS (1997) Inhibition of M-current in cultured rat superior cervical ganglia by linopirdine: mechanism of action studies. Neuropharmacology 36:1747–1753.

Chabbert C, Chambard JM, Sans A, Desmadryl G (2001a) Three types of depolarization-activated potassium currents in acutely isolated mouse vestibular neurons. J Neurophysiol 85:1017–1026.

Chabbert C, Chambard JM, Valmier J, Sans A, Desmadryl G (2001b) Hyperpolarization-activated (Ih) current in mouse vestibular primary neurons. Neuroreport 12:2701–2704.

Dayanithi G, Desmadryl G, Travo C, Chabbert C, Sans A (2007) Trimetazidine modulates AMPA/kainate receptors in rat vestibular ganglion neurons. Eur J Pharmacol 574:8–14.

Dechesne CJ, Mbiene JP, Sans A (1986) Postnatal development of vestibular receptor surfaces in the rat. Acta Otolaryngol 101: 11–18.

Dechesne CJ, Desmadryl G, Demêmes D (1987) Myelination of the mouse vestibular ganglion. Acta Otolaryngol 103:18–23.

Demêmes D, Dechesne CJ, Venteo S, Gaven F, Raymond J (2001) Development of the rat efferent vestibular system on the ground and in microgravity. Dev Brain Res 128:35–44.

Desmadryl G (1991) Postnatal developmental changes in the responses of mouse primary vestibular neurons to externally applied galvanic currents. Dev Brain Res 64:137–143.

Desmadryl G, Chambard JM, Valmier J, Sans A (1997) Multiple voltage dependent calcium currents in acutely isolated mouse vestibular neurons. Neuroscience 78:511–522.

Goldberg JM (1996) Theoretical analysis of intercellular communication between the vestibular type I hair cell and its calyx ending. J Neurophysiol 76:1942–1957.

Goldberg JM, Fernández C (1980) Efferent vestibular system in the squirrel monkey: anatomical location and influence on afferent activity. J Neurophysiol 43:986–1025.

Gómez-Casati ME, Katz E, Glowatzki E, Lioudyno MI, Fuchs P, Elgoyhen AB (2004) Linopirdine blocks $\alpha9\alpha10$-containing nicotinic cholinergic receptors of cochlear hair cells. J Assoc Res Otolaryngol 5:261–269.

Gu N, Vervaeke K, Hu H, Storm JF (2005) Kv7/KCNQ/M and HCN/h, but not $K_{Ca}2$/SK channels, contribute to the somatic medium after-hyperpolarization and excitability control in CA1 hippocampal pyramidal cells. J Physiol 566:689–715.

Holt JC, Lysakowski A, Goldberg JM (2006) Mechanisms of efferent-mediated responses in the turtle posterior crista. J Neurosci 26(51):13180–13193.

Holt JC, Stauffer EA, Abraham D, Géléoc SG (2007) Dominant-negative inhibition of M-like potassium conductance in hair cells of the mouse inner ear. J Neurosci 27:8940–8951.

Howard RJ, Clark KA, Holton JM, Minor DL (2007) Structural insight into KCNQ (Kv7) channel assembly and channelopathy. Neuron 53:663–675.

Hurley KM, Gaboyard S, Zhong M, Price SD, Wooltorton JR, Lysakowski A, Eatock RA (2006) M-like K^+ currents in type I hair cells and calyx afferent endings of the developing rat utricle. J Neurosci 26:10253–10269.

Ishiyama A, Lopez I, Wackym PA (1995) Distribution of efferent cholinergic terminals and alpha-bungarotoxin binding to putative nicotinic acetylcholine receptors in the human vestibular end-organs. Laryngoscope 105:1167–1172.

Ishiyama A, Lopez I, Wackym PA (1997) Molecular characterization of muscarinic receptors in the human vestibular periphery. Implications for pharmacotherapy. Am J Otol 18:648–654.

Ito K, Dulon D (2002) Nonselective cation conductance activated by muscarinic and purinergic receptors in rat spiral ganglion neurons. Am J Physiol 282:1121–1135.

Kharkovets T, Hardelin JP, Safieddine S, Schweizer M, El-Amraoui A, Petit C, Jentsch TJ (2000) KCNQ4, a K^+ channel mutated in a form of dominant deafness, is expressed in the inner ear and the central auditory pathway. Proc Natl Acad Sci U S A 97:4333–4338.

Kharkovets T, Dedek K, Maier H, Schweizer M, Khimich D, Nouvian R, Vardanyan V, Leuwer R, Moser T, Jentsch TJ (2006) Mice with altered KCNQ4 K^+ channels implicate sensory outer hair cells in human progressive deafness. EMBO J 25(3):642–652.

Kong WJ, Hussl B, Thumfart WF, Schrott-Fischer A (1998) Ultrastructural localization of ChAT-like immunoreactivity in the human vestibular periphery. Hear Res 119:96–103.

Kubisch C, Schroeder BC, Friedrich T, Lutjohann B, El-Amraoui A, Marlin S, Petit C, Jentsch TJ (1999) KCNQ4, a novel potassium channel expressed in sensory outer hair cells, is mutated in dominant deafness. Cell 96:437–446.

Lamas JA, Selyanko AA, Brown DA (1997) Effects of a cognition-enhancer, linopirdine (DuP 996), on M-type potassium currents (IK(M)) and some other voltage- and ligand-gated membrane currents in rat sympathetic neurons. Eur J Neurosci 9:605–616.

Lawrence J, Saraga F, Churchill JF, Statland JM, Travis KE, Skinner FK, McBain CJ (2006) Somatodendritic Kv7/KCNQ/M channels control interspike interval in hippocampal interneurons. J Neurosci 26:12325–12338.

Lerche C, Scherer CR, Seebohm G, Derst C, Wei AD, Busch AE, Steinmeyer K (2000) Molecular cloning and functional expression of KCNQ5, a potassium channel subunit that may contribute to neuronal M-current diversity. J Biol Chem 275:22395–22400.

Li GO, Kevetter GA, Leonard RB, Prusak DJ, Wood TG, Correia MJ (2007) Muscarinic acetylcholine receptor subtype expression in avian vestibular hair cells, nerve terminals and ganglion cells. Neuroscience 146:384–402.

Limón A, Pérez C, Vega R, Soto E (2005) Ca^{2+}-activated K^+ current density is correlated with soma size in rat vestibular-afferent neurons in culture. J Neurophysiol 94:3751–3761.

Lysakowski A, Goldberg JM (1997) A regional ultrastructural analysis of the cellular and synaptic architecture in the chinchilla cristae ampullares. J Comp Neurol 389:419–443.

Lysakowski A, Calin-Jageman L, Gaboyard S, Chatlani S, Price SD, Goldberg JM (2008) Developing the anatomical model of the vestibular calix ending: regions 3 and 4, the initial segment and heminode region. Abstracts of 45th Inner Ear Biology Meeting 2008:43.

Marlinski V, Plotnik M, Goldberg JM (2004) Efferent actions in the chinchilla vestibular labyrinth. J Assoc Res Otolaryngol 5:126–143.

Marrion NV, Adams PR, Gruner W (1992) Multiple kinetic states underlying macroscopic M-currents in bullfrog sympathetic neurons. Proc Biol Sci 248:207–214.

Mercado F, López IA, Acuna D, Vega R, Soto E (2006) Acid-sensing ionic channels in the rat vestibular endorgans and ganglia. J Neurophysiol 96:1615–1624.

Meves H, Schwarz JR, Wulfsen I (1999) Separation of M-like current and ERG current in NG108-15 cells. Br J Pharmacol 127:1213–1223.

Passmore GM, Selyanko AA, Mistry M, Al-Qatari M, Marsh SJ, Matthews EA, Dickenson AH, Brown TA, Burbidge SA, Main M, Brown DA (2003) KCNQ/M currents in sensory neurons: significance for pain therapy. J Neurosci 23:7227–7236.

Pérez C, Limón A, Vega R, Soto E (2005) KCNQ potassium channels in vestibular-afferent neurons. Assoc Res Otolaryngol Abstr 28:855.

Rabejac D, Devau G, Raymond J (1997) AMPA receptors in cultured vestibular ganglion neurons: detection and activation. Eur J Neurosci 9:221–228.

Risner JR, Holt JR (2006) Heterogeneous potassium conductances contributes to the diverse firing properties of postnatal mouse vestibular ganglion neurons. J Neurophysiol 96:2364–2376.

Rivera-Arconada I, López-Garcia JA (2005) Effects of M-current modulators on the excitability of immature rat spinal sensory and motor neurons. Eur J Neurosci 22:3091–3098.

Robbins J (2001) KCNQ potassium channels: physiology, pathophysiology, and pharmacology. Pharmacol Ther 90:1–19.

Rocha-Sánchez SMS, Morris KA, Kachar B, Nichols D, Fritzsch B, Beisel KW (2007) Developmental expression of Kcnq4 in vestibular neurons and neurosensory epithelia. Brain Res 1139:117–125.

Rome C, Luo D, Dulon D (1999) Muscarinic receptor-mediated calcium signaling in spiral ganglion neurons of the mammalian cochlea. Brain Res 846:196–203.

Romero M, Reboreda A, Sanchez E, Lamas JA (2004) Newly developed blockers of the M-current do not reduce spike frequency adaptation in cultured mouse sympathetic neurons. Eur J Neurosci 19:2693–2702.

Rossi ML, Martini M (1991) Efferent control of posterior canal afferent receptor discharge in the frog labyrinth. Brain Res 555:123–134.

Rüsch A, Lysakowski A, Eatock RA (1998) Postnatal development of type I and type II hair cells in the mouse utricle: acquisition of voltage-gated conductance and differentiated morphology. J Neurosci 18:7487–7501.

Safieddine S, Bartolami S, Wenthold RJ, Eybalin M (1996) Pre- and postsynaptic M3 muscarinic receptor mRNAs in the rodent peripheral auditory system. Mol Brain Res 40:127–135.

Sanguinetti MC, Jurkiewicz NK (1990) Two components of cardiac delayed rectifier K^+ current. Differential sensitivity to block by class III antiarrhythmic agents. J Gen Physiol 96:195–215.

Schnee ME, Brown BS (1998) Selectivity of linopirdine (DuP 996), a neurotransmitter release enhancer, in blocking voltage-dependent and calcium-activated potassium currents in hippocampal neurons. J Pharmacol Exp Ther 286:709–717.

Schroeder BC, Hechenberger M, Weinreich F, Kubisch C, Jentsch TJ (2000) KCNQ5, a novel potassium channel broadly expressed in brain, mediates M-type currents. J Biol Chem 275:24089–24095.

Selyanko AA, Delmas P, Hadley JK, Tatulian L, Wood IC, Mistry M, London B, Brown DA (2002) Dominant-negative subunits reveal potassium channel families that contribute to M-like potassium currents. J Neurosci 22:1–5.

Selyanko AA, Hadley JK, Wood IC, Abogadie FC, Delmas P, Buckley NJ, London B, Brown DA (1999) Two types of K^+ channel subunit, Erg1 and KCNQ2/3, contribute to the M-like current in a mammalian neuronal cell. J Neurosci 19:7742–7756.

Shapiro MS, Roche JP, Kaftan EJ, Cruzblanca H, Mackie K, Hille B (2000) Reconstitution of muscarinic modulation of the KCNQ2/KCNQ3 K^+ channels that underlie the neuronal M current. J Neurosci 20:1710–1721.

Shen Z, Marcus DC (1998) Divalent cations inhibit IsK/KvLQT1 channels in excised membrane patches of strial marginal cells. Hearing Res 123(1–2):157–167.

Shi W, Wymore RS, Wang HS, Pan Z, Cohen IS, McKinnon D, Dixon JE (1997) Identification of two nervous system-specific members of the erg potassium channel gene family. J Neurosci 17:9423–9432.

Søgaard R, Ljungstrøm T, Pedersen KA, Olesen SP, Jensen BS (2001) KCNQ4 channels expressed in mammalian cells: functional characteristics and pharmacology. Am J Physiol Cell Physiol 280(4):C859–C866.

Soto E, Salceda R, Cruz R, Ortega A, Vega R (2000) Microcomputer program for automated action potential waveform analysis. Comput Methods Prog Biomed 62:141–144.

Soto E, Limón A, Ortega A, Vega R (2002a) Características morfológicas y electrofisiológicas de las neuronas del ganglio vestibular en cultivo. Gac Méd Méx 138:1–13.

Soto E, Vega R, Budelli R (2002b) The receptor potential in type I and type II vestibular system hair cells: a model analysis. Hear Res 165:35–47.

Soto E, Pérez C, Limón A, Vega R (2004) M current in vestibular-afferent neurons from the rat. J Vest Res 14:190.

Soto E, Vega R, Luis E (2008) Developmental expression of inward rectifier K^+ currents in vestibular-afferent neurons of the rat. Assoc Res Otolaryngol Abstr 769:99.

Suh BC, Hille B (2002) Recovery from muscarinic modulation of M current channels requires phosphatidylinositol 4,5-bisphosphate synthesis. Neuron 35:507–520.

Suh BC, Hille B (2007) Regulation of KCNQ channels by manipulation of phosphoinositides. J Physiol 582:911–916.

Surti TS, Jan LY (2005) A potassium channel, the M-channel, as a therapeutic target. Curr Opin Investig Drugs 6:704–711.

Tejeda-Muñoz N (2008) Expresión del receptor muscarínico M1en neurona aferentes vestibulares de rata. Tesis de Licenciatura en Biomedicina. Universidad Autónoma de Puebla.

Wackym PA, Chen CT, Ishiyama A, Pettis RM, López IA, Hoffman L (1996) Muscarinic acetylcholine receptor subtype mRNAs in the human and rat vestibular periphery. Cell Biol Int 20:187–192.

Wang HS, Pan Z, Shi W, Brown BS, Wymore RS, Cohen IS, Dixon JE, McKinnon D (1998) KCNQ2 and KCNQ3 potassium channel subunits: molecular correlates of the M-channel. Science 282:1890–1893.

Wood CD, Manno JE, Manno BR, Odenheimer RC, Bairnsfather LE (1986) The effect of antimotion sickness drugs on habituation to motion. Aviat Space Environ Med 57:539–542.

Yamaguchi K, Ohmori H (1993) Suppression of the slow K^+ current by cholinergic agonists in cultured chick cochlear ganglion neurons. J Physiol 464:213–228.

Zhang H, Craciun LC, Mirshahi T, Rohacs T, Lopes CM, Jin T, Logothetis DE (2003) PIP2 activates KCNQ channels, and its hydrolysis underlies receptor-mediated inhibition of M currents. Neuron 37:963–975.

(Accepted 14 November 2008)
(Available online 21 November 2008)

Neuroscience Letters 468 (2010) 238–242

Contents lists available at ScienceDirect

Neuroscience Letters

journal homepage: www.elsevier.com/locate/neulet

Phospholipase C-mediated inhibition of the M-potassium current by muscarinic-receptor activation in the vestibular primary-afferent neurons of the rat

Cristina Pérez, Rosario Vega, Enrique Soto*

Instituto de Fisiología, Universidad Autónoma de Puebla, México

ARTICLE INFO

Article history:
Received 17 September 2009
Received in revised form 29 October 2009
Accepted 1 November 2009

Keywords:
Vestibular system
Inner ear
KCNQ
XE-992
Oxotremorine-M
U73122
Second messenger
Afferent neurons
Efferent system
Hair cells

ABSTRACT

The activation of the efferent vestibular system modifies the basal discharge and the dynamic response of primary-afferent neurons to head motion and gravitational stimuli. The efferent input to afferent neurons is mediated primarily by cholinergic synapses that activate both muscarinic and nicotinic receptors. Previously we had shown that the muscarinic-acetylcholine-receptor (mAChR) activation modulates the low-voltage-activated M-type potassium current ($I_{K,M}$) in the vestibular-afferent neurons. In this work we studied the second-messenger system mediating the inhibition of $I_{K,M}$ after mAChR activation. For this, voltage and current-clamp recordings were obtained in the cultured vestibular-afferent neurons of the rat. The $I_{K,M}$ was measured during its deactivation. Response to current-pulse injection was also studied. The use of the mAChR agonist oxotremorine-M significantly reduced the amplitude of the $I_{K,M}$ and modified the discharge response to current pulses from single spike to multiple spiking, reducing the adaptation of the electrical discharge. The intracellular perfusion of the phospholipase C (PLC) inhibitor U73122 significantly attenuated the inhibitory action of the mAChR receptor agonist oxotremorine-M. Its inactive analog U73343 produced no significant action. The use of the phosphatidylinositol 4,5 bis-phosphate (PIP_2) scavenger poly-L-lysine also led to a significant reduction of the $I_{K,M}$. Our results show that the mAChR mediated activation of PLC and subsequent PIP_2 depletion (caused by its hydrolysis), modulates the $I_{K,M}$ in the vestibular-afferent neurons, modifying their discharge response dynamics to current-pulse injection.

The vestibular system efferent synaptic terminals are found both on vestibular nerve afferents and on hair cells. The efferent neurons originate in the brain stem, and make synaptic contact with type II hair cells and with afferent neuron dendrites originating from type I hair cells (calyx bearing terminals) and from mixed neurons originating from type I and type II hair cells (dimorphic terminals). Efferent innervation is found in almost all of the acoustico-lateralis sensory systems, from neuromasts of the lateral line of fish and amphibians to the mammalian cochlea. In the vestibule the activation of the efferent system modifies the basal discharge and the dynamic response of primary-afferent neurons to head motion and gravitational stimuli [1]. The efferent synaptic input to afferent neurons is mediated primarily by cholinergic terminals that activate both muscarinic and nicotinic receptors. Previously we had shown that muscarinic-acetylcholine-receptor (mAChR) activation modulates the potassium M-current ($I_{K,M}$) in the vestibular primary-afferent neurons, leading to a modification of its dynamic response to electrical stimuli [15].

The $I_{K,M}$ is a voltage activated, low threshold, and noninactivating K^+ conductance. It is activated in the subthreshold range for the initiation of the action potential causing a membrane hyperpolarization, and in neurons contributes to the regulation of repetitive firing and excitability [3]. The $I_{K,M}$ is correlated with the expression of KCNQ-type potassium-channel subunits [22], and has been shown to be modulated by mAChR activation (from which it gets its name) and by other neurotransmitters that act via $G_{\alpha q/11}$ in a variety of neuron types [5,14,7]. The activation of the mAChR causes the closure of the KCNQ channels as a result of the hydrolysis of the membrane phospholipid, phosphatidylinositol 4,5 bis-phosphate (PIP_2), because the PIP_2 is required to maintain the KCNQ channels in an open state [25].

Five mAChR subtypes can be distinguished pharmacologically, and by their activation of second-messenger systems they are termed M1–M5. The odd-numbered receptors (M1, M3, and M5) are coupled to the $G_{\alpha q/11}$ subunit of the G protein and activate phospholipase C (PLC), whereas the M2 and M4 are coupled to the G_i and

* Corresponding author at: Instituto de Fisiología, BUAP, Apartado Postal 406, Puebla, Pue. 72000, Mexico. Tel.: +52 222 2295500x7316; fax: +52 222 2295500x7301.
E-mail addresses: esoto@siu.buap.mx, esoto2424@yahoo.com (E. Soto).

0304-3940/$ – see front matter © 2009 Elsevier Ireland Ltd. All rights reserved.
doi:10.1016/j.neulet.2009.11.004

G_o α subunits and inhibit adenylyl cyclase [4]. The PLC hydrolyzes the PIP_2 generating the second messengers diacylglycerol (DAG) and inositol 1,4,5-trisphosphate ($InsP_3$) that control diverse cellular processes among which is the gating of ionic channels like the KCNQ [20]. The PIP_2 directly activates all members of the KCNQ channels probably caused by an electrostatic interaction with a conserved region of basic amino acid residues located in the C-terminal region proximal to the S6 transmembrane domain [25].

With the aim to contribute to our understanding of the cellular mechanisms involved in the efferent control of the afferent neuron dynamics in the vestibular system, in this work we studied the second messengers (participation of PLC and PIP_2) mediating the inhibition of the M-current after mAchR activation in cultured vestibular-afferent neurons.

Experiments were made on young Wistar rats (postnatal days 7–10) before myelinization of the cell body was established [8]. Animal care and procedures were in accordance with the National Institutes of Health Guide for the Care and Use of Laboratory Animals.

Primary culture of the afferent neurons was previously described [13]. Briefly, the vestibular ganglia were dissected and placed in fresh L-15 tissue-culture medium, with 1.25 mg/mL of collagenase IA (Sigma Chemicals, St. Louis, MO, USA) and 1.25 mg/mL of porcine trypsin (USB, Cleveland, OH, USA), for 30 min at 37 °C. Then the tissue was mechanically dissociated and isolated cells were plated in 35-mm Nunclon™ tissue-culture Petri dishes (Nunc, Roskilde, Denmark) and maintained at 37 °C for 18–24 h in a 5% CO_2 tissue-culture incubator.

Experiments were done at room temperature (23–25 °C) and cells were continuously perfused by gravity-fed normal extracellular solution containing, in mM, NaCl 140, KCl 5.4, $MgCl_2$ 1.2, $CaCl_2$ 3.6, HEPES 10, and dextrose 10. Neurons maintained in the culture for 18–24 h were recorded using the patch-clamp technique in the whole-cell voltage clamp configuration. Patch-clamp pipettes were fabricated from 1.2-mm outside diameter borosilicate-glass capillary tubing (WPI, Sarasota, FL, USA) using a horizontal micropipette puller (P80/PC Sutter Instruments, San Rafael, CA, USA). Patch-pipette resistance was 1–3 MΩ when filled with the intracellular solution containing, in mM, NaCl 10, KCl 140, $CaCl_2$ 0.134, HEPES 5, EGTA 10, Mg-ATP 2, and Na-GTP 1. Data were recorded with an Axopatch 200B amplifier (Molecular Devices, Union City, CA, USA), the output of which was led to a 12-bit digital-analog converter (Digidata 1200, Molecular Devices) controlled by pClamp 9.0 software (Molecular Devices). The membrane capacitance (C_m) and series resistance (R_s) were measured on-line with the pClamp software. During the recordings, C_m and R_s were electronically compensated (80%). Data were lowpass filtered at 2 kHz and sampled at 5 kHz. The junction potential was calculated with the generalized Henderson liquid-junction potential equation. Voltages were not corrected for either liquid-junction potential (less than 3 mV in our experimental conditions).

The $I_{K,M}$ amplitude was investigated during its deactivation caused by a 1-s hyperpolarizing step to −60 mV and delivered from a holding potential of −20 mV. This protocol was used to take advantage of the slow deactivation time-course of the M-current. The deactivation-current amplitude was measured at −60 mV as the difference between the average of a 10-ms segment, taken 10–20 ms into the hyperpolarizing step, and the average during the last 20 ms of that step [3,18].

Current-clamp experiments were also done to study the effect of the various pharmacological agents used in the response of the vestibular-afferent neurons to a current-pulse injection. For these experiments cells were held at a membrane voltage of about −60 mV and square current pulses from 0.3 to 1 nA and 200 ms were injected.

Recordings were analyzed off-line using Clampfit 9.0 (Molecular Devices) and Origin 6.0 (Microcal Software, Inc., Northampton, MA, USA). The Student's *t*-test was used to assess statistical significance, with $P < 0.05$ indicating a significant difference. Results are shown as mean ± standard error of the mean (SE).

To study the effect of the PLC inhibition on the $I_{K,M}$ amplitude, we used the PLC inhibitor U73122 and its inactive analogue, U73343 (Sigma Chemicals, St. Louis, MO, USA). The mAChR agonist oxotremorine-M (oxo-M), poly-L-lysine, as a PIP_2 scavenger (Sigma Chemicals) and the KCNQ channel blocker XE-991 (from Tocris-Cookson, Inc. Ellisville, MO, USA) were also used. Because the action of U73122, U73343, and poly-L-lysine were at intracellular targets, they were dissolved in the intracellular solution used for filling of the recording pipette. Other drugs were applied using a theta tube coupled to a piezoelectric device (LSS-3200; Burleigh, Ontario, Canada) for a rapid extracellular solution exchange. Aliquots of all the drugs were prepared and stored in a freezer. The XE-991, oxo-M, and poly-L-lysine were dissolved in deionized water. The U73122 and U73343 were dissolved in an aqueous DMSO stock solution that once in the intracellular medium reached a concentration of 0.01% DMSO. For the experiments the aliquots were dissolved in the corresponding solution to reach the desired concentration before use.

Vestibular-afferent neurons of the rat in culture were identified by their birefringent round or ovoid somata under phase-contrast optics. The effect of oxo-M was studied in the $I_{K,M}$ deactivation protocol. The perfusion of the vestibular-afferent neurons with 10 μM oxo-M reduced the current amplitude by 58 ± 12% (Fig. 1A). The

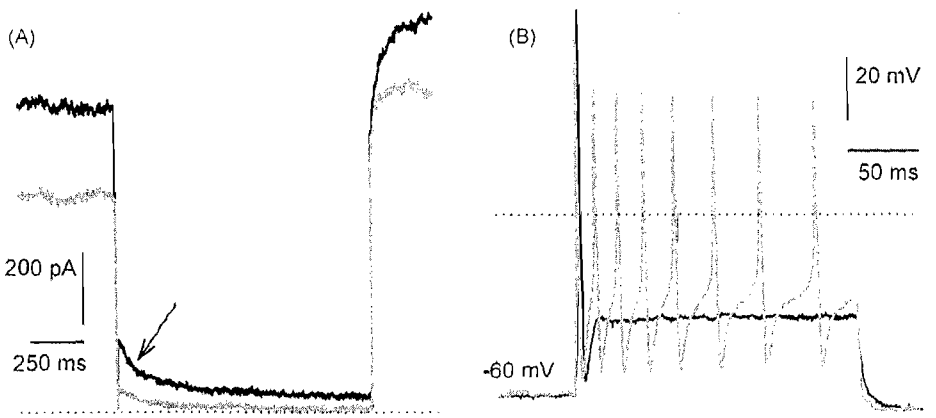

Fig. 1. Effects of oxo-M on the $I_{K,M}$ current deactivation and in the response to current pulses. In (A), the control (black trace) $I_{K,M}$ deactivation (arrow) was reduced after the perfusion of the cell with 10 μM oxo-M (gray trace). In (B), the response of a vestibular-afferent neuron (V_m = −60 mV) to a 0.6 nA, 200-ms current-pulse injection, in the control (black) and after the use of 10 μM oxo-M (gray). In this and the following graphs the dotted lines represent zero current or 0 mV.

action of oxo-M on the deactivation was completely blocked by the prior use of 1 μM atropine ($n=4$, data not shown). In current-clamp experiments, the use of 10 μM oxo-M depolarized the cell membrane potential by 5 ± 2 mV, and increased the excitability of the vestibular-afferent neurons from a typical single-action potential discharge to a repetitive 5 ± 2 action-potential discharge ($n=3$) (Fig. 1B).

To evaluate whether or not the activation of PLC participates in the modulation of the $I_{K,M}$ current caused by the activation of mAChR by oxo-M, the PLC inhibitor U73122 (3 and 10 μM) were added to the pipette filling solution. Ten minutes after the establishment of the whole-cell recording configuration, the application of 10 μM oxo-M decreased the amplitude of the $I_{K,M}$ by 40 ± 6% for the experiments using 3 μM U73122 ($n=4$; $P=0.24$ compared to the control oxo-M inhibition; Fig. 2A), and 23 ± 3% with 10 μM U73122 ($n=7$; $P=0.006$ compared to the control oxo-M inhibition; Fig. 2B). As a control, in the experiments in which oxo-M did not produce a significant effect (using 10 μM U73122), to discard the possibility that cells did not express the $I_{K,M}$ current, the KCNQ-channel blocker XE-991 (1 μM) was used after the oxo-M. The XE-991 caused a further $I_{K,M}$ decrease of 35 ± 3%, thus reaching a 64% decrease of the $I_{K,M}$ ($n=4$; $P=0.03$) (Fig. 2B), indicating that the $I_{K,M}$ was already expressed in the neurons and that the lack of a significant action of oxo-M was caused by the PLC inhibitor. In the experiments in which the oxo-M inhibitory action was not significantly modified (using 3 μM U73122), the addition of 1 μM XE-991 caused an additional decrease in the $I_{K,M}$ current amplitude of 12 ± 5% ($n=4$; Fig. 2A).

In current-clamp experiments done using 10 μM U73122 in the pipette, the use of 10 μM oxo-M caused a nonsignificant 1 mV depolarization of the membrane potential. Afterward the coapplication of oxo-M and 1 μM XE-991 caused a significant 7 ± 2 mV depolarization of the membrane potential and increased the action-potential discharge from 1 to 3 ± 1 action potentials ($n=4$), indicating that the $I_{K,M}$ was already functionally expressed by these cells (Fig. 2C).

As a control for the effect of U73122, the inactive analogue U73343 (3 and 10 μM) was also used in the recording pipette. With the use of 3 and 10 μM U73343, the perfusion of 10 μM oxo-M decreased the $I_{K,M}$ amplitude by 50 ± 11% and by 51 ± 3% ($n=4$ and 10) (Fig. 3A). In these experiments the oxo-M inhibitory effect was significantly greater than that obtained with the active inhibitor, 10 μM U73122 ($P=0.01$), and there was a nonsignificant difference with the inhibitory effect of the control of oxo-M (58 ± 12%; $P=0.65$, Fig. 1A). The coapplication of 10 μM oxo-M and 1 μM XE-991 additionally reduced the $I_{K,M}$ current amplitude by 9 ± 3% thus causing a 67% reduction of the $I_{K,M}$ current ($n=7$; $P=0.02$).

To study whether the depletion of the intracellular PIP_2 was responsible for the reduction of the $I_{K,M}$ amplitude, an experimental series using 100 μg/mL poly-L-lysine (a PIP_2 scavenger) in the recording pipette was done. It was found that after the first minute of the establishment of the whole-cell recording, the $I_{K,M}$ began to decrease systematically, attaining a 64 ± 4% ($n=4$) reduction after three minutes of the establishment of the whole-cell recording (Fig. 2B). These results indicate that PIP_2 is essential to maintain the $I_{K,M}$ amplitude.

Our results show that activation of the PLC mediates the modulation of the $I_{K,M}$ amplitude caused by the mAChR activation in the vestibular primary-afferent neurons of the rat. Our results are consistent with the PI-polyphosphate hypothesis that activation of PLC hydrolyses the PIP_2. This results in a depletion of the PIP_2 and in consequence the $I_{K,M}$ current is depressed [19,25].

Previous reports have shown that the use of the aminosteroid compound U73122 in tsA or CHO cells transfected with an M1 receptor and KCNQ2–KCNQ3 subunits completely blocked the mAChR action. In the superior cervical-ganglion neurons it was

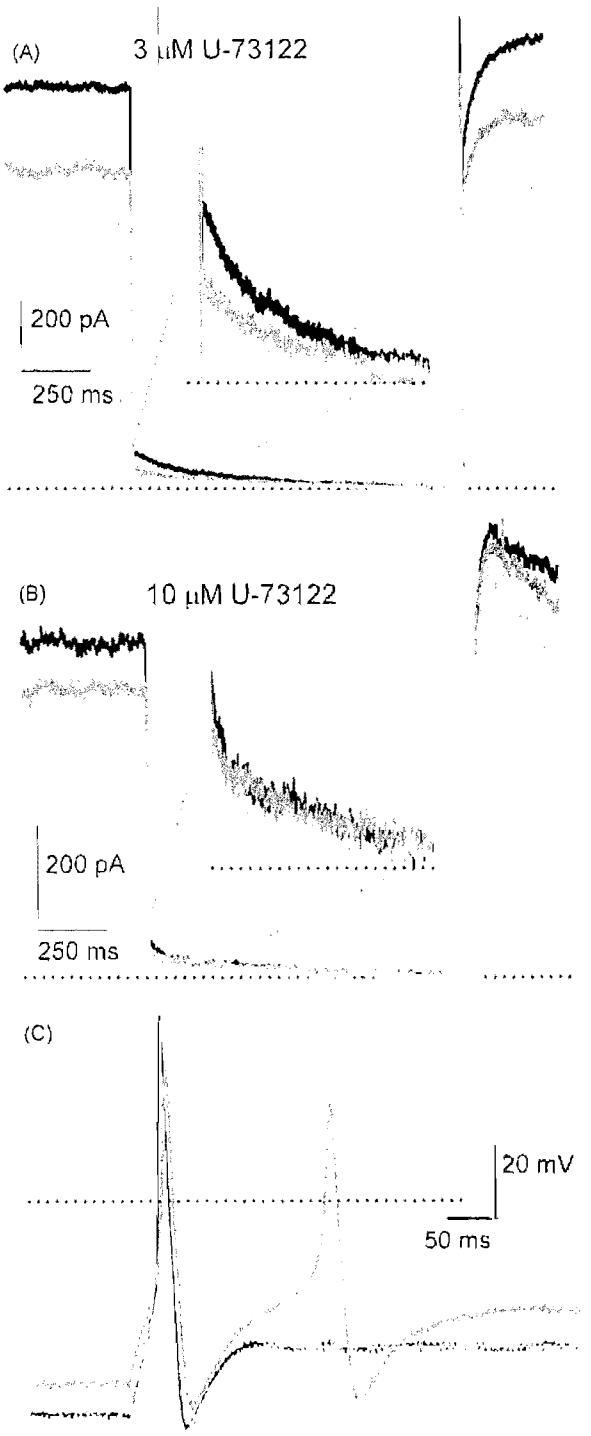

Fig. 2. Effects of the PLC inhibitor U73122 on the oxo-M action on the $I_{K,M}$. In (A), the recording of the $I_{K,M}$ deactivation in the control (black trace) and after the use of the PLC inhibitor U73122 (3 μM) produced a nonsignificant attenuation of the inhibitory effect of 10 μM oxo-M on the $I_{K,M}$ amplitude (dark gray trace). The addition of 1 μM XE-991 caused a significant decrease of the $I_{K,M}$ (light gray trace). In (B), a similar paradigm shows the decrease of the inhibitory effect of the oxo-M on the $I_{K,M}$ amplitude in the control (black) in the presence of 10 μM of U73122 (dark gray) and after 1 μM XE-991 use. In (C), the response of an afferent neuron (V_m = −60 mV) to a 0.8 nA, 200-ms current-pulse injection in the control (black) after the use of 10 μM oxo-M in the presence of 10 μM of U73122 (light gray) and during the coapplication of 10 μM oxo-M and 1 μM XE-991 (dark gray).

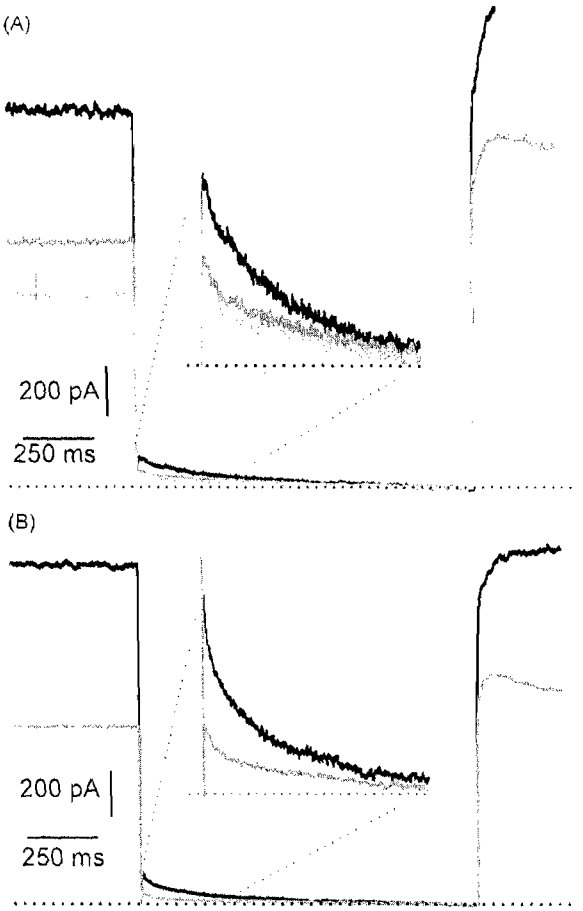

Fig. 3. Effect of the inactive analogue U73343 and the PIP_2 scavenger poly-L-lysine on the oxo-M action on the $I_{K,M}$. In (A), the $I_{K,M}$ deactivation recording in the control (black) was significantly reduced after the perfusion of 10 μM oxo-M in the presence of 10 μM U73343 (gray). After the perfusion of XE-991, there was an additional decrease of the $I_{K,M}$ (light gray). In (B), the use of poly-L-lysine in the intracellular solution caused a significant rundown of the $I_{K,M}$ after 3 min of establishing the whole-cell recording condition. The recording was done immediately after establishing the whole cell (black) and after 3 min (gray).

found that 3 μM U73122 blocked the inhibitory effect of oxo-M, reducing it from 80% to 20%, and that the inactive control compound U73343 had a weak inhibitory effect [19,24]. In contrast we found that the active compound U73122 produced a 61% reduction (from 58% to 23% of a maximum attained of 67% with XE-991) of the mAChR-caused M-current inhibition. The greater inhibition of the oxo-M effect found in the studies mentioned above could be caused by additional intracellular messengers participating in the control of the $I_{K,M}$ amplitude in our system. For example calcium has been found to modulate the $I_{K,M}$ amplitude in excised membrane patches obtained form the rat sympathetic neurons [17], and to cause a reduction of KCNQ4 currents expressed in CHO cells [6]. Other molecules such as $InsP_3$, DAG, NAD^+, cADP ribose, calmodulin, calcineurin, activators or inhibitors of PKC, tyrosine kinases, or myosin light-chain kinase have been suggested to modulate the M-current [14]. Furthermore the U73122 also had many side effects that were attributable to alkylation of various proteins [12], which may contribute to the variability of results between different cell types. Although differences between cells are highly expected, we cannot completely exclude that rundown of the M-current by dialysis of the intracellular medium, using whole-cell recording, may obscure the total effect of U73122. Nonetheless, in our previous work we found that the action of oxo-M on the $I_{K,M}$ in perforated patch experiments were not significantly different than values observed with whole-cell experiments [15].

Poly-L-lysine produces a local positive-electrostatic potential when it binds to the membrane and strongly attracts and effectively sequesters the multivalent PIP_2 [23]. It has been widely used in heterologous systems expressing KCNQ2–KCNQ3 subunits and M1 receptors [25,20]. The poly-L-lysine experiments in our system showed that intracellular PIP_2 is tonically activating the $I_{K,M}$ in the vestibular primary-afferent neurons.

The efferent vestibular system produces species-specific actions on primary-afferent neuron dynamics. In mammals [11] and in the toadfish [1], efferent activation increase background discharge and decrease the gain to angular motion stimuli. In the toadfish it has been shown that the decrease in sensitivity is mainly due to a reduction of hair cell receptor potential gain, consequent to an increase in the conductance of the cell membrane, whereas increase in background afferent discharge is due to excitatory conductance change occurring directly in the afferents [1]. In contrast combinations of excitation or inhibition were observed in frogs [16], turtles [2] and pigeons [10]. Differences can be accounted for by the relative density of efferent neurons innervating the hair cells or the afferent neurons, or due to the participation, aside from the acetylcholine, of other transmitters or modulators of the efferent synapse [21,9].

From a functional point of view, the inhibition of $I_{K,M}$ caused by the activation of mAChR, the subsequent stimulation of PLC, and depletion of PIP_2 results in an increased excitability of the vestibular-afferent neurons. These findings provide evidence about the mechanisms that underlie the excitatory response of the vestibular-afferent neurons to the influence of the cholinergic-efferent system.

Acknowledgements

The authors wish to thank Dr. Ellis Glazier for the editing of the English-language manuscript. This work was submitted in partial fulfillment of the requirements for the PhD degree of Cristina Pérez at the Posgrado en Ciencias Biomédicas, Instituto de Fisiología Celular, UNAM. This material is based on work supported by the Consejo Nacional de Ciencia y Tecnología, México (CONACyT) grant 46511 to ES and Vicerrectoria de Investigación (VIEP-BUAP)-CONACyT grants 20/SAL06-G and 20/SAL06-I to RV and ES. CP was supported by CONACyT fellowships 185855.

References

[1] R. Boyle, R.D. Rabbitt, S.M. Highstein, Efferent control of hair cell and afferent responses in the semicircular canals, J. Neurophysiol. 102 (2009) 1513–1525.
[2] A.M. Brichta, J.M. Goldberg, Responses to efferent activation and excitatory response-intensity relations of turtle posterior-crista afferents, J. Neurophysiol. 83 (2000) 1224–1242.
[3] D.A. Brown, P.R. Adams, Muscarinic suppression of a novel voltage-sensitive K^+ current in a vertebrate neuron, Nature 283 (1980) 673–676.
[4] M.P. Caulfield, N.J.M. Birdsall, International union of pharmacology. XVII. Classification of muscarinic acetylcholine receptors, Pharmacol. Rev. 50 (1998) 279–288.
[5] M.P. Caulfield, S. Jones, Y. Vallis, N.J. Buckley, G.D. Kim, G. Milligan, D.A. Brown, Muscarinic M-current inhibition via Gαq/11 and α-adrenoceptor inhibition of Ca^{2+} current via Gαo in rat sympathetic neurons, J. Physiol. 477 (1994) 415–422.
[6] J.M. Chambard, J.F. Ashmore, Regulation of the voltage-gated potassium channel KCNQ4 in the auditory pathway, Eur. J. Physiol. 450 (2005) 34–44.
[7] H. Cruzblanca, D.S. Koh, B. Hille, Bradykinin inhibits M current via phospholipase C and Ca^{2+} release from IP3-sensitive Ca^{2+} stores in rat sympathetic neurons, Proc. Natl. Acad. Sci. U.S.A. 95 (1998) 7151–7156.
[8] C.J. Dechesne, G. Desmadryl, D. Dememes, Myelination of the mouse vestibular ganglion, Acta Otolaryngol. 103 (1987) 18–23.
[9] D. Demêmes, I. Ryzhova, Ontogenesis of substance P in the rat peripheral vestibular system, Hear Res. 114 (1997) 252–258.
[10] J.D. Dickman, M.J. Correia, Vestibular efferent system in pigeons. Anatomical organization and effect upon semicircular canal afferent responsiveness, Ann. N. Y. Acad. Sci. 656 (1992) 927–930.

[11] J.M. Goldberg, C. Fernández, Efferent vestibular system in the squirrel monkey: anatomical location and influence on afferent activity, J. Neurophysiol. 43 (1980) 986–1025.
[12] L.F. Horowitz, W. Hirdes, B.C. Suh, D.W. Hilgemann, K. Mackie, B. Hille, Phospholipase C in Living Cells: activation, inhibition, Ca^{+2} requirement and regulation of M Current, J. Gen. Physiol. 126 (2005) 243–262.
[13] A. Limón, C. Pérez, R. Vega, E. Soto, Ca^{2+}-activated K^+ current density is correlated with soma size in rat vestibular-afferent neurons in culture, J. Neurophysiol. 94 (2005) 3751–3761.
[14] N.V. Marrion, Control of M-current, Annu. Rev. Physiol. 59 (1997) 483–504.
[15] C. Pérez, A. Limón, R. Vega, E. Soto, The muscarinic inhibition of the potassium M-current modulates the action-potential discharge in the vestibular primary-afferent neurons of the rat, Neuroscience 158 (2009) 1662–1674.
[16] M.L. Rossi, M. Martini, Efferent control of posterior canal afferent receptor discharge in the frog labyrinth, Brain Res. 555 (1991) 123–134.
[17] A.A. Selyanko, D.A. Brown, Intracellular calcium directly inhibits potassium M channels in excised membrane patches from rat sympathetic neurons, Neuron 16 (1996) 151–162.
[18] M.S. Shapiro, J.P. Roche, E.J. Kaftan, H. Cruzblanca, K. Mackie, B. Hille, Reconstitution of muscarinic modulation of the KCNQ2/KCNQ3K$^+$ channels that underlie the neuronal M current, J. Neurosci. 20 (2000) 1710–1721.
[19] B.C. Suh, B. Hille, Recovery from muscarinic modulation of M current channels requires phosphatidylinositol 4,5-bisphosphate synthesis, Neuron 35 (2002) 507–520.
[20] B.C. Suh, B. Hille, PIP_2 is a necessary cofactor for ion channel function: how and why? Annu. Rev. Biophys. 37 (2008) 175–195.
[21] R. Vega, E. Soto, Opioid receptors mediate a postsynaptic facilitation and a presynaptic inhibition at the afferent synapse of axolotl vestibular hair cells, Neuroscience 118 (2003) 75–85.
[22] H.S. Wang, Z. Pan, W. Shi, B.S. Brown, R.S. Wymore, I.S. Cohen, J.E. Dixon, D. McKinnon, KCNQ2 and KCNQ3 potassium channel subunits: molecular correlates of the M-channel, Science 282 (1998) 1890–1893.
[23] J. Wang, A. Gambhir, S. McLaughlin, D. Murray, A computational model for the electrostatic sequestration of PI(4,5)P2 by membrane-adsorbed basic peptides, Biophys. J. 86 (2004) 1969–1986.
[24] J.S. Winks, S. Hughes, A.K. Filippov, L. Tatulian, F.C. Abogadie, D.A. Brown, S.J. Marsh, Relationship between membrane phosphatidylinositol-4,5-bisphosphate and receptor-mediated inhibition of native neuronal M channels, J. Neurosci. 25 (2005) 3400–3413.
[25] H. Zhang, L.C. Craciun, T. Mirshahi, T. Rohacs, C.M. Lopes, T. Jin, D.E. Logothetis, PIP_2 activates KCNQ channels, and its hydrolysis underlies receptor-mediated inhibition of M currents, Neuron 37 (2003) 963–975.